MICROSTRUCTURAL AND THERMOELECTRIC CHARACTERISTICS OF P-TYPE CERAMICS IN THE Ca-Co-O SYSTEM

Mojca Presečnik

Doctoral Dissertation
Jožef Stefan International Postgraduate School
Ljubljana, Slovenia

Supervisor: Prof. Dr. Slavko Bernik, Jožef Stefan Institute, Jamova cesta 39, Slovenia

Evaluation Board:
Prof. Dr. Miran Čeh, Chair, Jožef Stefan Institute, Jamova cesta 39, Slovenia
Asst. Prof. Boštjan Jančar, Member, Jožef Stefan Institute, Jamova cesta 39, Slovenia
Prof. Dr. Miran Gaberšček, Member, Institute of Chemistry, Hajdrihova 19, Slovenia

MEDNARODNA PODIPLOMSKA ŠOLA JOŽEFA STEFANA
JOŽEF STEFAN INTERNATIONAL POSTGRADUATE SCHOOL



Mojca Presečnik

MICROSTRUCTURAL AND THERMOELECTRIC CHARACTERISTICS OF P-TYPE CERAMICS IN THE Ca-Co-O SYSTEM

Doctoral Dissertation

MIKROSTRUKTURNE IN TERMOELEKTRIČNE LASTNOSTI KERAMIKE TIPA P V SISTEMU Ca-Co-O

Doktorska disertacija

Supervisor: Prof. Dr. Slavko Bernik

Ljubljana, Slovenia, December 2016

Dedicated to my dear Julijan, to my precious daughter Brina and to my beloved son Matija

Acknowledgments

This PhD work was founded by the Slovenian Research Agency for which I am grateful.

I would like to thank Prof. Dr. Slavko Bernik for his supervision, guidance, encouragements, a lot of advice and unselfish help, especially in the field of chemistry, which is not my primary profession. I am thankful for our useful discussions, for setting the critical point of view, for sharing his experience with me and for being very understanding all along the way. I learned a lot from him. Thank you, Slavko!

Big thanks go to Dr. Matejka Podlogar. I am grateful for her unselfish help, for teaching me how to handle most of the devices in the lab and for her time spent with me on the FEG SEM, among others. Whenever I needed something or did not know how to handle something, she was always there for me, if not otherwise, with a good advice. Thank you Matejka, I will miss our conversations too ;)!

I would also like to thank Asst. Prof. Dr. Nina Daneu and Prof. Dr. Aleksander Rečnik for kindly accepting me to their office, for our useful talks and advice, for relaxed conversations, and for their unselfish help related to transmission electron microscopy.

Special thanks go to Dr. Johannes de Boor from the Institute of Materials Research in Cologne, Germany, who without knowing me, kindly responded to my request and enabled the much needed TE measurements, while here, at the Institute, we were still struggling with the TE device building. With this he made it possible for me to see if we are even on the right track with the development of the TE material. I cannot thank him enough for that. Besides, all the conversations we had about the measurements and about the results and reasons for them often opened my eyes and made me wonder what if.

I would like to thank Prof. Dr. Spomenka Kobe, our head of department, for being understanding and fair.

Special thanks go to Marjeta Maček Kržmanc from the K9 department and to Jena Cilenšek and Dr. Katarina Vojisavljević from the K5 department for technical assistance in the DTA/TG/MS measurements and hot-pressing sintering, respectively.

I would like to thank Edi Kranjc for the XRD measurements and useful discussions regarding the measurements, Luka Gruden and Asst. Prof. Dr. Andraž Kocjan from the former K6 department for teaching me to operate the Spark plasma sintering device, Dr. Zoran Samardzija who always helped me when I had problems with SEM, and Medeja Gec for teaching me how to prepare SEM and TEM samples. I would also like to thank Dr. Tadej Rojac for his advice and useful discussions in the field of mechano-chemistry.

A big thank you goes to Asst. Prof. Paul McGuiness who always found time for my English proofreadings and always devoted a sincere and heartfelt word to me, irrespective of the weather outside ☺.

Last but not least, I would like to thank all the wonderful people at the K7 department for all the fun times, laughter,

discussions, unselfish help, and so on and so on, especially (in alphabetical order) Sandra Drev, Mateja Košir, Darja Pečko, Matejka Podlogar, Rok Rudež, and Marko Soderžnik. “Hey “guys “, yes, our lives have taken different paths, but let us not break the bond, I wish you all, all the best”.

Then there is my entire family, especially Julijan, Brina, Matija, mami, Ivek, nona, dedi, Alenka, Zvone in Primož, there are no words which could express my gratitude for your unselfish support and standing right by my side all the way. Together we are like a well-established machine; it does not work if each small part does not participate. Hvala vsem, veliko mi pomenite in rada vas imam! Very special thanks go to you my dear Julijan, and to my precious Brina and Matija, you are my everything and I love you infinitely.

Abstract

In quest of energy efficiency and sustainability enormous amounts of produced waste heat have been completely neglected so far. The thermoelectric devices (TE) offer only viable possibility to exploit it by direct conversion into the electrical energy. The oxide TE materials are attractive for high-temperature applications, chemically stable and also environmentally friendly and non-toxic, made from abundant and low cost elements. However, to compete with the state-of-the art TE materials in the sense of TE figure of merit (zT), energy and cost of their processing, a significant improvement of their zT is required, as well as optimization of the methods for synthesis and processing.

The topic of my PhD research was the development of the promising p-type thermoelectric oxide $Ca_3Co_4O_9$ (Ca349) ceramics. I studied the influence of starting oxide powders on the formation of the Ca349 compound using solid state synthesis methods. While the same fine grained single-phase Ca349 material was used, I studied the influence of various processing methods on the microstructural features (morphology and size of grains, degree of texturing and density) and TE characteristics of the Ca349 ceramics. Finally I also studied doping the Ca349 compound with WO_3, analysing the influence of high valence and heavy W^{6+} ions on the microstructural features and the TE characteristics.

Use of relatively coarse grained starting powders of $CaCO_3$ and Co_3O_4 confirmed sluggish formation of the Ca349 compound at temperatures around 900 °C reported in the literature. However, use of fine powders enabled the formation of a single-phase Ca349 already after a single calcination at much lower temperature of 760 °C for 12 hours, which was also beneficial in further processing of the Ca349 ceramics. A mechano-chemical treatment of the same fine starting powder mixture resulted only in its amorphization; however, it enhanced its reactivity resulting in a single-phase Ca349 ceramics after only 4 hours of calcination at 760 °C. Furthermore I studied the influence of different processing methods, some already reported in the literature, modified and also novel not reported yet. It showed that they influence the key microstructural features (shape, size and thickness of grains, degree of texturing and density) differently, affecting the TE characteristics. Fully textured and dense Ca349 ceramics was also obtained; however, contrary to general expectations, modestly textured and porous Ca349 ceramics had comparable electrical conductivity and Seebeck coefficient at about 3-times lower thermal conductivity and hence much higher zT of 0.31 at 600 °C, which is the highest zT reported for pristine Ca349. The results showed the direction and possibilities for microstructural enhancement of the TE characteristics; while indicating possibilities for further improvements beyond currently obtained zT, for its major increase optimised microstructure should be combined also with proper doping.

Doping with WO_3 resulted in the formation of solid solution $Ca_3Co_{3.88}W_{0.12}O_9$, indicating much lower solid-solubility than previously reported. Incorporation of W^{6+} into the Ca_2CoO_3-layers slightly increased the Seebeck coefficient and significantly decreased thermal

conductivity; however, due to also significantly decreased electrical conductivity the obtained zT value was decreased in comparison to the undoped sample.

Povzetek

V novejšem času je na vseh področjih velik poudarek na energetski učinkovitosti in trajnostnem razvoju. Pri tem so bile povsem spregledane ogromne količine odpadne toplote in njihova koristna izraba. Tukaj nastopijo termoelektrične (TE) naprave, ki edine lahko direktno pretvorijo odpadno toploto v električno energijo ne glede na velikost vira. Oksidni TE materiali so primerni za uporabo pri visokih temperaturah zaradi kemične stabilnosti in ekološke sprejemljivosti, saj so nestrupeni in narejeni iz elementov z zadostnimi naravnimi zalogami, ki so zato cenejši. Da bi bili primerljivi z doslej najboljšimi in najbolj uporabljenimi TE materiali, tako glede faktorja kvalitete (zT) kot tudi po vloženi energiji in stroških za proizvodnjo, je potrebno občutno zvišanje njihovega zT-ja in optimizacija metod sinteze in procesiranja.

Tema disertacije je bil razvoj obetavne oksidne TE keramike p-tipa na osnovi spojine $Ca_3Co_4O_9$ (Ca349). Preučevala sem vpliv začetnih prahov na tvorbo spojine Ca349 pri klasični keramični sintezi. V nadaljevanju sem pri vseh postopkih procesiranja keramike Ca349 uporabila enofazni drobnozrnati Ca349 material in študirala njegov vpliv na mikrostrukturo (morfologija in velikost zrn, stopnja teksturiranosti in gostota) in TE lastnosti Ca349 keramike. V zaključku sem keramiko Ca349 dopirala z WO_3 in preučila vpliv visoko valenčnega in težkega iona W^{6+} na mikrostrukture lastnosti ter TE značilnosti.

Uporaba relativno grobih začetnih prahov $CaCO_3$ in Co_3O_4 je potrdila počasnost reakcije in nastanek spojine Ca349 okoli 900 °C. Z uporabo finih, atritorsko pomletih začetnih prahov, je spojina Ca349 nastala že po prvi 12 urni kalcinaciji pri 760 °C, torej mnogo hitreje in pri precej nižji temperaturi. Uporaba tako pripravljenega materiala Ca349 se je pokazala kot prednost tudi v nadaljnjem procesiranju keramike Ca349. Z mehano-kemijsko obdelavo je zmes izhodnih prahov postala amorfna, spojina Ca349 ni nastala, povečala pa se je reaktivnost, tako da je spojina Ca349 nastala že po 4 urah kalcinacije pri 760 °C. V nadaljevanju sem preučevala vpliv različnih metod procesiranja keramike, in sicer nekatere metode, že poročane v literaturi, spremenjeno metodo in povsem novi metodi, ki pri keramiki Ca349 še nista bili uporabljeni. Pokazalo se je, da imajo metode različen vpliv na mikrostrukturne značilnosti ter TE lastnosti. Po splošnih pričakovanjih naj bi bila dobra TE keramika Ca349 z dobrimi TE lastnostmi visoko teksturirana in gosta, kar je bilo v raziskavi tudi doseženo. Vendar pa je najvišji zT z vrednostjo 0,31 pri 600 °C imela zmerno teksturirana in porozna keramika Ca349 z zelo primerljivo električno prevodnostjo in Seebekovim koeficientom, a kar 3-krat nižjo termično prevodnost kot povsem teksturirana in gosta. Po mojem najboljšem vedenju gre za najvišjo poročano vrednost zT za nedopirano keramiko Ca349.

Rezultati procesiranja keramike Ca349 so nakazali smernice in možnosti za izboljšanje TE lastnosti z mikrostrukture in tudi, da so možne še nadaljnje izboljšave. Za bistveno povišanje zT pa bi bilo potrebno tudi ustrezno dopiranje.

Raziskovala sem dopiranje Ca349 spojine z WO_3, kjer je nastala trdna raztopina $Ca_3Co_{3.88}W_{0.12}O_9$ z veliko manjšo trdno topnostjo, kot

je bilo poročano. Vgrajevanje W^{6+} iona v Ca_2CoO_3 plasti je povzročilo rahlo zvišanje Seebeckovega koeficienta in občutno znižanje termične prevodnosti. Hkrati pa se je znižala tudi električna prevodnost in negativno vplivala na zT dopiranih vzorcev v primerjavi z nedopiranimi.

Contents

List of Figures ..... ***xvii***

List of Tables ..... ***xix***

Abbreviations ..... ***xxi***

Symbols ..... ***xxv***

1 Introduction ***1***

1.1 Thermoelectric Effects 2

1.1.1 ..... Seebeck effect 2

1.1.2 ..... Peltier effect 4

1.1.3 ..... Thomson effect 5

1.2 Applications of the thermoelectric affect 5

1.2.1 ..... Efficiency and the thermoelectric figure of merit 7

1.2.1.1 ... “Efficiency” of a single thermoelectric material 8

1.3 Electrical and thermal transport properties 9

1.3.1 ..... Carrier concentration 9

1.3.2 ..... Effective mass 10

1.3.3 ..... Thermal conductivity 10

1.3.3.1 ..... Electronic thermal conductivity 10

1.3.3.2 ..... Lattice thermal conductivity 11

1.3.4 ..... Phonon-Glass-Electron-Crystal or PGEC 11

1.4 Thermoelectric materials 11

1.4.1 ..... Oxide thermoelectrics 13

1.4.1.1 ..... Wide-Bandgap Semiconductor Oxides 14
1.4.1.2 ..... Layered Oxychalcogenides 14
1.4.1.3 ..... Perovskite-type oxide materials 14
1.4.1.4 ..... Layered Cobalt-based oxide materials 15
1.4.1.4.1 ..... Na_xCoO 15
1.4.1.4.2 ..... Ca-Co-O system 17
1.4.1.4.2.1 ..... $Ca_3Co_4O_9$ crystal structure 17
1.4.1.4.2.2 .. Synthesis of the $Ca_3Co_4O_9$ compound and the microstructure 18
1.4.1.4.2.3 ..... Texturing and the microstructural characteristics 20
1.4.1.4.2.4 ..... Doping for enhanced TE properties 21

2 Aims and hypothesis *23*

2.1 Description of the problem 23

2.2 Aims and goals of the dissertation 25

3 Material processing and characterization *27*

3.1 Synthesis 27
3.1.1 ..... Solid state synthesis 27
3.1.1.1 ..... Classical ceramic solid-state procedure 27
3.1.1.1.1 ..... WO_3-doped $Ca_3Co_4O_9$ 27
3.1.1.2 ..... Mechano-chemical synthesis 28

3.2 Processing 33
3.2.1 ..... Spark plasma sintering (SPS) 33
3.2.1.1 ... Free-edge spark plasma sintering or spark plasma texturing (SPT) 34
3.2.2 ..... Other processing methods 34
3.2.2.1 ..... Hot pressing - HP 34
3.2.2.2 ..... Free edge spark plasma texturing - SPT 34

3.2.2.3 .....Novel cold pressing of calcinated Ca349 pellet 35
3.2.3 .....Thermoelectric characterization 35
3.2.4 .....Other characterizations methods 35
3.2.4.1 .....Particle size measurements 35
3.2.4.2 .....Differential thermal analysis-DTA, thermal-gravimetric analysis-TG and mass spectrometry-MS 35
3.2.4.3 .....Densities measurements 36
3.2.4.4 .....X-ray powder diffraction (XRD) 36
3.2.4.5 .....Scanning electron microscopy (SEM) 36

4 Synthesis of single-phase $Ca_3Co_4O_9$ ceramics and their processing for a microstructure-enhanced thermoelectric performance *37*

5 The Thermoelectric Compound $Ca_3Co_4O_9$ – Synthesis and Characteristics *53*

6 Influence of a mechano-chemical treatment on the synthesis and characteristics of p-type thermoelectric $Ca_3Co_4O_9$ ceramics.....*59*

7 Microstructural and thermoelectric properties of WO_3-doped $Ca_3Co_4O_9$ ceramics.....*69*

8 Conclusions *77*

References *81*

Bibliography *89*

Biography *91*

List of Figures

Figure 1.1: The schematic presentation of the Seebeck effect. . 2
Figure 1.2: The schematic presentation of the Seebeck effect in an open circuit. 3
Figure 1.3: The Seebeck effect schematic presentation in the single material. 4
Figure 1.4: The schematic presentation of the Peltier effect. . 5
Figure 1.5: The schematic presentation of the Thomson effect. . 5
Figure 1.6: (a) Conventional thermocouple from metal or alloy; (b) micro thermocouples on the substrate [12]. 6
Figure 1.7: Schematic presentation of the thermoelectric generator (left) and thermoelectric refrigerator (right)[12]. . 6
Figure 1.8: The scheme of the TE module made from p-n couples wired electrically in series and thermally in parallel [7]. ... 6
Figure 1.9: Demonstration of TE efficiency as a function of temperature and thermocouple material figure of merit [12]. ... 9
Figure 1.10: Presentation of maximised zT, which is comprised from compromised thermal conductivity (κ) and Seebeck coefficient (S) with electrical conductivity (σ) [7]..... 10
Figure 1.11: Graphical presentation of time development of the bulk TE materials with new concepts and technologies for achieving higher zT values [30]. 12
Figure 1.12: Presentation of the TE materials according to the working temperature, environment impact and abundancy [36]. .. 13
Figure 1.13: BiCuSeO crystal structure [47]. 14
Figure 1.14: (a) Schematic crystal structure of ideal perovskite oxide SrTiO3 (Pm-3m) and (b) crystal structure of distorted perovskite $CaMnO_3$ (Pnma)[37]..... 15
Figure 1.15: Schematic crystal structures of layered cobalt oxides (a) Na_xCoO_2, (b) $Ca_3Co_4O_9$, and (c) $Ca_3Co_4O_9$ structure model projected parallel to a-axis [37,63] 16
Figure 1.16: The development of the oxide TE materials through time [61]. 17
Figure 1.17: Phase diagram for the CaO-CoO system in air [68]. 18
Figure 3.1: The milling parameters in planetary mill with cylindrical vial needed for description of energetics of the high-energy milling process [113]. 28
Figure 3.2: Schematical presentation of the planetary mill and of the cylindrical milling vessel. (See Fig. 3.1) [114]. 29

Figure 3.3: The consequences of the high-energy collisions between milling balls and powder particles [114].....29
Figure 3.4: Schematically presented configuration of the SPS (left) and SPT (right) processing methods [96].....34

List of Tables

Table 3.1: The mill, the milling vial and balls parameters ... 33

Abbreviations

TE	. . . Thermoelectricity
TEG	. . . Thermoelectric generator
RTG	. . . Radioisotope thermoelectric generator
emf	. . . Electromotive force
PGEC	. . . Phonon-glass-electron crystal
SPS	. . . Spark plasma sintering
FAS	. . . Field-assisted sintering
PECS	. . . Pulsed electric current sintering
Ca349	. . . $Ca_3Co_4O_9$
SG	. . . Sol-gel
HT	. . . Thermal hydro-decomposition method
MC	. . . Mechano-chemical treatment
HP	. . . Hot-pressing
MA	. . . Magnetic alignment
CPP	. . . Cold high-pressure pressing
TGG	. . . Templated grain growth
SPT	. . . Free-edge SPS or Spark plasma texturing
CS	. . . Conventional, classic sintering
CP	. . . Cold pressing of sintered Ca349 pellet without post annealing
CP-920	. . . Free-edge cold pressing of sintered Ca349 pellet with post annealing
CM	. . . Combined method for TE measurements
XRD	. . . X-ray powder diffraction
SEM	. . . Scanning electron microscopy
EDXS	. . . energy-dispersive x-ray spectrometry
DTA	. . . Differential thermal analysis
TG	. . . Thermal-gravimetric analysis
MS	. . . Mass spectrometry

Abbreviations/sample labelling used in Chapter 4

Ca326	. . . $Ca_3Co_2O_6$
UT	. . . Coarse grained powder
AM	. . . Attrition milled powder
CS-920 sample	. . . Classical sintered *sample* at 920°C
SPT-920 sample	. . . SPT prepared *sample* using the already classically sintered pellet at 920°C

SPT sample	. SPT prepared *sample* using raw only compacted powder
HP sample	. *Sample* prepared with hot-pressing

CP sample	.	*Sample* prepared only with CP of the calcinated pellet
CP-920 sample	.	Free-edge CP *sample* with subsequent annealing at 920°C
AM-760_1 *sample*	.	AM *sample* single calcinated at 760°C
AM-760_2 *sample*	.	AM *sample* twice calcinated at 760°C
UT-760_1 *sample*	.	UT *sample* single calcinated at 760°C
AM-860_1*sample*	.	AM *sample* single calcinated at 860°C
UT-860_2 *sample*	.	UT *sample* twice calcinated at 860°C
IP	.	In-plane measurements
OP	.	Out-of-plane measurements

Abbreviations/sample labelling used in Chapter 5

B	.	Untreated powder mixture
MC10	.	MC treated powder mixture for 10h

Abbreviations/sample labelling used in Chapter 6

UT	.	Attrition milled powder mixture, which was not MC treated
MC1	.	MC treated batch (300 rpm, 23 balls)
MC2	.	MC treated batch (360 rpm, 23 balls)
MC3	.	MC treated batch (300 rpm, 16 balls)
MCx-y	.	y is the milling time in hours
MC2-15	.	MC2 powder mixture milled for 15h

MC-600-4h *sample*	.	MC *sample* annealed at 600°C for 4h
UT-600-4h *sample*	.	UT *sample* annealed at 600°C for 4h
MC-760-2h *sample*	.	MC *sample* annealed at 760°C for 2h
UT-760-2h *sample*	.	Ut *sample* annealed at 760°C for 2h
MC-760-4h *sample*	.	MC *sample* annealed at 760°C for 4h
UT-760-4h *sample*	.	UT *sample* annealed at 760°C for 4h
UT-760-12h *sample*	.	UT *sample* annealed at 760°C for 12h
OR	.	As-parched original powder mixture
MC-760-12 *sample*	.	MC *sample* annealed at 760°C for 12h
MC-920 *sample*	.	MC *sample* sintered at 920°C for 12h
UT-920 *sample*	.	UT *sample* sintered at 920°C for 12h

Abbreviations/sample labelling used in Chapter 7

RE^{3+}	.	Rare-earth element ions

Symbols

S	. . .	Seebeck coefficient, thermopower, electromotive force
zT	. . .	Dimensionless thermoelectric figure of merit
z	. . .	Thermoelectric figure of merit also TFM
σ	. . .	Electrical conductivity
κ	. . .	Thermal conductivity
V	. . .	Voltage
ΔV	. . .	Electrical potential difference
T	. . .	Temperature
ΔT	. . .	Temperature difference
$°C$	. . .	Degree Celsius
K	. . .	Degree Celvin
I	. . .	Electric current
Q	. . .	Heat generation or removal rate
Π	. . .	Peltier coefficient dependent of the material
q	. . .	Heat absorption or release rate
ţ	. . .	Thomson coefficient
η	. . .	Efficiency of a single TE material
Z_m	. . .	Single material TE performance
T_H	. . .	Temperature at the hot side
T_C	. . .	Temperature at the cold side
$\overline{T}$	. . .	Average Temperature
Z_D	. . .	Device TE performance
κ_e	. . .	Electronic thermal conductivity
h	. . .	Planck’s constant
k	. . .	Boltzmann’s constant
n	. . .	Carrier concentration
m^*	. . .	Effective mass
ρ	. . .	Electrical resistivity
μ	. . .	Carrier mobility
κ_l	. . .	Lattice thermal conductivity
L	. . .	Lorentz factor
E_b	. . .	Kinetic energy of the ball
m_b	. . .	Mass of the ball
V_b	. . .	Velocity of the ball inside the vial
E_s	. . .	The remained kinetic energy of the ball

V_s	. . .	Velocity of the ball in the moment towards the equilibrium state
ΔE_b	. . .	Kinetic energy transformed from the single ball to the powder particles

K_a . . Rate of elasticity

N_b . . Number of balls

φ_b . . Empirical factor

n_v . . Ratio between the number of finite and contained balls in the vial

$N_{b,V}$ . . Number of balls which can be contained in the vial

H_V . . Height of the vial

D_V . . Diameter of the vial

d_b . . Diameter of the balls

ΔE_b^* . . Kinetic energy transformed from the balls (finite number) to the powder particles or Ball impact energy

ϵ . . Calculated parameter

n_v . . Ratio between N_b and $N_{b,V}$

n_s . . Ratio between N_b and $N_{b,S}$

$N_{b,S}$ . . the number of balls needed to cover one third of the inner surface wall

α_b . . acceleration of balls

W_p . . the rotational speed of the supporting disk

W_V . . the rotational speed of the vial

R_p . . the distance between the rotational axes

R_V . . radius of the milling vial

D_V . . diameter of the milling vial

ρ_b . . density of the ball

v_1 . . ball-impact frequency

K . . empirical parameter

E_{cum} . . cumulative kinetic energy

t . . milling time

m_p . . powder mass

f . . Lotgering factor

P . . Ratio of the peak intensity in the given range

P_o . . Ratio of the peak intensity for a randomly oriented specimen (JCPDS cards, No. 21-0139)

α . . Thermal diffusivity

c_p . . Specific heat

Eb_{cr} . . Critical ball impact energy

$Ecum_{cr}$ . . Critical cumulative energy

Chapter 1

Introduction

In the 21st century the fast development, comfort demands, growing world population and mobility are tremendously increasing the world energy consumption, which is associated with the elevated use of fossil fuel and consequently global warming, respectively. To decrease the pollution and save the environment, green energies, such as the well-known photovoltaics, wind energy and biomass, have been developed to meet the increased energy demand associated with the process of civilization. But, as promising as they seem, unfortunately, still none of them can compete with the cost and convenience of fossil fuels. An alternative answer to the same question would be enhancing efficiency in the use of existing energy resources.

In most cases, poor efficiency occurs due to heat loss during energy transformation. Home heating, automotive exhaust, and industrial processes all generate huge amounts of unused heat, which represents almost up to 70% of all produced heat, and that could be converted to electricity. Consequently, a great deal of interest was devoted to the thermoelectric (TE) energy conversion, because of the ability to convert a temperature gradient into electrical energy (associated with the heating or cooling effect) and vice versa.

One way to improve the energy sustainability is through the scavenging of waste heat with thermoelectric generators (TEGs), with the help of the so-called "Seebeck effect". On the contrary, with the external electrical energy input, the phenomena called the "Peltier effect" can be used for creating the temperature gradient. The TE devices are unique solid-state devices, in which charge carriers serve as the working fluid, and in addition, they have no moving parts, they are silent, reliable and scalable. Their use is usually specialised in areas of science, where the cost is not the main consideration, like, medical, military and space applications. The Mars rover "Curiosity" is powered by a radioisotope thermoelectric generator (RTG) which converts the heat released by naturally decaying plutonium dioxide into electricity, some devices are used as a remote power for oil pipelines and sea buoys, and nevertheless also for achieving auxiliary power to improve the overall system efficiency, for instance in factories to recover industrial waste heat [1,2]. Thermoelectrics have long been too inefficient to be cost-effective in most applications [3]. In the mid-1990 some of the theoretical predictions suggested there is a possibility to enhance the TE efficiency through the nanostructural engineering [4]. Simultaneously, research of complex bulk materials (such as skutterudites [5], clathrates [5] and Zintl phases [6]) showed that high efficiency could indeed be obtained [7].

The performance of the TE material is given by the thermoelectric figure of merit (zT) of a material. To maximize it, a variety of conflicting properties needs be optimized in the

way the material has a large thermopower (absolute value of the Seebeck coefficient), high electrical conductivity, and low thermal conductivity. As these transport characteristics are interrelated, this can be a rather challenging task. As every story has a beginning, for thermoelectricity, it all starts with the fundamental thermoelectric effects discovered centuries ago.

In this chapter, the fundamental thermoelectric effects, application and efficiencies; electrical and thermal transport properties, and an overview of the current research progress will be introduced and discussed.

1.1 Thermoelectric Effects

The mechanism of the conversion between thermal energy and electrical energy is based on the thermoelectric effect, which includes three thermodynamically reversible effects, namely the Seebeck effect, Peltier effect and Thomson effect [8].

1.1.1 Seebeck effect

In 1821, T. J. Seebeck firstly discovered that electrical potential can be established at a junction of two dissimilar metals when the circuit was placed in temperature gradient [9]. He noticed a deflected needle if placed in the vicinity of a closed loop, formed from two dissimilar conductors, when one of the junctions was heated. He then concluded that interaction was a magnetic phenomenon (the thermomagnetic effect) [10]. The term "thermoelectricity" was introduced in 1823 by Ørsted, who redirected the conceptualization of those experiments: "Seebeck has discovered that one can establish an electric circuit in metals without the interposition of any liquid. One establishes the current in this circuit by disturbing the equilibrium of temperature." By the 1840s, it was tacitly assumed Seebeck discovered thermoelectricity [11], which is today known as the Seebeck effect, shown in Fig. 1.1.

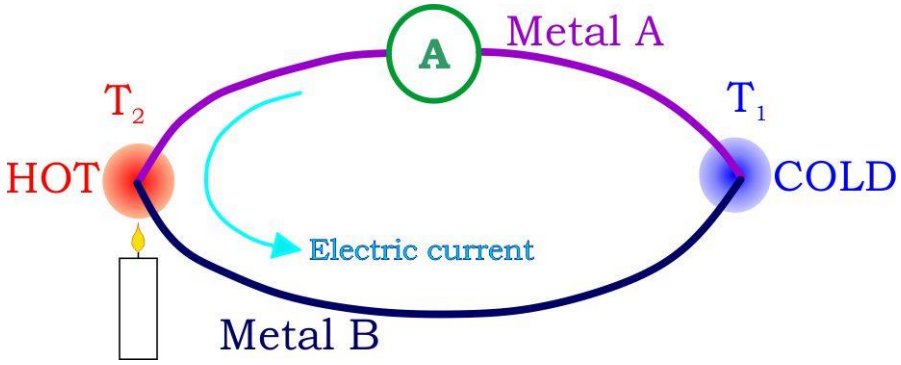


Figure 1.1: The schematic presentation of the Seebeck effect.

An electric current (electromotive force-emf) appears in every closed loop, where the junctions are at a different temperature. Therefore, when having a temperature difference at two junctions, consequently we also have an electrical potential difference (voltage, ΔV_{out}) at the two terminals, as illustrated in Fig. 1.2. The developed TE voltage in the given temperature difference (ΔT) is proportional to the temperature difference and the linear relation is given as

$$S_{AB} = \frac{\Delta V_{out}}{\Delta T}, \quad (1.1)$$

where the S_{AB} is the proportionality constant between two materials *A* and *B* in the circuit and is called the "relative Seebeck coefficient". It is expressed in units of V/K or V/°C (commonly μV/K or μV/°C).

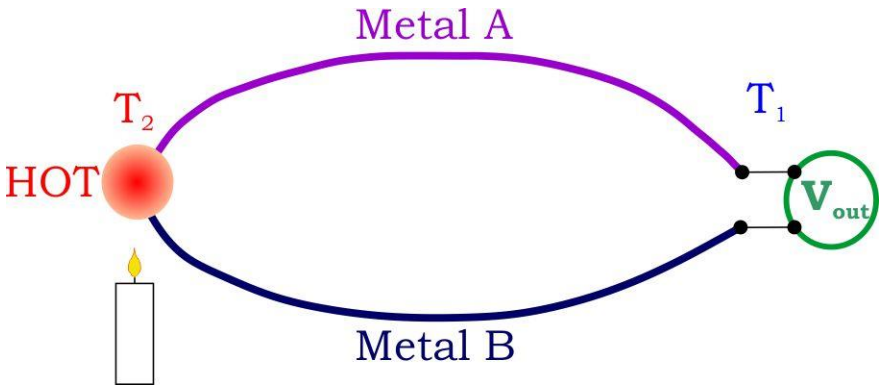


Figure 1.2: The schematic presentation of the Seebeck effect in an open circuit.

As already described above, the same will happen also when having a single material as depicted in Fig. 1.3. In the case when the temperature difference (ΔT) between the two ends of the same material is small, the Seebeck coefficient of this material is given by

$$S = -\frac{\Delta V}{\Delta T} \quad (1.2)$$

where the ΔV is the TE voltage between the two ends of the same material.

At this point the Eq. 1.1 can be rewritten with Eq. 1.2 as

$$S_{AB} = S_B - S_A = \frac{\Delta V_A}{\Delta T} - \frac{\Delta V_B}{\Delta T} \quad (1.3)$$

where the S_A and S_B are the absolute Seebeck coefficients of the material *A* and *B*, whose intrinsic properties depend on the nature of both materials [8].

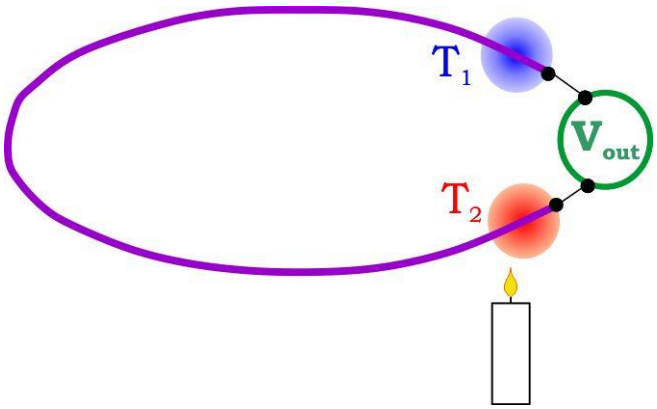


Figure 1.3: The Seebeck effect schematic presentation in the single material.

By convention α is the symbol for the Seebeck coefficient, but the Seebeck coefficient is often referred to as the thermal emf or thermopower. In the following text, S will be used, which is also very common. The sign of S is positive, if the emf causes a current flow in a clockwise direction around the circuit, meaning it is generally governed by the positive charge carriers (holes). In that case we talk about the positive p-type semiconductor or conductor, if the main charge carriers are electrons, we have the n-type semiconductor or conductor [12].

1.1.2 Peltier effect

A complementary effect was discovered by Peltier [22], approximately 12 years later, who observed that in the vicinity of the junction between dissimilar conductors with passing current a temperature change emerges. However, he was not aware of the importance of his discovery. The true nature of the Peltier effect was explained by Lenz [13] in 1838, who resolved that heat absorption or generation at the junction between two conductors deepens upon the direction of the current flow [10]. In a closed loop formed with two dissimilar conductors and applied electric current, heat may be generated at one junction but removed at another as shown in the schematic of Fig. 1.4. The heat generated or removed at the junction is proportional to the electric current (I) and the relation can be given as

$$Q = (\Pi_A - \Pi_B) \cdot I \tag{1.4}$$

where Q is the heat generation or removal rate and Π_A and Π_B are the material dependent Peltier coefficients of the materials A and B [8].

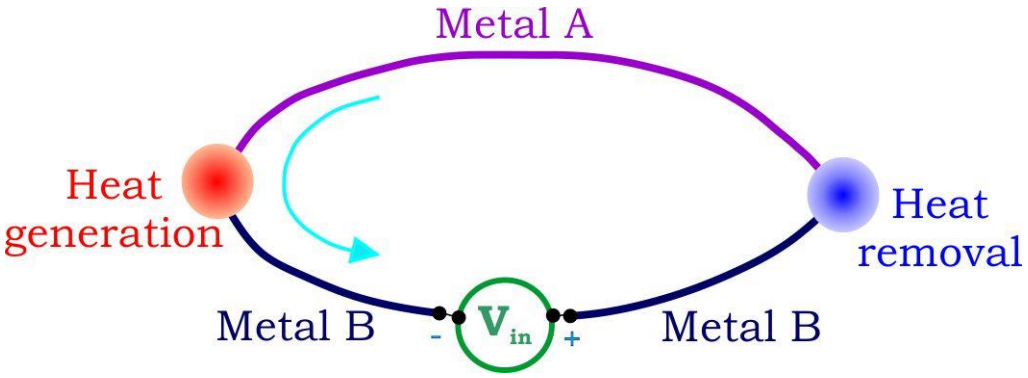


Figure 1.4: The schematic presentation of the Peltier effect.

1.1.3 Thomson effect

In 1851 the Seebeck and Peltier coefficients were correlated by W. Thomson (Lord Kelvin)[14], who, in addition, predicted also the existence of the third thermoelectric effect, the Thomson effect. This effect is an evolution or absorption of heat when electric current passes through a circuit composed of a single material that has a temperature difference along its length.

The absorbed or released heat can be calculated as

$$q = \text{ţ} \cdot I \cdot \nabla T \tag{1.5}$$

where q is the heat absorption or release rate, ţ is the Thomson coefficient, (I) is the electric current and (∇T) is the temperature gradient. When we have a positive temperature gradient (current flowing towards the hot side), the material absorbs heat and the Thomson coefficient is positive, as illustrated in Fig. 1.5 [8].

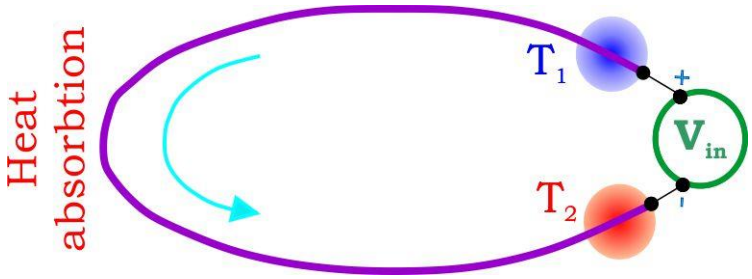


Figure 1.5: The schematic presentation of the Thomson effect.

1.2 Applications of the Thermoelectric Effect

Today the TE technology is revolving around modern-day thermocouples and their application in power generation and refrigeration.

Conventional metallic thermocouples, as shown in Fig.1.6 (a), are made from metal or metal alloys. When their junction is located in a hot or cold environment compared to the ambient, they generate small voltages and small amounts of electrical power when connected to a resistive load with the help of the Seebeck effect. Most common applications are in sensors to operate control systems (air conditioning equipment, refrigerators, central heating units) or in measurements of temperature. The thermocouples can operate also the other way around as a heat pump with the help of the Peltier effect [12].

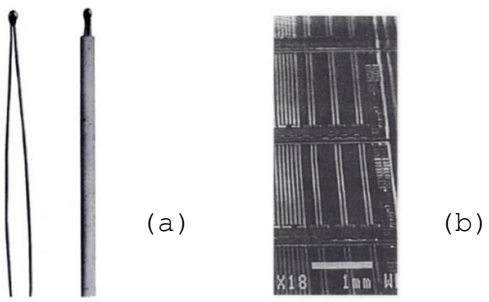


Figure 1.6: (a) Conventional thermocouple from metal or alloy; (b) micro thermocouples on the substrate [12].

Another branch of thermocouples are those made from modern semiconductors. As shown in the scheme in Fig.1.7 a TE generator or cooler consists of n- and p-type semiconductors which are electrically connected in series and thermally in parallel. When a temperature gradient is applied to a material, the mobile charge carriers at the hot-end tend to diffuse to the cold end, consequently the electrical potential is formed, because of the Seebeck effect.

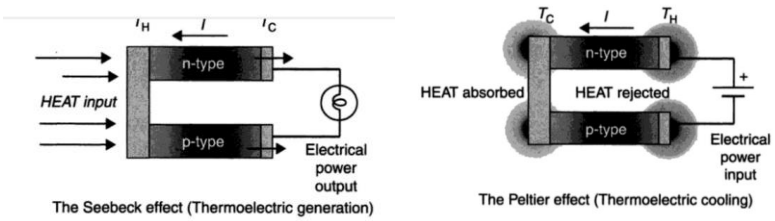


Figure 1.7: Schematic presentation of the thermoelectric generator (left) and thermoelectric refrigerator (right) [12].

Recently, thin film structures made it to the forefront because of increased use in sensor applications. Usually, the thermocouples here are micrometre wide and laid down by a variety of techniques onto the supporting electrically insulating thin film substrate, as shown in Fig. 1.6 (b) [12].

Generated voltages of semiconductor thermocouples are still modest, hundreds of microvolts per degree, so in practice a large number of thermocouples are needed to form a useful module, as shown in Fig. 1.8. The TE module construction does not differ much despite two different applications. Ideally the geometry of the thermoelements should be wire-like (long and thin) for generation of electricity and squat (short and fat) for refrigeration [12].

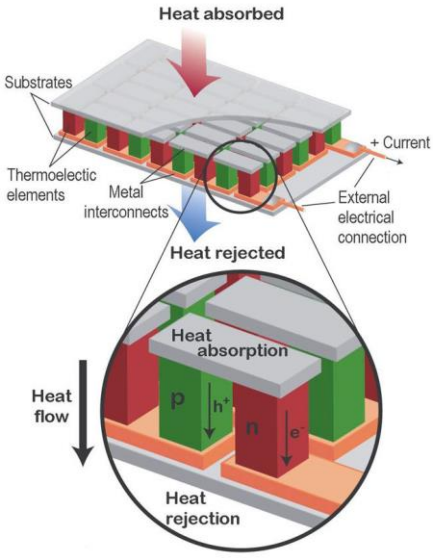


Figure 1.8: The scheme of the TE module made from p-n couples wired electrically in series and thermally in parallel [7].

1.2.1 Efficiency and the thermoelectric figure of merit

The engineers have been in search of efficient and economically viable thermoelectric generators (TEGs) since the 19th century. The relationship between physical properties of TE materials and the efficiency of a simplified thermopile or TEG was in 1909 mathematically expressed by Edmund Altenkirch. The Altenkirch's parameters and variables (emf, thermal and electrical conductivity) were later used by the famous Russian scientist, Abram F. Ioffe who integrated them into the Z group (quantity Z or parameter Z) to calculate the efficiency of thermoelectric devices [15].

The Ioffe's parameter Z is given by the formula [16]

$$Z = \frac{S^2\sigma}{\kappa} \tag{1.6}$$

where:
Z – complex characteristic of the TE material pair properties, [1/K];
S – electromotive force of the thermoelectric device;
σ – electric conductivity of the TE material pair;
κ – thermal conductivity of the TE material pair.

According to Ioffe, Z is the most important indicator of thermoelements [13]. This parameter was introduced to calculate the efficiency of devices having the following features [16]:

- device arms are formed by a pair of materials A and B of the p/n type;
- electromotive force of each of materials A and B is the same;
- thermal and electric contact of materials A and B is ideal;
- difference in temperatures between the hot junction and the cold junction of the device is very small;
- physico-chemical properties of materials A and B do not vary with time.

It is very important to emphasize that the Ioffe's "ideal thermoelectric device" is equivalent to a pair of materials A and B being in perfect contact with each other [15, Polozine, 2014, pp.1261].

When taking this into consideration the performance of TE material pairs can also be evaluated with the parameter Z.

In the last sixty years the Z parameter has been well accepted. It is called the "Thermoelectric Figure of Merit" [17,18,19] or TFM, and it serves as a much needed tool for evaluation and comparisons of the TE performance worldwide. Because the material properties (S, σ and κ) are temperature dependent, the performance in the scientific papers is often expressed as the product of Z by temperature T. This product is a zT, a dimensionless quantity of the TE materials performance. Usually the product zT coincides with the maximum performance of the material and so far the highest obtained value has not exceeded 2.4. [20] according to the latest reports [15].

1.2.1.1 "Efficiency" of a single thermoelectric material

The maximum "efficiency" η of a single TE material is defined by the equation [12]:

$$\eta = \frac{\sqrt{1+Z_m\overline{T}}-1}{\sqrt{1+Z_m\overline{T}}+\frac{T_C}{T_H}} \cdot \frac{T_H-T_C}{T_H} \quad (1.7)$$

where:
T_H – temperature of the TE material pair hot side;
T_C – temperature of the TE material pair cold side;

$$\overline{T} = \frac{T_H+T_C}{2} \quad (1.8)$$

Regarding that nowadays η of modern TE materials is from 5 to 15 %, the search for new materials goes on, as there are physical predictions this is possible [21]. When considering the progress and evolving knowledge on the TE materials, the efficiency could reach 21 % in the next decade [15].

However, when talking about TE devices the efficiencies of modern heat engines for electric power generation based on the TE material are much smaller, in the range of 2 to 8 % (different reference sources), typically around 5% [22]. Here the efficiency for a power generation does not depend only on materials zT anymore, but also on other device factors [15]. As already mentioned zT properties are T dependent and in addition divergent for both (p- and n-type) materials in a device. If these properties are assumed to be temperature independent within an arm, and that the contact resistance at the hot and cold junctions is negligible, Z_D (D; label for device) equates the Z_m of material in Eq. 1.7 [12]. In that case the maximum efficiency of the device, namely of the TE module is given in Eq. 1.9

$$\eta = \frac{\sqrt{1+Z_D\overline{T}}-1}{\sqrt{1+Z_D\overline{T}}+\frac{T_C}{T_H}} \cdot \frac{T_H-T_C}{T_H} \quad (1.9)$$

A thermoelectric converter is a heat engine and like all heat engines it obeys the law of thermodynamics, consequently the efficiency limit of a TE power generation corresponds to the Carnot efficiency (the second term in Equations 1.7 and 1.9 [12].

As seen in Fig. 1.9 large temperature differences in the thermocouple from thermoelectric materials are desirable as they enable an increase in the available heat for conversion as dictated by the Carnot efficiency. For instance, the thermocouple with an average figure of merit of 3 x 10^{-3}/K would have to operate over a temperature difference of 500 K to have an efficiency of 20% [12].

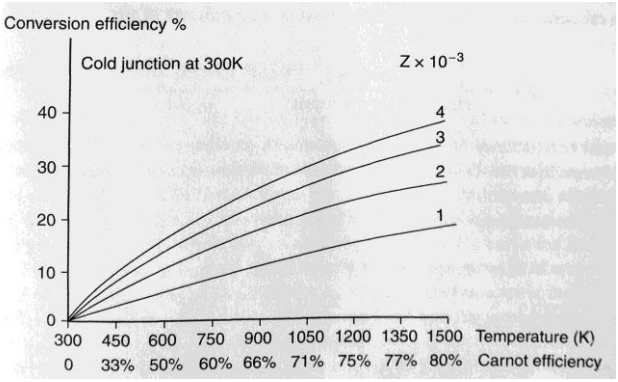


Figure 1.9: Demonstration of TE efficiency as a function of temperature and thermocouple material figure of merit [12].

1.3 Electrical and Thermal Transport Properties

A good and efficient TE material should possess high electrical conductivity (σ) to maximize the output current through minimizing the internal resistance, high Seebeck coefficient (S) in order to maximize the thermoelectric voltage for a given temperature gradient, and low thermal conductivity (κ) in order to maintain the temperature gradient. However, those three properties are correlated and improving one of them may often lead to an offset from another, constraining the enhancement in zT.

1.3.1 Carrier concentration

All three parameters (σ, S and κ) used for classification of zT are functions of the carrier concentrations. It is clear that electrical conductivity and Seebeck coefficient are related inversely, and that electronic contribution to the thermal conductivity κ_e is generally around 1/3 of the total thermal conductivity, also increasing with the carrier concentration [12].

For a high S coefficient there should only be a single type of carriers, as mixed p- and n-type conduction will cancel out the induced Seebeck voltages. Low carrier concentration usually means high Seebeck coefficient (see Equation 1.10), however also low electrical conductivity (see Equation 1.11). For metals or degenerate semiconductors (parabolic band, energy-independent scattering approximation [23]) the Seebeck coefficient is given by:

$$S = \frac{8\pi^2 k_B^2}{3eh^2} m^* T \left(\frac{\pi}{3n}\right)^{2/3} \tag{1.10}$$

where h is the Planck's constant, k is the Boltzmann's constant, n is the carrier concentration and m^* is the effective mass of the carrier.

The electrical conductivity (σ) and electrical resistivity (ρ) are related to n through the carrier mobility μ:

$$\frac{1}{\rho} = \sigma = ne\mu \tag{1.11}$$

As seen from Figure 1.10 the maximum peak of figure of merit typically occurs somewhere between 10^{19} and 10^{21} carriers per cm^3 (depending on the material system), which tells us a compromise

between large S, high electrical conductivity and low thermal conductivity should be made. Such carrier concentrations are usually found between common metals and semiconductors, that is in heavily doped semiconductors, respectively [7].

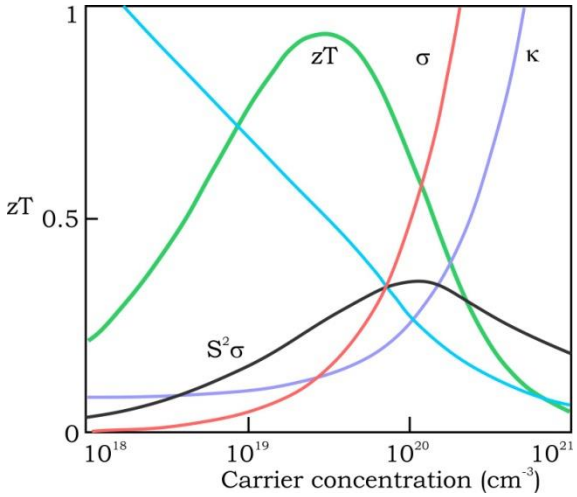


Figure 1.10: Presentation of maximised zT, which is comprised of compromised thermal conductivity (κ) and Seebeck coefficient (S) with electrical conductivity (σ) [7].

1.3.2 Effective mass

Here we have another conflict between thermopower and electrical conductivity. As seen from Equation 1.11 the electrical conductivity is related to carrier concentration through the carrier mobility. The mobility is related with the effective mass of the carriers. If the carriers are heavy with larger effective mass, they will move with slower velocities, and therefore small mobilities, which will in turn result in low electrical conductivity. On the contrary large effective masses produce high thermopower, as seen from Equation 1.10. Consequently, a compromise must be made between high effective mass and high mobility, which is a rather complex task, as their relationship depends on the electronic structure, scattering mechanisms and anisotropy. According to C.M. Bhandary and M. Rowe [24] decoupling of those two properties should be possible in anisotropic crystal structures. Materials where the elements have small electronegativity differences have usually high mobility and low effective masses. The opposite can usually be found in ionic structures with narrow bands. There is no recipe yet which effective mass is optimum, as good TE material can be found in a variety of conductors and semiconductors, from low mobility, high-effective-mass oxides [25] and chalcogenides [26] to high-mobility, low-effective-mass SiGe and GaAs [7].

1.3.3 Thermal conductivity

1.3.3.1 Electronic thermal conductivity

For maximum possible zT we need low total thermal conductivity. Total thermal conductivity comprises two sources of heat transport. The first one comes from electrons and holes transporting heat (κ_e), and the second one from phonons travelling through the lattice (κ_l), as given by the equation:

$$\mathfrak{k} = \mathfrak{k}_e + \mathfrak{k}_l \tag{1.12}$$

Most of the electronic term (κ_e) is directly related to the electrical conductivity through the Wiedermann–Franz law:

$$\mathfrak{k}_e = L\sigma T = ne\mu LT \tag{1.13}$$

where L is the Lorentz factor, 2.4 x $10^{-8}J^2K^{-2}C^{-2}$ for free electrons. The L can slightly change, particularly with carrier concentration, and especially in low-carrier-concentration materials where it can be reduced by as much as 20% from the free-electron value [7].

1.3.3.2 Lattice thermal conductivity

Lattice thermal conductivity is related to lattice vibrations and hence thermal conductivity by phonons. The lowest lattice thermal conductivities can be found in glasses, although in general they are not good TE materials. According to Slack [27], the thermal conductivity in glass is a random walk of energy through a lattice which leads to the concept of a minimum thermal conductivity κ_{min}. Main heat carriers are phonons with widely varying wavelengths and mean free paths [28] (from less than 1 nm to greater than 10 μm) creating a need for phonon scattering agents at a variety of length scales [7].

1.3.4 Phonon-Glass-Electron-Crystal or PGEC

Thermoelectrics require a rather unusual material for good performance, the so-called PGEC material. Meaning the materials have lattice thermal conductivities similar to amorphous materials (phonon mean free paths are as short as possible) but have an electronic structure that can be described as for crystalline solids (the electron mean free paths are as long as possible), which can maintain high electrical conductivity [29].

1.4 Thermoelectric Materials

Lately much has been done in the field of TE materials regarding the development of new approaches as well as enhancing the TE performance. Summarised reported zT values per publishing years with labelling of various approaches used are shown in Fig. 1.11 [30]. When considering that TE materials have been developed since the discovery of the thermoelectricity, the progress can be divided into three generations according to zT values [31]. The first generation are the thermoelectrics with average zT of around 1, and devices from them with 4-6% efficiency, depicted in the left purple part of Fig. 1.11. The second generation almost doubled the zT reaching 1.3-1.7 at high temperatures. This was achieved by introduction of nanostructures and compositional in-homogeneities [32]. The expected efficiencies here are 11%-15%, as shown in the middle blue part of Fig. 1.11. The third generation exhibits the highest zT, reaching 1.8 [33] and higher [34] and is still under development. The predicted device conversion efficiencies increase to around 15-20% as shown in the right yellow part of Fig. 1.11. However, in recent years not only a high zT is important anymore, but the development is moving towards low-cost and earth-abundant elements [30].

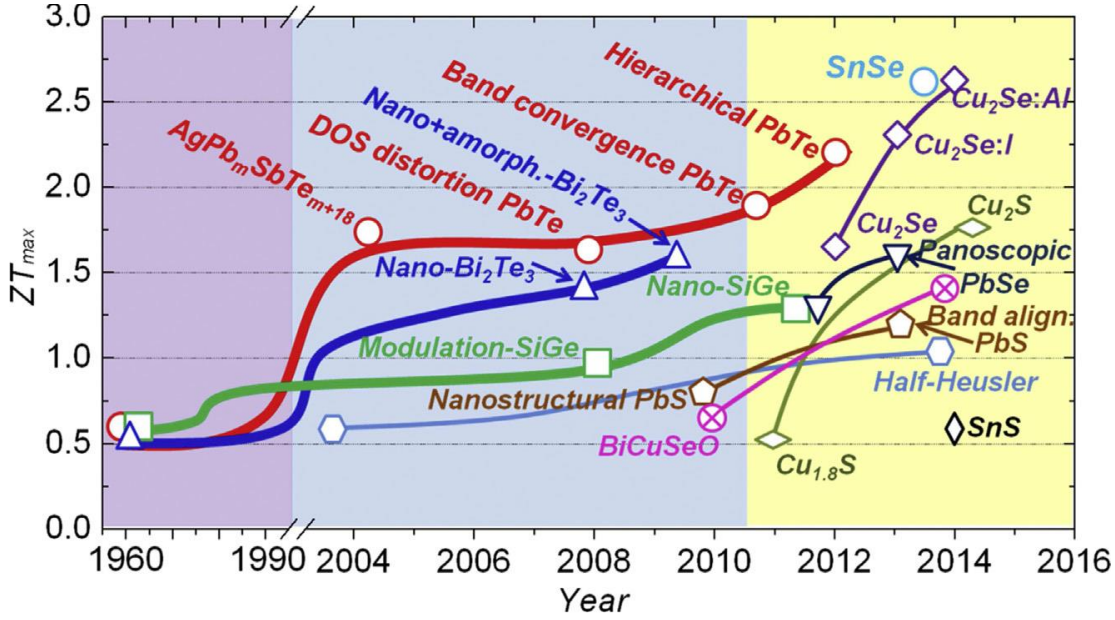


Figure 1.11: Graphical presentation of time development of the bulk TE materials with new concepts and technologies for achieving higher zT values [30].

From Fig. 1.11 it can be seen that the highest efficiencies are achieved by using new concepts and technologies which can control the transport of phonons and electrons, for instance producing super lattice structures; or with introducing all-scale hierarchical architectures, which allow effective phonon scattering on all relevant length scales, from atomic-scale lattice disorder and nanoscale endotaxial precipitates to mesoscale grain boundaries. With these methods zT of 2.2 -2.4 [20,34] were achieved. The highest zT of 2.6 ± 0.3 at 650 °C to our knowledge was reported by Zhao et al. [35]. They attribute this remarkably high zT to the intrinsically ultralow lattice thermal conductivity along the b axis, which is the consequence of enormously high Grüneisen parameters, which reflect the anharmonic and anisotropic bonding.

In addition to the efficiency division of TE materials, they can be divided also according to the working temperature on three regions as shown in Fig. 1.12 [7,36]: Bi_2Te_3- based low-, PbTe-based middle- and SiGe-based high-temperature ranges, with typical temperatures varying from <400 K, 600 K-900 K and >900 K, respectively.

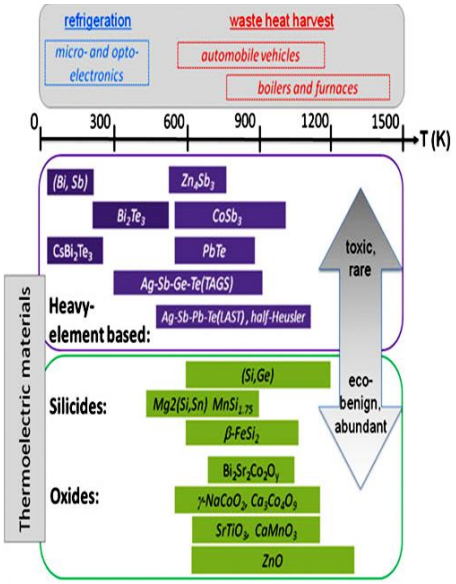


Figure 1.12: Presentation of the TE materials according to the working temperature, environment impact and abundancy [36].

Although the above-mentioned materials remain the cornerstone of commercial applications, they have several drawbacks. For instance Pb, Bi and Te are environmentally hazardous, which restricts them from several applications. Some of the alloys are also prone to oxidation or sublimation when operating in air at high temperatures. Moreover, employing these heavy metals should be avoided, as they are usually toxic, low in abundance as natural resources, and are not environmentally friendly. For this reason the oxide TE materials have been considered as good potential candidates as they are more suitable for high temperature applications because of their structural and chemical stabilities, oxidation resistance, consisting of earth abundant elements and low cost.

1.4.1 Oxide thermoelectrics

Oxide materials are important in a wide range of technological applications including electronics, magnetic devices, sensors, fuel cells, refractories, thermal barrier coatings, optical devices, biomaterials and many more. Despite their benefits, they were initially overlooked as possible TE materials, as they were in general depicted more as insulators [37]. However, there are some drawbacks likely to occur, like exfoliation of metal electrodes because of the different expansionary coefficients of the metal and ceramics, and the possibility of high contact resistance.

The situation about oxide TE changed, when in 1997 Terasaki et al. [38] found that Na_xCoO_2 crystals exhibited metallic electrical resistivity (200 $\mu\Omega$cm) and, shockingly, had the large value for thermopower (S) of 100 μV/K. This may result in zT of 1, considering the relatively high thermal conductivity ($\kappa \approx$ 4 W/mK to 5 W/mK) of Na_xCoO_2 [37]. This discovery lit a fire in researcher's minds to explore high efficiency oxide materials. In this chapter, several representative oxide TE materials are introduced and discussed.

1.4.1.1 Wide-Bandgap Semiconductor Oxides

Wide-bandgap semiconductors, also known as transparent (bandgap 1.5 eV to 3.5 eV) conducting oxides (TCO), such as ZnO (3.37 eV) [39,40], SnO_2 (3.6 eV) [41,42], and In_2O_3 (3.6 eV) [43] are well-known n-type oxide thermoelectric materials. Because of the broad s-p band and large electron mobility they have large power factors of 10^{-3} W/mK^2 to 10^{-4} W/mK^2. Overall they exhibit rather low figures of merit, mostly due to very high thermal conductivity ($\kappa \approx 5$ W/mK to 10 W/mK). However, there are some reports increasing the optimism. Ohtaki et al. [44] reported a nanocomposite of Al/Ga co-doped ZnO ($Zn_{0.96}Al_{0.02}Ga_{0.02}O$) with $zT \approx 0.65$ at 1273 K (Fig.1-16), further, Berardan et al. [43] reported the zT of 0.45 at 1273 K for the composition $In_{1.8}Ge_{0.2}O_3$ (Fig 1.15), where the addition of Ge to In_2O_3 causes precipitation of fine particles of $In_2Ge_2O_7$ impurity phase, which results in lower κ. Finally, Koumoto and co-workers [45] investigated $(ZnO)_mIn_2O_3$ compounds with a layered structure and observed that the figure of merit increased with increasing the number of ZnO layers [37].

1.4.1.2 Layered Oxychalcogenides

BiCuSeO is a promising p-type TE material composed by alternatively stacking the insulating oxide $(Bi_2O_2)^{2+}$ layer acting as a charge reservoir and the conductive selenide $(CuSe_2)^{2+}$ layer constituting conduction pathways, as shown in Fig. 1.13. Pristine BiCuSeO exhibits low thermal and electrical conductivity. But it was recently reported by Zhao [46] that BiCuSeO based compounds showed excellent charge transport behaviour due to hole introduction by replacing Bi^{3+} with Sr^{2+}, resulting in a high zT of 0.76 [47]. Good results were achieved also in the highly textured $Bi_{0.875}Ba_{0.125}CuSeO$, where after three hot-forging steps a two-fold increase in carrier mobility was achieved, resulting in zT of 1.4 650 °C [48]. Another way to improve efficiency of this compound is with grain refinement (200-400nm) [49].

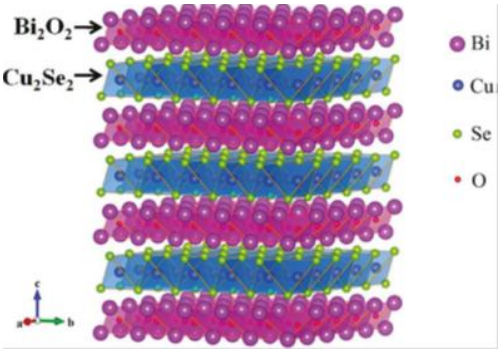


Figure 1.13: BiCuSeO crystal structure [47].

1.4.1.3 Perovskite-type oxide materials

Perovskite-type oxides are represented by the general formula ABO_3, where A is typically a rare-earth, alkaline-earth or alkali cation and B is the 3d, 4d, or 5d transition metal. As seen from Fig. 1.14 the *A* cation is located in the centre of eight corner-shared $[BO_6]^{8-}$ octahedra. This group shows good thermoelectric properties at high temperatures on doping at A and B cationic sites [37]. The two most representative systems are $SrTiO_3$ and $CaMnO_3$.

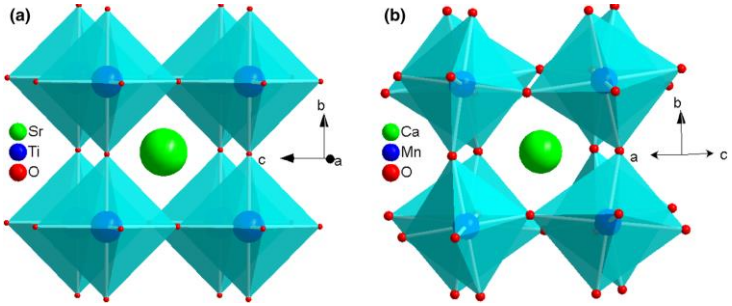


Figure 1.14: (a) Schematic crystal structure of ideal perovskite oxide $SrTiO_3$ (Pm-3m) and (b) crystal structure of distorted perovskite $CaMnO_3$ (Pnma) [37].

$SrTiO_3$ and layered titanate phases exhibit good TE properties due to their excellent electronic transport and stability at high temperatures, and are good potential n-type TE materials. According to the literature, the best results were obtained by doping [50,51] and by using combustion synthesis and SPS [52]. Polycrystalline $SrTiO_3$:Nb showed the highest figure of merit of 0.37 at 1000 K [50], whereas a thin film of $SrTiO_3/SrTiO_3$:Nb superlattice was reported to exhibit the largest estimated zT of 2.4 at room temperature [51]. Furthermore, with doping $SrTiO_3$ can form a superlattice Ruddlesden-Popper structure, expressed as $SrO(SrTiO_3)_n$ or $Sr_{n+1}TinO_{3n+1}$. This superlattice structure is very similar to the one found in the layered cobaltates, as is composed of perovskite-type $(SrTiO_3)_n$ block layers and rock salt SrO layers stacking along the c-axis [50,53,8]. Titanate phases, however, also have a few drawbacks, they exhibit high thermal conductivity ($\kappa_{300K} \approx 10$ W/mK), due to the dominant contribution from the lattice thermal conductivity, which is indicating on Umklapp-type phonon-phonon interaction. Another disadvantage is the oxidation of Ti^{3+} to Ti^{4+} under air at high temperatures, leading to instability of the phases [37].

Other promising oxides in this class are $CaMnO_3$ and $LaMnO_3$, which possess a larger Seebeck coefficient (800 μV/K and 450 μV/K, respectively, at 300 K) [53] and lower thermal conductivity. In both systems p- or n-type conduction can be established, depending on aliovalent substitutions on either the A- or B-site [37]. The performance can be improved either by doping on both sites or by synthesis methods, which predominantly generate a smaller grain size [54,55]. The highest figures of merit reported among the $CaMnO_3$ compositions are Yb-doped $CaMnO_3$ with zT = 0.2 [56] at 1000 K, the Dy-doped $CaMnO_3$ with zT = 0.2 at 1273 K [53], and the Nb-doped $CaMnO_3$ with zT > 0.3 at 1073 K [57].

1.4.1.4 Layered Cobalt-based oxide materials

Cobalt-oxide-based layered structured crystals including Na_xCoO_2, $Ca_3Co_4O_9$, and their derivative compounds have been developed as p-type materials having rather high TE performance. This group of compounds has to date reached unity or larger for the maximum zT [58].

1.4.1.4.1 Na_xCoO Na_xCoO_2 has a hexagonal layered structure where the CdI_2-type CoO_2 layer and charge-balancing Na^+ ions are alternatively stacked along the c-axis. The CoO_2 layer is rhombohedrally distorted with edge-sharing CoO_6 octahedra stacked in alternating fashion (…ABC CBA…). In this way two different types of trigonal prismatic sites are yielded, and they are partially occupied by Na^+ ions (Fig. 1.15a). In such layered

structure electrons and phonons have different paths, thus this could be a prototype of the "nanoblock integration'' and Na_xCoO_2 crystal structure can be regarded as a prototype phonon-glass-electronic crystal [59]. The ordered CoO_2 layers serve as electronic transport layers, while the disordered Na^+ blocks serve as phonon-scattering regions to give low thermal conductivity. According to Koshibae et al. and Wanf et al. [60,61] the CdI_2-type CoO_2 blocks in layered cobalt oxides favour the low-spin state of Co^{3+} and Co^{4+}, which results in large thermopower at high temperatures. Despite good TE properties in Na_xCoO_2 single crystal, those are worse in the polycrystalline Na_xCoO_2 ceramics achieving zT value of 0.8 [62]. Besides, Na_xCoO_2 ceramics application as a high-temperature thermoelectric oxide is limited due to its hygroscopicity in air, and the volatility of sodium above 800 °C [37].

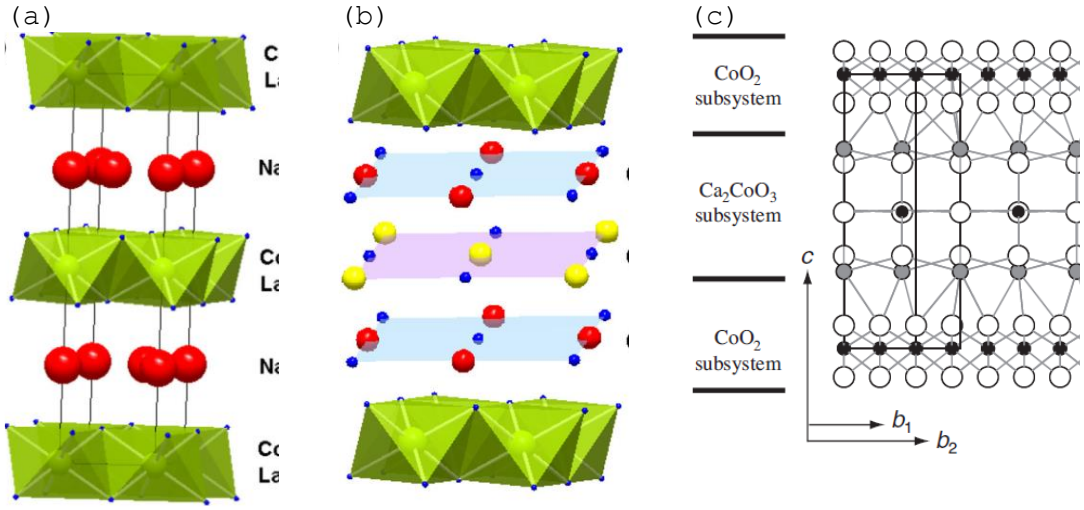


Figure 1.15: Schematic crystal structures of layered cobalt oxides (a) Na_xCoO_2, (b) $Ca_3Co_4O_9$, and (c) $Ca_3Co_4O_9$ structure model projected parallel to a-axis [37,63].

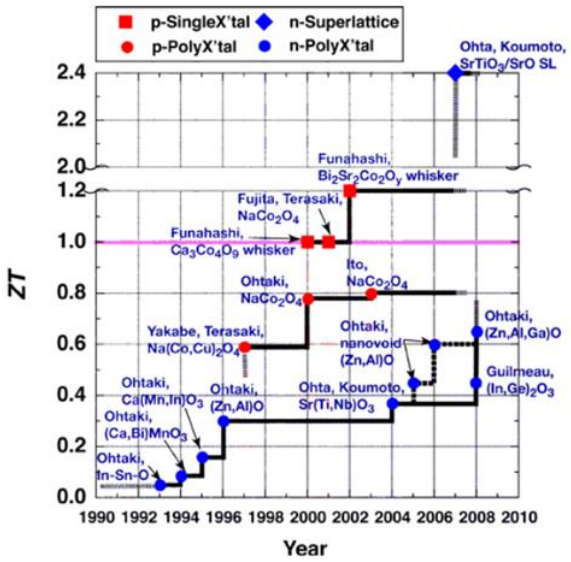


Figure 1.16: The development of the oxide TE materials through time [61].

1.4.1.4.2 Ca-Co-O system

1.4.1.4.2.1 $Ca_3Co_4O_9$ crystal structure The crystal group of misfit layered cobalt oxide was identified by Leligny et al. [64], who successfully performed the structure analysis of the electrically conductive modulated layered cobalt oxide $Bi_2M_3Co_2O_y$ with M=Sr, Ca and Ba [65], which was synthesised in relation to the superconductor Bi2201 [59]. A series of thallium and bismuth cobaltates, $Tl□[(Sr,Ca)_{1-□}O]_{1+x}CoO_2$, $Bi□[A_{0.75}Bi_{0.25}O]_{(3+3x)/2}CoO_2$ (A = Ca, Sr), and $[Bi_{0.87}SrO_2]_2[CoO_2]_{1.82}$ were then produced, which represents the first oxides with a misfit-layered structure [37].

Approximately 16 years ago, Miyazaki et al. [66,67] succeeded to synthesise misfit layer cobalt oxides $[Ca_2CoO_{3.34}]_{0.62}[CoO_2]$ and $[Ca_2(Co_{0.65}Cu_{0.35})_2O_4]_{0.63}[CoO_2]$ by the solid state reaction at 920 °C. The synthesis took about 20 hours in an oxygen gas flow and it was repeated three times to obtain a homogenous sample. However, this was not the first successful synthesis of the Ca349 compound, the synthesis of the $Ca_3Co_4O_9$ was conducted before requiring even longer times [68]. Due to a still not fully defined structure, the $[Ca_2CoO_3]_{0.62}[CoO_2]$ compound was/is expressed as $Ca_9Co_{12}O_{28}$ [69], $Ca_2Co_2O_5$ [58], $Ca_3Co_4O_9$ and so on. These inconsistencies are the consequence of an incommensurate structure, which is difficult to describe with rational chemical formulas, besides these cobalt oxides change their composition by the possible substitution and/or their nonstoichiometry [67].

First descriptions of the Ca349 crystal structures were reported independently by Masset et al. [70] and Miyazaki et al. [66]. Masset et al. described the structure as $[Co_{10}^{3+}Co_{16}^{4+}O_{52}][Ca_{32}^{2+}Co_{16}^{2+}O_{43}]$ but Miyazaki et al. reported it as $[Ca_2CoO_{3.34}]_{0.614}[CoO_2]$. Both groups succeeded in identifying that crystal consists of CdI_2-type CoO_2 layer and interleaving the Ca-Co-O rock-salt layer [59].

Both sub-layers, a CdI_2-type hexagonal CoO_2 subsystem and a rock salt-type Ca_2CoO_3 subsystem, are stacked alternatively along the c-axis. Both subsystems share a common a- and c-axis and angle, but have different and incommensurate *b* parameters (see Fig. 1.15 b and c).The resulting structural formula can thus be described as $[Ca_2CoO_3][CoO_2]_{(b1/b2)}$, where $b1/b2 \sim 1.62$. The b1 parameter belongs to the rock salt and b2 to the CoO_2 subsystem, respectively [67,70]. Such a layered structure and the discordance between the sublattices of these two types of layers makes it such that this kind of composite crystals is expected to exhibit strong anisotropy, which reflects itself in the plate-like grain morphology, and in transport properties, respectively. There were a few studies confirming the two-dimensional nature of the transport properties in the Ca349 crystals (S of 240 μV/K, σ of 434 S/cm, both determined in the a-b planes, out-of-plane κ 3 W/mK) [70,71]. It was shown that Ca349 conductivity is governed by the in-plane conductivity, which coincides with the a-b planes of the Ca349 crystal/compound. In-plane conduction is usually much larger than the out-of-plane conduction, whose direction coincides with the c-axis.

What is interesting in this structure is also that among the different layered cobaltate systems, the $Ca_3Co_4O_9$ stands out as the system containing one cation with nominally different oxidation states, namely Co^{2+} in the rocksalt buffer layers (Ca_2CoO_3) and Co^{4+} and Co^{3+} in the octahedral CoO_2 layers [70]. The compound has also two crystalographically distinct Co ion sites see Fig. 1.15), where each of them plays a different role. To

preserve the overall charge neutrality of both sub-layers, the holes from positively charged CoO layer in the rock-salt system are transferred to the CoO_2 negatively charged layer. This results in increased mobile hole concentration, which is essential for breaking the electron-hole symmetry of the half-filled Co-band in the CoO_2 layers, and thus enabling the high thermoelectric power in the strongly correlated CoO_2 subsystem, and making the Ca349 compound p-type TE oxide. From this one can conclude that the CoO_2 sheets are responsible for the conduction and the rock-salt layers can be regarded as a charge reservoir, which introduces hole carriers into the CoO_2 conduction sheets [66,72,73,74]. Moreover, Satake et al. [75] showed that the rock-salt layer controls the lattice thermal conductivity due to phonon scattering; i.e., the in-plane thermal conductivity reduces by increasing the number of rock-salt layers, while leaving the electronic properties of the CoO_2 blocks unperturbed.

Such crystal nature therefore requires observance of all aforementioned features, especially when characterizing the TE properties for which we know they strongly depend on the microstructure, i.e. density, size and morphology of the grains and texturing. All these properties will be thoroughly discussed in the next few chapters.

Considering that quite some time has passed from the first Ca349 synthesis, in the next few paragraphs the main findings and attempts to improve the TE figure of merit, either by synthesis, texturing or doping, will be presented, respectively.

1.4.1.4.2.2Synthesis of the $Ca_3Co_4O_9$ compound and the microstructure

According to the phase diagram two phases are present in the system CaO and CoO, the $Ca_3Co_2O_6$ (Ca326) phase and the $Ca_3Co_4O_9$ (Ca349) phase [68]. The Ca349 phase is stable up to 926 °C where it decomposes into the Ca326 phase and the CoO-rich solid solution as seen in Fig. 1.17.

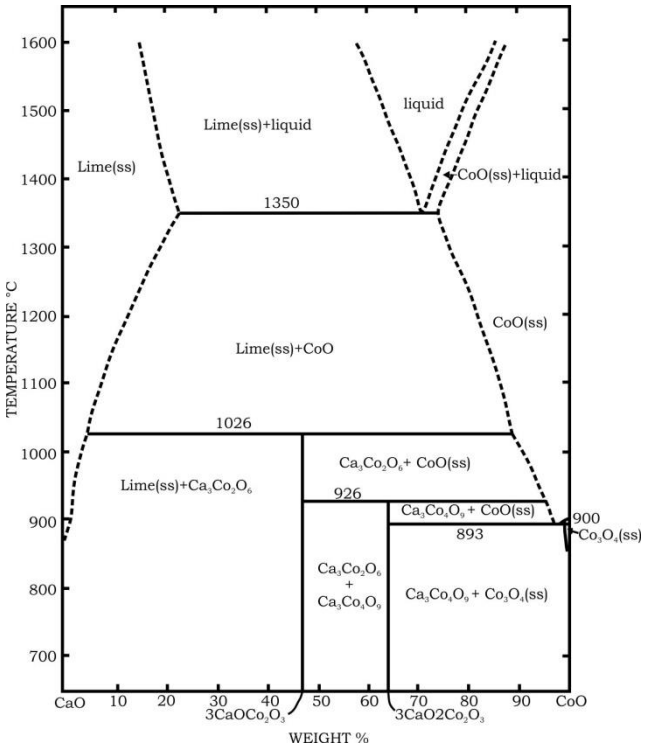


Figure 1.17: Phase diagram for the CaO-CoO system in air [68].

The Ca349 compound can be synthesised by quite a few different methods, for instance with the solid state reaction [76,68], with sol-gel routes (SG) [77,78,79], and with a thermal hydro-decomposition method (HT) of acetate salts [80]. On the other hand, the simple chemical solution deposition method is also known, and has been derived for depositing $Ca_3Co_4O_9$ films onto Si substrates [81], however it cannot be used for fabricating bulk samples.

The most common method used is the solid state reaction. Usually it is performed in two steps, from $CaCO_3$ and Co_3O_4 powders, starting with calcination at temperatures around 900-920 °C for 24h, and followed by grinding and subsequent annealing at the same temperatures [68,76, 82].

When we look at the other two synthesis methods, sol-gel route and a thermal hydro-decomposition method of acetate salts, respectively, we can notice that lower calcination temperatures (650-800 °C) and times were required for the formation of the fine single phase Ca349 powder, which needs to be further pressed and sintered at at least 850 °C and higher to prepare bulk ceramics. The final sintered microstructures obtained with these methods are fine-grained, rather dense, and the samples showed TE properties up to 0.29 [79]. In comparison to the conventionally prepared pristine Ca349 ceramics it seems that such a microstructure is preferable. The conventionally prepared Ca349 ceramics has namely the round plate-like grains, with lengths up to 5 μm and with random distribution. It has usual porosity of around 65% of the theoretical density, which is calculated on the basis of the ideal composition and is 4.68 g/cm^3 [70] and the reported zTs are up to 0.07 at 700 °C [83]. Here it is important to mention that until now, in the big majority of the studies the influence of the synthesis on the size, on the shape and on the thickness of the Ca349 grains has not been analysed as well as the influence of the morphology on the TE properties. Consequently we can only deduce what was the grain morphology in conventionally prepared Ca349 samples from the included micrographs, where it seems that the plate-like grains are rather round, regular shaped and relatively thick. The conventional preparation requires repeated cycles of calcination and intermediate grinding to prepare single-phase Ca349 ceramics and hence longer heat treatment process at higher temperatures in comparison to the SG or the HT methods.

In the reports, however, the studies about influence of the starting precursors on the conditions of the heat treatment (calcination and sintering temperatures and times) to prepare single phase Ca349 ceramics, and consequently their microstructure and TE characteristics, were essentially neglected. Hence we decided to analyse the formation of the single phase Ca349 ceramics by using fine starting oxides of $CaCO_3$ and Co_3O_4 and compare them with preparation when using purchased coarse grain starting powders, which were also used in most of the reported studies. We showed that commonly reported sluggishness of the solid state synthesis simply results from the low reactivity of course grained reactants, while with the use of fine starting powders of $CaCO_3$ and Co_3O_4 the single phase Ca349 ceramics can be obtained already after single calcination at temperature as low as 760 °C.

Another method, which could be adequate and interesting for the Ca349 synthesis and enhancing its TE properties, is the so-called mechano-chemical synthesis. The term “mechano-chemistry”, is

mostly used for the solid state reactions triggered under the influence of mechanical forces, usually imposed with high-energy ball collisions in the mill [84,85]. The consequences of such high energy collisions are decreasing the particle size and hence specific surface enlargement, amorphization, input of the crystal defects, plastic and elastic deformations and nevertheless also chemical reactions [86]. It was shown that starting-powder mixtures treated with the MC method in some cases enable the synthesis of compounds that could not be prepared with the classical ceramic procedures [87]. According to the reports, in the case of TE materials, the MC processing also enables preparation of highly refined microstructures and hence better TE characteristics [88], therefore all the features which could be useful for the Ca349 phase formation and good TE properties. Hence we decided to mechano-chemically synthesize the Ca349 compound, and analyze the influence of the parameters of high-energy milling on the powder mixture of $CaCO_3$ and Co_3O_4, the synthesis of the Ca349 phase, and the microstructure and TE characteristics of the Ca349 ceramics. We showed that the MC treatment results in the amorphization and enhanced reactivity of the starting powder mixture, leading to the synthesis of the single phase Ca349 after significantly shorter calcination time, and further enabled preparation of fine-grained Ca349 ceramics with about 2 times higher zT value in comparison to the literature reports for the classically prepared undoped one.

However, besides fine-grained samples with the proper morphology, there are also other ways to enhance the TE properties. Because of the large anisotropy in the electrical transport properties (according to Bhattacharaya [89] the room temperature values of in-plane and out-of-plane resistivity in the single crystal are 18.9 and 90.1 mΩcm, respectively) and distinct plate-like morphology of grains, it was generally considered that the best way to optimize the microstructure and the TE performance in the Ca349 compound would be to prepare highly textured and dense Ca349 ceramics [90,91]. In the next few paragraphs various fabrication methods for achieving highly textured and hence dense bulk ceramics will be presented. However, my work clearly showed that a compromise between the degree of texturing and density resulted in a favorable microstructure and, to the best of my knowledge, the highest zT value of 0.31 at 600 °C for the pristine Ca349 ceramics.

1.4.1.4.2.3Texturing and the microstructural characteristics Many processing methods have been investigated, such as hot-pressing (HP) [90,91], magnetic alignment (MA) [92], cold high-pressure pressing (CPP) [93], templated grain growth (TGG) [94], spark-plasma sintering (SPS) [95] and free-edge SPS or Spark plasma texturing (SPT) [96]. Samples prepared with the HP usually show homogenously distributed plate-like shaped grains aligned almost perfectly perpendicular to the applied stress. The degree of grains alignment, length and thickness depends on the applied stress (different ranges from 5 to 30 MPa) and is usually in the range from 5 to 15 μm, and around 0.2 μm, respectively. The temperatures and times used by the HP differ as well and they typically range from 850 to 920 °C and are sintered for 5-24h, respectively. The densities vary from 94 — 99% of the theoretical value. Very similar, highly textured microstructure with densities up to 99% was achieved with the SPT method (a modified edge-free SPS method) of the pre-sintered pellet, but here in comparison to the HP decisively shorter sintering time is needed. The zTs in such fully textured and dense samples were from 0.15 to 0.18 at

about 700 °C [76,96]. Slightly lower zT around 0.14 were achieved in the samples processed by the normal SPS method [97]. These samples had almost full density of 99.6%, however without evident grain alignment (i.e. texturing). The grain length is usually slightly increased in comparison to the conventionally prepared sample. Another method that offers a relatively pronounced grain texturing is the cold high-pressure pressing (CPP); extremely high pressures of 3 GPa are used for compacting the starting powder mixture into the pellets. The CPP ceramics had densities around 98%, the grain-growth was inhibited in comparison to conventionally prepared samples and the zT values were around 0.11 [93].

In most reports a single processing method to prepare Ca349 ceramics was studied and only rarely two or more different processing methods are compared. Therefore, it is hard to make an objective comparison about the influence of the processing method on the microstructure, i.e., the density, size and morphology of the grains and texturing, and the TE characteristic of the Ca349 ceramics. For this reason we made a study with the same single phase Ca349 starting material for preparation of the Ca349 ceramics using various processing methods: i) already-reported in the literature (conventional sintering – CS, hot pressing – HP, free-edge spark-plasma sintering of a sintered pellet – SPT), ii) modified (free-edge SPS of a pellet from just compacted powder – SPT) and ii) novel (cold pressing of sintered Ca349 pellet without post annealing – CP, a free-edge cold pressing of sintered Ca349 pellet with post annealing – CP-920).

1.4.1.4.2.4Doping for enhanced TE properties The third option to improve the TE characteristics is the doping. In the Ca349 system the dopants substitute either Ca-sites or Co-sites. Generally it is believed that if doping on Co-sites, then the band structure and the transport mechanism are affected, and a great change in the physical properties is expected. On the other hand, if doping on Ca-site, only the charge carrier concentration can be altered with not so much impact on the band structure [98,99]. There have been many attempts to improve the Ca349 TE properties with various dopants. Starting with rare-earth ions (La, Pr, Dy, Ho, Er, Yb and Lu) and substitution on the Ca-site, which generally resulted in increased Seebeck coefficient and decreased lattice thermal conductivity, with the largest zT report of 0.36 at 800°C for Lu doped Ca349 sample [100,101]. Substitutions were made also with alkali (Na, K) and alkaline-earth metals (Mg, Sr, Ba), where often only modest, if any, improvements in electrical conductivity and S were gained, with the highest reported zT up to 0.22 [102,103]. There were also attempts of substitutions on Co-site, however without specific targeting to either the Co-sites in the CoO_2 layers or in the Ca_2CoO_3 layers. In these studies mostly the transitional elements (Ti, Mn, Ni, Pt, Cu, Zn, Fe) were used [104,105,106] and the zT values up to 0.28 were reported. Some of the best zT values were reported for doping with Pb, Sb, Bi, and Ag [107,108,100]. Here the Ag and Lu substitutions for Ca atom and the existence of Ag as nano-inclusions lead the material to the highest reported zT till date, reaching 0.61 at 845 °C [100].

The influence of doping with the high valence ions like Cr^{6+}, Mo^{6+}, W^{6+} on the thermoelectric characteristics of the Ca349 ceramics was reported in the low-temperature range from 5 K to 350 K [104,106,109]. However, these reports are not complete and discuss only one or two of the TE characteristics, newer all three together. Nevertheless, it can be summarized that in general they increase the Seebeck coefficient, decrease electrical conductivity and decrease thermal conductivity of the Ca349 ceramics. In the case of W-doping, which is also a very heavy

element, only one work made by Fu et al. [106] was reported, where the influence on the electrical conductivity was studied; it decreased with increasing the addition of WO_3 for the composition $Ca_3Co_{4-x}W_xO_9$, (x = 0.1, 0,2, 0.3 and 0.4). They resolved that W^{6+} substitutes Co^{2+} in the Ca_2CoO_3 layers and determined the solid solubility limit in the range $0.4 < x < 0.5$; however, the microstructural aspects were not examined.

In order to fully assess the influence of WO_3-doping on the microstructure development and TE characteristics in the temperature range from 40 °C to 600 °C I prepared $Ca_3Co_{4-x}W_xO_9$ ceramics for x from 0 to 0.2 by the classic ceramic procedure using fine powders of $CaCO_3$, Co_3O_4 and WO_3.

Chapter 2

Aims and Hypothesis

2.1 Description of the Problem

In the last decades among the TE materials the oxide TE materials have attracted a lot of attention. The TE materials, namely, offer the only viable possibility for direct conversion of the waste heat into the electrical energy regardless the size of source and in an environmentally friendly way. The oxide TE materials are in comparison to the state-of-the-art TE materials (BiTe, BiSe,BiSb, PbTe, etc.) light, nontoxic and much cheaper, made from abundant elements, and they can be used at high temperatures up to 800 °C. However, their TE characteristics are still much behind the state-of-the-art materials, thus significant improvement of the thermoelectric figure of merit (zT) is required to fulfil requirements for efficient applications. It should also be stressed that oxide TE materials are typically synthesised at much higher temperatures and longer times, hence their preparation requires more energy than processing of the classical TE metallic alloys. It is somehow contradicting that materials used for harvesting the waste heat produce a significant amount of the waste heat while processed. Hence, energy and cost-effective processing of the oxide TE materials is another imperative for their successful utilization.

The $Ca_3Co_4O_9$ (Ca349) is a promising p-type oxide thermoelectric. Its synthesis using classical ceramic procedure from powders of $CaCO_3$ and Co_3O_4 was generally reported to be very sluggish and requires several calcinations for 24 hours at temperatures between 900 °C and 920 °C with intermediate grindings to prepare the single phase material. Afterwards, final sintering at 920 °C is still required to prepare the desired samples of the Ca349 ceramics, whose zT values were typically below 0.06 at 700 °C. On the contrary, however, studies of the sol-gel and hydrothermal synthesis showed that single-phase Ca349 powder could be prepared at significantly lower temperatures in the range from 650 °C to 800 °C and in a much shorter time. Such powders were fine grained and enabled preparation of the homogeneous and fine grained Ca349 ceramics by sintering at temperatures from 850 °C to 920 °C, having much better thermoelectric characteristics with zT values even up to 0.29 at 700 °C. Such distinct differences in synthesis and characteristics of obtained Ca349 ceramics can largely result from the reactivity of the starting precursors affecting formation, composition, structure and microstructure of the obtained Ca349 compound. Accordingly, the use of fine starting powders of $CaCO_3$ and Co_3O_4 could significantly enhance the preparation of the Ca349 compound by the classical ceramic procedure, facilitating its formation at lower temperatures and in shorter calcination times. Well recognized advantages of the

mechano-chemical method in synthesis of various materials could be beneficial also in the synthesis of the Ca349 ceramics, which has not been examined yet. The use of highly reactive starting precursors in solid-state synthesis could also positively influence the morphology of Ca349 grains and in general microstructural features of the prepared Ca349 ceramics for improved TE characteristics, which was also mostly neglected in reported studies.

The Ca349 compound has a complex misfit layered structure, where each of the sub-structural CoO_2 and Ca_2CoO_3 layers plays a different role in transport characteristics, which are additionally affected by a discordance between these layers; hence a compound exhibiting strong anisotropy in physical properties. Accordingly, the electrical and thermal conductivity in the single crystal are noticeably higher in an in-plane direction (a-b planes) than in an out-of-plane (c-axis) direction. The Seebeck coefficient is structurally much less dependent. Such structure also dictates a distinct plate-like morphology of the Ca349 grains. Structural and morphological characteristics of the Ca349 phase indicate that in polycrystalline Ca349 ceramics a proper microstructure can significantly contribute to the enhancement of the TE characteristics. It was generally anticipated that highly textured and dense microstructure would be favorable to gain Ca349 ceramics with high zT. Various processing methods were studied so far to prepare such highly textured Ca349 ceramics. However, while highly porous Ca349 ceramics with completely random orientation of the plate-like grains had zT of about 0.06, fully textured and dense ceramics had zT of about 0.17. Although it is a three-fold increase, the obtained zT value is somehow disappointing still being much below the zT for the single crystal Ca349 of 0.8. Microstructural features present in the polycrystalline ceramics could actually be an advantage and contribute to the improvement of the TE characteristics in regard to the single crystal, which raises a question about what kind of a microstructure would be required. While grain boundaries usually represent an obstacle for the movement of the charge carriers and hence mean higher electrical resistivity, it is also known that their effects could also be minimized by proper processing tailoring their nature. On the other hand the grain size directly influences the density of grain boundaries, which can contribute to the so-called energy filtering for the increased Seebeck coefficient. It is also known that higher porosity usually means lower thermal conductivity of ceramics and in the case of Ca349 ceramics porosity is closely related to the degree of texturing. Accordingly, enhancement of the TE characteristics of the Ca349 ceramics requires optimization of the complete procedure from the synthesis of Ca349 compound to the final processing of the Ca349 ceramics in order to gain a favorable microstructure in regard to the grain size and morphology, grain alignment and porosity.

Compared to the pristine Ca349 ceramics, noticeable influence on the TE properties with increased zT to about 0.5 was achieved by doping of the Ca349 compound on Ca- or Co-site. High 6+ valence ions of Cr and Mo were reported for the temperature range 5 K to 350 K to increase S and decrease thermal conductivity, while for W^{6+} only a decrease of electrical conductivity was given. For the TE oxides their characteristics at higher temperatures are important. In the case of W, which is also a very heavy element, it would therefore be interesting to fully examine the influence on all TE characteristics of Ca349 also at higher temperatures.

2.2 Aims and Goals of the Dissertation

The topic of my PhD research was the development of the TE p-type Ca349 ceramics. I studied the influence of starting oxide powders and the methods of synthesise on the formation of the Ca349 compound, and afterwards the influence of various processing methods on the obtained microstructural features (morphology of the grains, density, degree of texturing) and consequently the TE characteristics of the Ca349 ceramics.

At first I studied the synthesis of the Ca349 compound using the classical ceramic procedure from purchased commercially available and relatively coarse starting oxides powders of $CaCO_3$ and Co_3O_4. Afterwards I exploited the possibility to improve the classical ceramic solid state synthesis of the Ca349 compound, either by use of the fine starting powders obtained by attrition milling of $CaCO_3$ and Co_3O_4, or by mechano-chemical (MC) synthesis also from the fine starting powders of $CaCO_3$ and Co_3O_4. I analysed the influence of starting powders on the formation of the Ca349 compound depending on the calcination temperature and time, phase compositions, microstructural features (density, size and morphology of the grains) and finally TE properties. The study of MC treatment involved examining the influence of the milling parameters (i.e. ball impact energy, ball impact frequency and cumulative energy) on the characteristics of the treated powder mixture and its phase composition for possible formation of the Ca349 phase, and formation of the Ca349 compound after calcination of the MC treated powder mixture.

Once, I had the fine single phase Ca349 material, the second goal was to study the influence of different processing methods on the microstructure. I analysed the microstructural features (density, degree of texturing and also the size and morphology of the grains) in correlation with the processing parameters and obtained TE characteristics of the Ca349 ceramics to determine these key elements that affect the possibility of improving TE characteristics for higher zT. Using the same starting Ca349 material enabled a comprehensive comparison among processing methods and was certainly an advantage compared to the previous studies reported in literature, which were mostly limited to single or maximum two processing methods in preparation of the Ca349 ceramics. Among the already studied processing methods I used classical solid state synthesis, hot-pressing (HP) and free-edge spark plasma sintering (SPT) of the sintered pellet. In addition I modified the SPT by using a pellet from just compacted powder and not the sintered one. Finally, I also used novel methods which were previously not yet reported for the Ca349 ceramics, a cold pressing of sintered pellet of Ca349 ceramics and free-edge cold pressing of sintered pellet of Ca349 ceramics with post-annealing. To find out how the density and the microstructure anisotropy influence each of the TE parameters (Seebeck coefficient, electrical and thermal conductivity) a comparison between fully dense highly textured and highly porous Ca349 ceramics was made by measurements of the TE parameters simultaneously on the same block of the sample in both directions, parallel and perpendicular to the applied stress.

Within the third part of my PhD research I studied the influence of WO_3-doping on the formation, composition, microstructure and TE characteristics of the Ca349 ceramics in the temperature range from 40 to 615 °C.

Chapter 3

Material Processing and Characterization

As already mentioned in Chapter 1 two main synthesis methods, the classical ceramic solid-state procedure and mechano-chemical synthesis, were used in this work. Therefore, a few facts about both of them will be given, with the emphasis on the mechano-chemical method which is less familiar and needs to be clarified in order to understand our work in Chapters 5 and 6. In addition, basic grounding will be given in the frame of not so familiar processing methods, namely the edge-free SPS, and different TE characterisation used in our research, respectively.

3.1 Synthesis

3.1.1 Solid state synthesis

3.1.1.1 Classical ceramic solid-state procedure

Classical solid state synthesis is the easiest way to make many solid state materials by the direct reaction of their components at high temperatures. Often it is a relatively slow process, controlled by the atomic diffusion; however it can be accelerated by reducing the particle size and with a possible presence of crystal defects, especially vacancies and interstitials. Moreover, the diffusion/synthesis can also be improved with a repeated cycle of calcination-milling-calcination, gaining better homogeneity of the material and completed reactions between the source materials, but at a possible cost of introducing contamination. The repeated heat treatment technique can also result in the presence of unwanted phases [110].

In my PhD research classical solid state synthesis of the Ca349 was studied either by using commercial (as purchased) $CaCO_3$ and Co_3O_4 starting powders with average particle sizes of 2.5 μm and 1.38 μm, respectively, or with the same powders attrition milled to the average particle size of 0.45 μm and 0.36 μm, respectively. Starting powders were mixed in the molar ratio 9:4, homogenized for 2 hours in a planetary mill in absolute ethanol media and subsequently dried. The powder mixtures were uniaxially pressed with pressures of 200-220 MPa into pellets. The pellets were calcined at temperatures of 600 °C – 920 °C for different durations, namely 2 – 20h. The detailed synthetic processes in this research can be found in each chapter.

3.1.1.1.1 WO_3-doped $Ca_3Co_4O_9$ Samples of $Ca_3Co_{4-x}W_xO_9$ for x=0, 0.02, 0.05, 0.1 and 0.2 were prepared using classical solid state

synthesis from attrition milled powders of $CaCO_3$ and Co_3O_4, and from purchased fine WO_3 powder with average particle size of approximately 40 nm. Homogenised mixtures of all starting powders were then uniaxially pressed with 250 MPa and sintered for four times at 900 °C for 20h in air with intermediate grindings in the agate mortar.

3.1.1.2 Mechano-chemical synthesis

The term "mechanochemistry" was first introduced by Friedrich Wilhelm Ostwald in 1887 and 1893 [84,111]. It was defined as a special chemistry branch, which deals with the chemical and physical changes of substances subjected to the mechanical energy and it applies for substances in all aggregate states. In the last few decades the term is used mostly for the solid state reactions triggered under the influence of mechanical forces, usually imposed with high-energy ball collisions in the mill [84,85]. The solid is often processed mechanochemically with a view that it would increase the reactivity. In this case, we are talking about the "mechanochemical or mechanical activation" [112,85].

However, alhough it may seem the mechanochemical process is very straightforward, there are many very complex processes going on during the transmission of mechanical energy into the powder particles, which are still not fully understood. Describing the energetics of the high energy milling is difficult because of the numerous milling parameters, which must be taken into consideration. The parameters are presented in Fig. 3.1 and Fig. 3.2 [113,114]. However, it can be stated with certainty what are the consequences of the high-energy collisions between milling balls and powder particles presented in Fig. 3.3 [114].

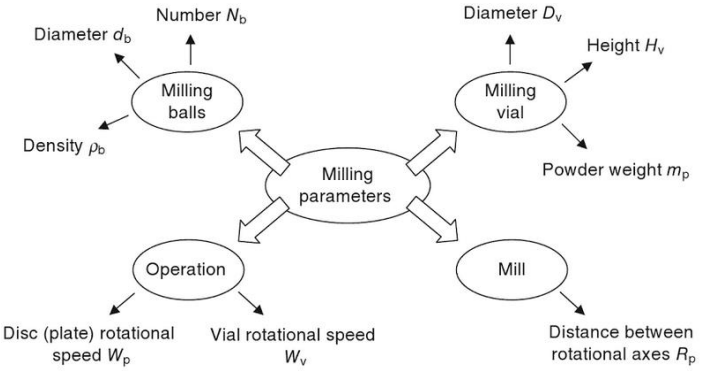


Figure 3.1: The milling parameters in planetary mill with cylindrical vial needed for description of energetics of the high-energy milling process [113].

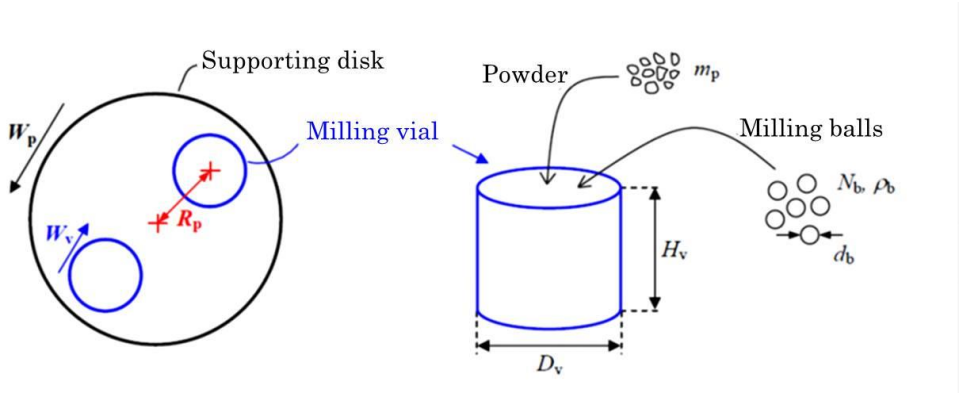


Figure 3.2: Schematical presentation of the planetary mill and the cylindrical milling vessel. (See Fig. 3.1) [114].

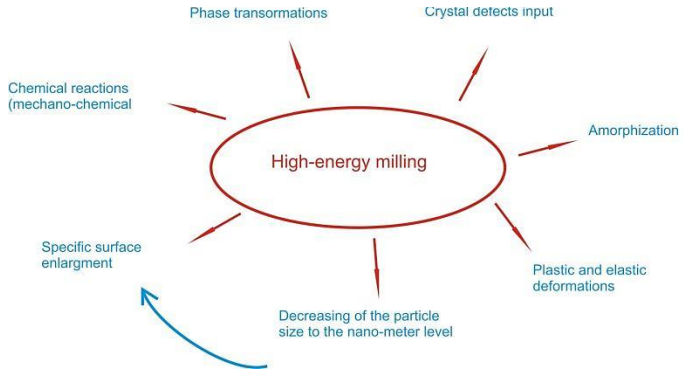


Figure 3.3: The consequences of the high-energy collisions between milling balls and powder particles [114].

The milling parameters are involved in the mathematical models to correlate them to the ball impact energy as well as with the frequency with which the balls collide on the inner wall of the vial, i.e., the ball-impact frequency.

It is known that a part of the kinetic energy of the ball is transferred to the powder, and another part remains in the ball after collision. When the total kinetic energy of the ball is transferred to the powder particles, we are talking about ideal plastic collision; on the contrary we have the ideal elastic collision. So the amount of ball's kinetic energy transferred to the powder is the ball energy.

Burgio et al. [115] derived kinematic equations to describe the velocity and the acceleration of the balls in the vial of a planetary mill. He proposed that the ball does separate from the vessel's wall at some point of acceleration, makes a few collisions, and goes back to the "equilibrium" state with the milling vessel. At this state there is no kinetic energy loss or energy transfer on the system, only on the powder particles.

With Equation 3.1 he described the kinetic energy of the ball Eb, "launched" at a given moment from the vessel's wall.

$$E_b = \frac{m_b \cdot V_b^2}{2} \tag{3.1}$$

where m_b is the mass of the ball and V_b the velocity of the ball inside the vial launched at a given moment from the vessel's wall.

The remained kinetic energy of the ball Es, the part after the collision with powder particles, can be described with Equation 3.2, where the V_s is the velocity of the ball in the moment when it starts to move in the "equilibrium" state with the vial.

$$E_b = \frac{m_b \cdot V_s^2}{2} \tag{3.2}$$

The kinetic energy transformed from the ball to the powder particles is given by the divergence of Equations 3.1 and 3.2.

$$\Delta E_b = E_b - E_s = \frac{m_b}{2}\left(V_b^2 - V_s^2\right) \tag{3.3}$$

The term is valid in the case of ideal plastic collision. Usually factor K_a is added to Equation 3.3, which is the rate of elasticity of the depended collision [115].

$$\Delta E_b = K_a \cdot \frac{m_b}{2}\left(V_b^2 - V_s^2\right) \tag{3.4}$$

For the ideal elastic collision $K_a = 0$, which means the whole kinetic energy stays on the ball and it is not transformed to the powder particles, namely the $\Delta E_b = 0$. For the ideal plastic collision $K_a = 1$. In this case the whole kinetic energy is transferred to the system (Equation 3.3).

Magini [116] studied the influence of the collision elasticity factor $K_a$on the Ti-Al system. He proved the assumption of the ideal plastic collision or $K_a = 1$ (Equation 3.4) can be considered in the initial milling phase only, since the plasticity and elasticity of the collision depend mainly on the degree to which the balls are coated, and on the elastic properties of the balls and the milled powder.

The ΔE_b energy in Equation 3.3 is valid for a single ball, however, in the real experiment, we are dealing with a finite number, N_b, of balls that hinder each other so that kinetic energy must be modified by an empirical factor , φ_b, which is able to account for the degree of filling of the vial. In this case the empirical factor φ_b is added to Equation 3.4.

$$\Delta E_b^* = \varphi_b \cdot \Delta E_b = \varphi_b \cdot K_a \cdot \frac{m_b}{2}\left(V_b^2 - V_s^2\right) \tag{3.5}$$

The empirical factor φ_b is given by Equation 3.6 [115].

$$\varphi_b = 1 - n_v^{\varepsilon} \tag{3.6}$$

Where n_v is the ratio between N_b, a finite number of the balls, and $N_{b,V}$, the number of the balls that can be contained in a simple cubic arrangement in the vial, with height H_V and diameter D_V (Equation 3.7). At this point we take into account the diameter of the balls d_b (Equation 3.8). The parameter ϵ is usually larger than 1 for ordinary milling balls and vials used in high-energy milling (see Equation 3.11).

$$n_V = \frac{N_b}{N_{b,V}} \tag{3.7}$$

$$N_{b,V} = \frac{D_V^2 \cdot H_V}{2 \cdot d_b^3} \tag{3.8}$$

From Equations 3.6, 3.7, 3.8 it is evident that when only one ball is in the vial or $N_b = 1$, the $n_V \to 0$ and $\varphi_b \to 1$, respectively. In this case the $\Delta E_b^* = \Delta E_b$, so we use Equation 3.4. In the case when the vial is absolutely filled with balls or $N_b = N_{b,V}$, the $n_V = 1$, $\varphi_b = 0$ and $\Delta E_b^* = 0$, respectively [114]. (See Equations 3.5, 3.6, 3.7)

In Equation 3.6 we have the parameter ε. To calculate it, the additional condition must be introduced. It was empirically discovered [117,118,119] that power consumption is heavily diminished when the vial is filled with balls in such a way that one third of the inner surface wall is covered. This is attributed to the reciprocal hindering of the balls, which decreases the effective transfer of the kinetic energy from the balls to the powder particles. Consequently, the factor n_s was introduced, which is the ratio between N_b and $N_{b,S}$, which is the number of balls needed to cover, in a simple cubic arrangement, one third of inner surface wall (Equations 3.9, 3.10).

$$n_S = \frac{N_b}{N_{b,S}} \tag{3.9}$$

$$N_{b,S} = \frac{\pi \cdot (D_V - d_b) \cdot H_V}{3 \cdot d_b^2} \tag{3.10}$$

For the conditions where the vial's wall is one third covered ($n_S = 1$), the authors have derived the border condition for empirical hindering factor φ_b to be 0.95 [115]. In this case the reciprocal hindering of the balls is small. If we introduce the border condition of $\varphi_b = 0.95$ for $N_b = N_{b,S}$ (valid for $n_S = 1$) into Equation 3.6, we can calculate the parameter ε.

$$0{,}95 = 1 - \left(\frac{N_{b,S}}{N_{b,V}}\right)^{\varepsilon} \tag{3.11}$$

On the basis of the ball's movement analysis, the equations for balls velocity and acceleration in the vial of a planetary mill were derived [115]. The balls acceleration a_b and velocity $V\mathrm{b}$ (see Equation 3.1) and V_s (see Equation 3.2) are given with Equations 3.12, 3.13 and 3.14.

$$a_p = \left(\left(W_p^2 R_p\right)^2 + \left(W_V^2 R_V\right)^2\right)^{1/2} \tag{3.12}$$

$$V_b = \left(\left(W_p R_p\right)^2 + W_V^2 \left((D_V - d_b)/2\right)^2 \cdot \left(1 - 2W_V/W_p\right)\right)^{1/2} \tag{3.13}$$

$$V_s = \left(\left(W_p R_p\right)^2 + W_V^2 \left((D_V - d_b)/2\right)^2 + 2W_p R_p W_V \cdot (V - d_b)/2\right)^{1/2} \tag{3.14}$$

Where W_p is the rotational speed of the supporting disk, W_V is the rotational speed of the vial, R_p is the distance between the rotational axes, R_V and D_V are the radius and diameter of the milling vial and d_b is the radius of the ball.

If we introduce the equations for velocities V_b and V_s (Equations 3.13 and 3.14) into Equation 3.5, we can evaluate the ball-impact energy, ΔE_b^*, the energy that is transferred at collision to the powder particles (Equation 3.15). ρ_b is the density of the ball.

$$\Delta E_b^* = \frac{1}{2} \cdot \varphi_{a_b} \cdot K \left(\rho_b \frac{\pi d_b^3}{6} \right) \cdot W_p^2 \left(\left(\frac{W_V}{W_p} \right)^2 \left(\frac{D_V - d_b}{2} \right)^2 \cdot \left(1 - 2\frac{W_V}{W_p} \right) - 2R_p \left(\frac{W_V}{W_p} \right) \cdot \left(\frac{D_V - d_b}{2} \right) - \left(\frac{W_V}{W_p} \right)^2 \left(\frac{D_V - d_b}{2} \right)^2 \right) \quad (3.15)$$

The ball-impact frequency v_1 of the single ball is defined with Equation 3.16 [115].

$$v_1 = K \cdot (W_p - W_V) \quad (3.16)$$

The value K depends on the geometry of the mill and on the ball diameter. It tells us how many collisions are made by a single ball in one second when the absolute spinning frequency of the mill is one revolution per second. Magini [120] has shown that the K value can be evaluated to be approximately 1.5 for ball diameter around 10 mm, which is employed in most cases.

If we assume that the milling parameters are adjusted correctly and the milling vial is filled so that the reciprocal hindering of the balls is negligible, the number of the balls N_b in the vial is the only parameter that affects the ball- impact frequency (Equation 3.17).

$$v_t = N_b \cdot K \cdot (W_p - W_V) \quad (3.17)$$

If we compare the equations for ball-impact energy, ΔE_b^*, and for ball-impact frequency v_t, we can conclude [114]:

Changing the number of balls within the non-hindering region affects the ball-impact frequency, while maintaining the same ball-impact energy (Equation 3.17).

On the other hand, the diameter and the density of the balls can be changed in order to set the ball-impact energy without affecting the ball-impact frequency (Equation 3.15).

The cumulative kinetic energy E_{cum} is defined as the weight-normalized product of the ball-impact energy, the ball-impact frequency, and the milling time given with Equation 3.18.

$$E_{cum} = (\Delta E_b^* \cdot v_t \cdot t)/m_p \quad (3.18)$$

Where ΔE_b^* is ball-impact energy, v_t is ball-impact frequency, t is milling time and m_p is powder mass.

It has been demonstrated that ΔE_b^* is related to the path of the reaction and v_t to the transformation kinetics. Every system can react differently to an amorphous phase or toward crystalline compound. Different paths are usually characterised by different activation states. The synthesis of the amorphous phase requires

low activation energy. This represents a condition in which the powder can "cumulate" the energy transferred during the milling action and the transformation kinetics is simply a function of a total energy released by a milling tools. These kinds of reactions are called "cumulative reactions" [121]. To form a crystalline compound, the overcoming of a definite energy threshold or critical ball-impact energy is required [118,122], above which only a crystalline compound is formed. This means that the reaction can proceed only if during a single hit the ball-impact energy transferred to the trapped powder is sufficient to overcome its activation energy. Through experiments the authors [122] defined also the minimum cumulative energy necessary to obtain an amorphous product.

For the mechano-chemical milling we used commercial $CaCO_3$ and Co_3O_4 starting powders in the molar ratio 9:4, which were homogenized for 2 hours in a planetary mill in absolute ethanol media and subsequently dried. Prior to the preparation of the mixture, both starting powders were attrition milled for 6 hours in absolute isopropanol media to obtain fine powders and subsequently dried at 150 °C. For all three series of the MC treatment described in Chapter 5 and 6, batches of powder mixtures weighing 3.5 g were used.

The MC treatment was performed in a Fritsch Pulverisette 5 planetary mill using vidia composite milling vial and milling balls, respectively. In Table 3.1 all the characteristics which were used at experiments, and which are described in Chapters 5 and 6 are gathered, respectively. They were calculated using Equations 3.15, 3.17 and 3.18.

Table 3.1: The mill, the milling vial and the balls parameters.

Fritsch Pulverisette 5		Milling vial (vidia)		Milling balls (vidia)	
R_p [m]	0.125	D_V [m]	0.09	d_b [m]	0.01
k	-2.19	H_V [m]	0.038	ρ_b [kg/m^3]	15920
W_p [r/s]	5 - 6			N_b	23 and 16
t [h]	2-20h				

3.2 Processing

3.2.1 Spark plasma sintering (SPS)

The Field-assisted sintering technology (FAS) or spark plasma sintering (SPS) or pulsed electric current sintering (PECS) are the names most widely used for this synthesis technique. It differs from the hot pressing in the way the heat is produced and transmitted. The SPS consists of a mechanical loading system, which is placed in a controlled atmosphere (vacuum or protective gas at atmospheric pressure) and which at the same time acts as a high-power electrical circuit. Because the materials used for tooling have a good electrical conductivity, low voltages (typically around 10 V) produce high currents (1-10 kA), which results in efficient Joule heating [123]. Simultaneously to the heating, also the uniaxial loading up to 250 kN can be used. Despite, there are still debates whether the controlling mechanism is Joule heating or plasma generation due to the spark, this technique is very useful as it increases the kinetics of sintering

(reduces the total duration and energy costs), achieves rapid densification and limits the grain growth [96].

3.2.1.1 Free-edge spark plasma sintering or spark plasma texturing (SPT)

This method uses the same principles as the SPS method. The only difference at this modified method is to allow free expansion perpendicular to the pressing direction by using a mould with a diameter much larger than the diameter of the sample, as presented in Fig. 3.4. [96]. The result is dense and highly textured ceramics with lamellar grains aligned perpendicular to the direction of applied pressure.

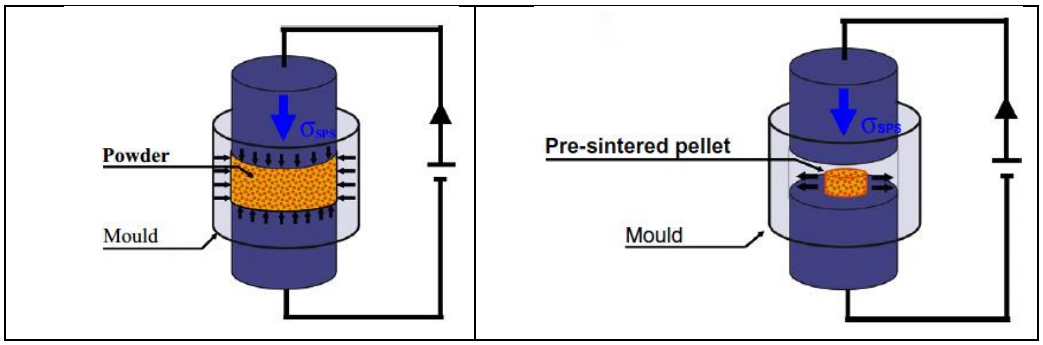


Figure 3.4: Schematically presented configuration of the SPS (left) and SPT (right) processing methods [96].

3.2.2 Other processing methods

For preparation of the Ca349 ceramics using various processing methods (i.e. hot pressing (HP), spark plasma texturing of the sintered sample (SPT-920), spark plasma texturing of only compacted powder (SPT), cold pressing of calcinated *pellets* (CP) and free-edge cold pressing of calcinated *pellets* with additional annealing (CP-920), the same starting single-phase Ca349 material, prepared by classical ceramic procedure from mixture of fine attrition milled powders of $CaCO_3$ and Co_3O_4 by calcination at 760 °C for 12 h, was used, either as pellets obtained after calcination or powder prepared by grinding calcined pellets.

3.2.2.1 Hot pressing - HP

For HP the pellets with a diameter of 12 mm were uniaxially pressed at 220 MPa and placed into a corundum model with an inner diameter of 26 mm, which allowed lateral deformation, they were sintered at 800 °C for 16 h under a uniaxial pressure of 25 MPa.

3.2.2.2 Free edge spark plasma texturing - SPT

SPT samples were prepared either as reported in the literature, namely the Ca349 pellets already classically sintered at 920 °C for 2 hours (SPT-920) were placed in a graphite die with a diameter larger than a pellet and sintered at 900 °C for 2 min under the uniaxial pressure of 50 MPa, or the green pellets of *just compacted powder* of the Ca349 phase, which was uniaxially pressed with 760 MPa (label SPT), were used and treated as described for the previous sample.

3.2.2.3 Novel cold pressing of calcinated Ca349 pellet

A novel method in the preparation of the Ca349 ceramics is the cold pressing of sintered pellets of the Ca349 ceramics in a die which is otherwise used for pressing powders into pellets. Two variants of the cold pressing were used: i) cold pressing without post-annealing (CP) and ii) free-edge cold pressing with post-annealing (CP-920). In the case of the CP the calcined pellet was uniaxially pressed with 380 MPa in the stainless-steel die with the same diameter as the pellet under a pressure of 380 MPa. In the case of CP-920 the calcinated pellets with diameter of 16 mm were uniaxially pressed with 210 MPa in the stainless-steel die with a diameter of 22 mm and afterwards annealed at 920 °C for 20 hours. The details are described in Chapter 4.

3.2.3 Thermoelectric characterization

The TE characteristics of the samples, the electrical conductivity (σ), the Seebeck coefficient (S) and the thermal conductivity (κ), used to determine the figure of merit zT, were analyzed in two different ways from room temperature up to about 627 °C. One set of TE measurements was made by a method usually used and reported in the literature, which is a combination of different measurements to obtain TE parameters; the Seebeck coefficient (S) and the electrical conductivity (σ) were measured simultaneously in a He atmosphere on a single custom-built device while the thermal conductivity was determined in accordance to the equation $\kappa = \alpha c_p \rho$ from the separate measurements of a thermal diffusivity (α) by the commercial laser-flash apparatus, specific heat (c_p) by the DSC and density (ρ) by the Archimedes' method. Detailed description of TE characterization is presented in Chapter 4. I labeled this combined method as CM. Here it has to be mentioned that zT values determined by the CM are the combination of the σ and S measured in the in-plane □direction and κ in the out-of-plane direction, and hence, in the case of textured samples because of the anisotropy of the TE parameters, likely overestimated in accordance with the degree of texturing. Hence another set of measurements of selected samples was made using a Z-meter, which enabled measurements of all three TE parameters (σ, S, κ) simultaneously on the sample in the same direction in vacuum (detailed description is presented in Chapter 4). A combination of both methods for measurement of the TE parameters enabled comprehensive comparison of different processing methods with their influence on the microstructure and consequently the TE characteristics of the Ca349 ceramics. Measurements of the selected sample by the CM and Z-meter showed that results are well comparable within reasonable variation of ± 10 %. The comparison is presented in the supplementary material of Chapter 4.

3.2.4 Other characterizations methods

3.2.4.1 Particle size measurements

The particle size of the powders was determined using a Horiba LA-920 laser-scattering particle-size-distribution analyzer.

3.2.4.2 Differential thermal analysis-DTA, thermal-gravimetric analysis-TG and mass spectrometry-MS

The thermal characteristics of the powders up to 1200 °C were analysed using differential thermal analysis (DTA), thermal-gravimetric analysis (TG) and mass spectrometry (MS) to follow

the reactions, mass changes and released CO_2 with temperature, respectively. The study was performed in air with a heating rate of 10 °C/min using a simultaneous thermal analysis instrument, (STA) Netzsch Jupiter 449, coupled with a mass spectrometer (MS) 403C Aëoloss.

3.2.4.3 Densities measurements

Densities were measured using a density-measurements system Densitec (Metar sa, Matran, Switzerland).

3.2.4.4 X-ray powder diffraction (XRD)

The phase composition of the samples and the formation of the Ca349 phase were analysed with X-ray diffraction (XRD) analysis using an X'Pert PRO MPD (Cu-Kα, 2θ range 5 – 80 °).

3.2.4.5 Scanning electron microscopy (SEM)

The samples were grinded and polished in a different cross-section direction to access the microstructure in "in-plane" and "out-of-plane" direction. They were coated with a few nanometers thick carbon coating to prevent surface charging. In the case of fractured samples, which mostly serve for grain morphology and texturing observations, they were coated with a few nanometers thick layer of gold.

The microstructural analysis was carried out in JEOL JSM-5800 scanning electron microscope equipped with an energy-dispersive X-ray spectrometer (EDXS) and an Oxford Instruments Link Isis software system for the compositional analysis of the phases.

Chapter 4

Synthesis of Single-Phase $Ca_3Co_4O_9$ Ceramics and Their Processing for a Microstructure-Enhanced Thermoelectric Performance

In this chapter, a paper entitled "**Synthesis of single-phase $Ca_3Co_4O_9$ ceramics and their processing for a microstructure-enhanced thermoelectric performance**", by authors M. Presečnik, J. de Boor and S. Bernik, is presented.

The purpose of the work presented in this article was firstly to study and optimize classical ceramic solid-state synthesis of the single-phase Ca349 ceramics from the powder mixture of $CaCO_3$ and Co_3O_4, followed by analysis of different processing methods to gain knowledge and assess possibilities for microstructural enhancement of the TE characteristics of the Ca349 ceramics.

The $Ca_3Co_4O_9$ (Ca349) phase was synthesised using either purchased, rather coarse grained powders of $CaCO_3$ and Co_3O_4, or these powders attrition milled to fine grain size of about 0.5 μm. The use of coarse grained powder mixture required several calcinations at 900 °C for 24 hours with intermediate grindings to get Ca349 compound with minor contents of secondary phases. However, the use of fine attrition milled powders resulted in the formation of the single-phase Ca349 ceramics already after single calcination for 12 hours at a much lower temperature of 760 °C. Such ceramics was highly porous with completely random orientation of small and very thin plate-like grains of irregular shape, and had a surprisingly high zT of 0.094 at 627 ^{0}C, which is about 50% higher than reported in the literature for classically prepared pristine Ca349 ceramics. The use of such single-phase Ca349 material with preferred grain morphology turned out to be excellent for further processing of the Ca349 ceramics.

In further work the preparation of the Ca349 ceramics was studied using various processing methods: i) those already reported in the literature (classical sintering – CS, hot pressing – HP, free-edge spark-plasma sintering of the sintered pellet – SPT), ii) newly modified (SPT with use of pellets of just compacted powder) and iii) novel (cold pressing of a calcined Ca349 pellet without post annealing – CP and free-edge cold pressing of a calcined Ca349 pellet with post annealing – CP-920). The influence of processing on the microstructural features, i.e., the density and degree of texturing, size and morphology of the grains, and resulting TE characteristic of the Ca349 ceramic were analysed. It showed that at the distinct plate-like morphology of grains,

the degree of texturing and density strongly correlates. Depending on the processing the Ca349 ceramics with different densities ranging from about 50% to 100% were obtained having either completely randomly orientated plate-like grains or fully aligned (textured), respectively. Samples with random grain orientation or lower degree of texturing and hence high porosity had lower thermal conductivity (κ), lower electrical conductivity (σ) and high Seebeck coefficient (S). By increasing texturing and hence increased density, κ increased in both directions (in-plane and out-of-plane), S remained similar, while σ increased mainly along the plate-like grains in the in-plane direction. The highly porous sample without any texturing and random grain orientation had a zT value of 0.09 at 600 °C. In the fully textured and dense sample prepared by the modified SPT using pellets from only compacted Ca349 powder the zT value increased to 0.17, while in the literature typical values of 0.14 are reported for samples prepared by usual SPT method using sintered pellets. The highest zT value of 0.31, which is to the best of our knowledge also the highest zT reported in the literature for pristine Ca349 ceramics, was obtained in the sample prepared by a novel method of the free-edge cold pressing with a subsequent annealing (CP-920). The sample had a modestly textured microstructure with density of about 65% and well preserved starting morphology of fine, irregular shaped and thin plate-like grains. In comparison to the fully textured sample it had similar σ, higher S and about 3-times lower κ of 0.47 W/mK, which is among the lowest reported.

Contrary to general expectation that fully textured ceramics is favourable for high zT, the results clearly showed that a compromise between the density and degree of texturing is required while keeping preferred fine morphology of grains. In general, the results dictate that the imperative for achieving high zT in pristine Ca349 ceramics is to prepare the single phase Ca349 ceramics in a single calcination step at the lowest possible temperature, which ensures favourable morphology of the Ca349 grains, while in further processing it has to be preserved at the development of a proper microstructure for the degree of texturing and density. Any thickening of the plate-like grains with rounding of their shape, which resulted from higher temperatures and longer times of heat-treatment showed in lower zT values.

Available online at www.sciencedirect.com

ScienceDirect

Ceramics International 42 (2016) 7315–7327

CERAMICS INTERNATIONAL

www.elsevier.com/locate/ceramint

Synthesis of single-phase $Ca_3Co_4O_9$ ceramics and their processing for a microstructure-enhanced thermoelectric performance

M. Presečnik[a,b,*], J. de Boor[c], S. Bernik[a]

[a]Jožef Stefan Institute, Jamova cesta 39, 1000 Ljubljana, Slovenia
[b]Jožef Stefan International Postgraduate School, Jamova cesta 39, 1000 Ljubljana, Slovenia
[c]Institute of Materials Research, German Aerospace Center, Linder Höhe, Cologne, Germany

Received 21 December 2015; received in revised form 22 December 2015; accepted 14 January 2016
Available online 28 January 2016

Abstract

Single-phase $Ca_3Co_4O_9$ with a high porosity, having a ZT of 0.09 at 627 °C, was successfully prepared by a simple solid-state reaction using fine powders of $CaCO_3$ and Co_3O_4 after a calcination at 760 °C for 12 hours. It was excellent either for the preparation of the starting powder for the processing of the $Ca_3Co_4O_9$ ceramics or for direct processing. The influence of already-reported processing methods (classic sintering, hot pressing, free-edge spark-plasma sintering (SPS) of a sintered pellet) and new methods, such as free-edge SPS of a pellet from just-compacted powder, cold pressing of a sintered pellet without post annealing, and free-edge cold pressing of a sintered pellet with post-annealing, on the preparation of $Ca_3Co_4O_9$ ceramics was studied. The results showed how the density, the grain morphology and the microstructural anisotropy can all influence the thermoelectric characteristics of $Ca_3Co_4O_9$ ceramics measured in directions parallel and perpendicular to the applied pressure. While the fully dense (99%) and perfectly textured ceramics prepared by the free-edge SPS of a pellet from just-compacted powder had a ZT of 0.17, the highest ZT of 0.31 was obtained for the free-edge cold-pressed and annealed ceramics with modest texturing and low density (65%), having a very low κ of 0.47 W/mK. The results also showed that thin and irregular-shaped plate-like grains with sharp edges are preferred, while their thickening accompanied by rounding of their shape resulted in a reduced thermoelectric performance. The study revealed both the possibilities and the limitations for enhancing the TE characteristics of $Ca_3Co_4O_9$ ceramics just through microstructure optimisation.
© 2016 Elsevier Ltd and Techna Group S.r.l. All rights reserved.

Keywords: $Ca_3Co_4O_9$; Synthesis; Processing; Microstructure; Thermoelectric properties

1. Introduction

Thermoelectric (TE) materials have attracted much attention due to their potential in power-generation devices, i.e., TE modules, which provide the only viable method to convert waste heat directly into electricity in an efficient, economical and environmentally friendly manner. Since Terasaki et al. [1] reported that the transition-metal oxide $NaCo_2O_4$ exhibits a large thermopower and a low electrical resistivity, oxide TE materials became very promising for high-temperature applications, since they are, in contrast to the otherwise thermoelectrically much better conventional TE alloys, very stable in air (oxidizing atmospheres) at elevated temperatures, as well as being cheaper and non-toxic. While $NaCo_2O_4$ is known to be highly unstable, due to its poor resistance to humidity and volatility at elevated temperatures [2,3], $Ca_3Co_4O_9$ (Ca349) is much better in this regard and at the same time also very promising for further enhancements of its TE properties. The properties of Ca349 are closely related to its complex, misfit layered structure consisting of a CoO_2 layer of the CdI_2 type, ensuring an electrically conductive and an insulating Ca_2CoO_3 layer of the rock-salt type. The mismatch and the weak connection between these two substructure types contribute to the phonon scattering for a reduced thermal conductivity [4]. Such a structural anisotropy suggests the anisotropy of the TE characteristics. It was reported that single crystals of Ca349 showed good TE characteristics,

*Corresponding author at: Jožef Stefan Institute, Jamova cesta 39, 1000 Ljubljana, Slovenia. Tel.: +386 14773178; fax: +386 14773930.
E-mail address: mojca.presecnik@ijs.si (M. Presečnik).

http://dx.doi.org/10.1016/j.ceramint.2016.01.128
0272-8842/© 2016 Elsevier Ltd and Techna Group S.r.l. All rights reserved.

with a ZT as high as 0.87 at 700 °C [5], mostly as a result of the high Seebeck coefficient S of 240 μV/K and the high conductivity σ of 434 S/cm, both determined in the a–b planes, and less due to the relatively high thermal conductivity κ of about 3 W/mK. However, the use of single crystals is very limited for major applications due to their expense, and for large-scale production the synthesis route is unsuitable. Much more feasible is the use of polycrystalline Ca349 ceramics, which unfortunately have much lower TE characteristics, expressed as ZT values of about 0.1 at 700 °C [6]. The main reasons for the low ZT values of polycrystalline ceramics in comparison to single crystals are their much lower electrical conductivity in the range 20–50 S/cm and a lower Seebeck coefficient in the range 100–180 μV/K, so that the typically much lower thermal conductivity κ of around 1–1.5 W/mK cannot compensate [7–14]. In contrast to single crystals with fully expressed properties solely related to the composition and crystal structure, polycrystalline ceramics are handicapped by complex microstructural features such as: density, grain size and grain size distribution, grain orientation, grain boundaries and the connectivity among the grains. Hence, optimisation of the microstructure provides important opportunities to improve the TE characteristics of polycrystalline Ca349 ceramics.

The phase diagram of the CaO–CoO system was reported by Woermann and Muan [15]. Two binary phases are present in the system: a $Ca_3Co_4O_9$ phase (Ca349) and a $Ca_3Co_2O_6$ phase (Ca326). The $Ca_3Co_4O_9$ phase is stable up to 926 °C when it decomposes into the $Ca_3Co_2O_6$ (Ca326) and the CoO solid solution with CaO (CoOss). The $Ca_3Co_2O_6$ phase decomposes at 1026 °C into a solid solution of CaO with CoO (CaOss) and a solid solution of CoO with CaO (CoOss). They also found that the reactions of these phases' formation from $CaCO_3$ and Co_3O_4 are extremely sluggish, taking several weeks with intermediate grinding steps to obtain single-phase samples. They also reported that the two reactions, i.e., $CaCO_3 = CaO + CO_2$ and $Co_3O_4 = 3CoO + 1/2O_2$, both occur in the temperature range 880–900 °C. According to most reports in the literature, the synthesis of Ca349 is normally performed using a classic ceramic procedure in two steps from $CaCO_3$ and Co_3O_4, then calcination at temperatures 900–920 °C for around 24 hours, followed by repeated annealing with intermediate grinding at the same temperatures [7,15–22]. Calcinations at 750 °C or 800 °C for 12 hours were found to be unsuccessful, which required an additional calcination at 850 °C for 12 hours, followed by final annealing at a temperature just below 920 °C for about a day to obtain single-phase Ca349 [19,23,24]. However, fine-grained powders of single-phase Ca349 were obtained at lower temperatures in the range from 650 to 800 °C and with shorter firing times using a sol-gel Pechini synthesis method from Ca- and Co-nitrates [25–28] and a thermal hydro-decomposition method of acetate salts [29]. The pellets prepared from such powders were subsequently sintered at temperatures of at least 850 °C and higher [27,28].

The microstructure of the Ca349 samples is typically highly porous (with densities only about 70% of theoretical) with randomly oriented, plate-like grains of the Ca349 phase with sizes up to about 5 μm in the case of samples classically prepared from oxide powders and much finer in those prepared from sol-gel powders [11,28]. At 600 °C the samples had a Seebeck coefficient in the range from 120 to 170 μV/K and an electrical conductivity σ from 20 to 70 S/cm. While the classically prepared samples had a thermal conductivity of about 1.1 W/mK, it was much lower for the sol-gel-prepared samples with values of κ in the range from 0.4 to 0.9 W/mK, which was explained by the high porosity of the fine-grained microstructure [28]. For the Ca349 ceramics prepared from the $CaCO_3$ and Co_3O_4 powders, the highest ZT values of about 0.04 were reported in the literature [12]. In the case of the sol–gel samples, noticeably higher ZT values were reported in the range from 0.1 to 0.29 [25,28].

In order to optimize the microstructure and the TE performance of the Ca349 ceramics, many processing methods were investigated, such as hot pressing (HP) [30], magnetic alignment (MA) [31], cold high-pressure pressing (CPP) [32], templated grain growth (TGG) [33] and spark-plasma sintering (SPS) [34,29]. In comparison with a conventional preparation, all these processing techniques have shown that they enable the preparation of dense and textured Ca349 ceramics, i.e., the two main microstructural features believed to improve the TE characteristics of the Ca349 ceramics most significantly [36]. Cold high-pressure pressing (CPP) [32], which differs from conventional preparation only in the use of extremely high pressure, i.e., 3 GPa, to make pellets for the final sintering from the Ca349 powder, resulted in almost fully dense samples with densities up to 98% of theoretical and with pronounced microstructural texturing of the plate-like Ca349 grains in a direction perpendicular to the pressing axis. Similar densities and low, if any, texturing were obtained with the spark-plasma sintering (SPS) of already classically pre-sintered pellets of Ca349 [7–11,30,34,37,38]. Nevertheless, the samples prepared by CPP and SPS showed similar TE characteristics, which were mostly determined in the direction perpendicular to the pressing direction for the electrical conductivity (σ) and the Seebeck coefficient (S), and in a parallel direction for the thermal conductivity (κ). The samples prepared by the CPP method had, at 630 °C (900 K), an electrical conductivity σ of about 75 S/cm, a Seebeck coefficient S of 190 μV/K and a thermal conductivity κ of about 2.3 W/mK, which led to a ZT of about 0.11 [32]. At the same temperature the SPS samples had a higher σ in the range from 100 to 120 S/cm, an S value of about 170 μV/K, a κ of about 2.1 W/mK and a ZT of about 0.14 [7–11,30,34,37,38]. Nearly perfect microstructural texturing of the Ca349 samples, having densities up to 99% of theoretical, was obtained with hot pressing (HP) [7,8,10,12,16,24,29,30,39] and by employing a modified edge-free SPS method (SPT) [35] on the already pre-sintered pellets. The samples showed slightly enhanced TE characteristics with the following values at 630 °C: σ from 100 to 170 S/cm, S in the range 160–170 μV/K and a much broader range of k from 1.6 to 5.3 W/mK, as well as a ZT in the range from 0.15 to 0.18. Very seldom are there reports of the TE parameters being measured in highly textured samples in both directions. The results of Wu et al. [27] showed a much higher σ of 450 S/cm

in the perpendicular direction than in the parallel (62 S/cm), a slightly higher S in the perpendicular direction (157 S/cm) than in the parallel direction (148 S/cm) and a much lower κ in the parallel direction (1.35 W/mK) than in the perpendicular one (2.7 W/mK). As a result, the obtained ZT value at 630 °C was much higher in the perpendicular direction (0.16) than in the parallel (0.045).

In this work the influence of the precursor's particle size on the synthesis of the Ca349 phase from powders of $CaCO_3$ and Co_3O_4 was studied. It clearly showed that the use of fine-grained starting powders enables the preparation of the pure Ca349 phase at relatively low temperatures and with short sintering times. Furthermore, using single-phase Ca349 powder, the effect of processing on the microstructure and the TE properties of the Ca349 ceramics was studied. We used different processing methods, such as conventional sintering, hot pressing and SPT. However, besides the pre-sintered pellets of Ca349, which were generally used for the SPS and SPT processing, in accordance with reports in the literature, we also used pellets of compacted-only Ca349 powder. Another novelty in this work was the preparation of Ca349 ceramics by cold pressing the pre-sintered Ca349 pellets, either in a stainless-steel die with the same diameter as the pellet, and without subsequent annealing, or in a die with a larger diameter, followed by annealing. The microstructures and the TE characteristics were analyzed in the directions perpendicular and parallel to the applied pressure to elucidate the influence of processing on the microstructure and the TE characteristics of the samples.

2. Experimental

The synthesis of the $Ca_3Co_4O_9$ compound was studied by employing the classic ceramics procedure, using $CaCO_3$ (Alfa Aesar, stock 011403Lot G23W035, 99.5% metals basis, 5 μm) and Co_3O_4 (Alfa Aesar, stock 45806, Lot B29T027, 99.7% metals basis, 2–6 μm), either as obtained powders (label UT, coarse grained) or additionally attrition milled for 6 hours to obtain fine powders (label AM). The particle size of the powders was determined using a Horiba LA-920 laser-scattering particle-size-distribution analyzer. The average particle size of the untreated $CaCO_3$ was about 2.5 μm with a broad and bimodal size distribution, and this was reduced in the AM powder to about 0.45 μm with a narrow size distribution. The untreated Co_3O_4 powder already had quite a narrow size distribution, with an average particle size of about 1.38 μm, while in the AM powder it was even narrower, with a much lower average particle size of about 0.36 μm. Mixtures of the $CaCO_3$ and Co_3O_4 powders in the molar ratio 9:4 were homogenized for 2 hours in a planetary mill in absolute ethanol media and subsequently dried. The powder mixtures, one from the coarse UT and the other from the fine AM starting powders, were uniaxially pressed with 200 MPa into pellets with a diameter of 12 mm and a thickness of about 3 mm. The pellets were calcined either at 760 °C for 12 hours or at 860 °C for 12 hours. While the samples from the UT powder mixture were twice calcined at both temperatures, with intermediate grinding, the samples from the AM powder mixture were calcined only once. The phase composition of the samples and the formation of the Ca349 phase were analyzed after each calcination with X-ray diffraction (XRD) analysis using an X'Pert PRO MPD (Cu-K_α, 2Θ range 5–80 °). The microstructures of the polished cross-sections of the pellets were also analyzed using a JEOL JSM-5800 scanning electron microscope (SEM) equipped with an energy-dispersive x-ray spectrometer (EDXS) and an Oxford Instruments Link Isis software system for the compositional analysis of the phases. The single-phase calcined Ca349 samples prepared from the AM powder mixture were used for the preparation of the Ca349 powder by grinding in an agate mortar for subsequent processing using a variety of methods. For the classic sintering (label CS) the pellets with a diameter 12 mm and a height of either about 3 mm or about 12 mm were uniaxially pressed at a pressure of 220 MPa and sintered in air at 920 °C for 20 hours (sample label CS-920). For the hot pressing (label HP) the pellets with a diameter of 12 mm and a height of about 10 mm were uniaxially pressed at 220 MPa and placed into a corundum model with an inner diameter of 26 mm, which allowed lateral deformation. The HP samples were sintered at 800 °C for 16 h under a uniaxial pressure of 25 MPa (label HP). Using the free-edge SPS processing (SPT), the samples were prepared in two ways, either with the use of Ca349 pellets with a diameter of 10 mm and a height of 14 mm, already classically sintered at 920 °C for 2 hours (label SPT-920), or by using raw pellets of the same dimensions prepared just by compacting the Ca349 powder at a pressure of 760 MPa (label SPT). Both types of Ca349 pellets were placed in a graphite die with a diameter of 19.5 mm, which allowing free lateral deformation of the sample during the processing. The samples were treated using spark-plasma sintering system (Dr. Sinter, SPS Sintex inc.) in vacuum (3×10^{-4} bar), under a uniaxial pressure of 50 MPa and at a dwell temperature of 900 °C for 2 min, obtained with a pulsed electric current (3 V, 1100 A). The as-prepared SPT samples were afterwards grinded to remove the graphite foil from the surface for further characterizations. For the processing with cold pressing (CP), pellets sintered at 760 °C for 12 hours were used, having a diameter of either 10 mm or 16 mm. The pellets with a diameter of 10 mm were placed into the stainless-steel die with the same diameter and uniaxially pressed under a pressure of 380 MPa. In this way samples with heights of about 8 mm (initially about 11 mm) were prepared, which were afterwards not annealed (samples labeled CP). The pellets with a diameter of 16 mm and a height of about 6 mm were placed into the stainless-steel die with a diameter of 22 mm and pressed with a pressure of 210 MPa. The obtained pellets with a diameter of 22 mm and a height of about 3.5 mm were very compact; nevertheless, they were annealed at 920 °C for 20 hours (label CP-920).

The phase compositions of the Ca349 samples prepared by the classic sintering (CS) method, the hot pressing (HP), the free-edge spark-plasma sintering (SPT) and the cold pressing (CP) were checked with x-ray powder-diffraction analysis

(XRD). The degree of orientation for the textured specimens was evaluated using the Lotgering factor, for which a value of f is calculated using the XRD peak intensity [40]:

$$f = \frac{(P-Po)}{(1-Po)} P = \left(\frac{\Sigma I\,(00l)}{\Sigma I\,(hkl)}\right),$$

where P is the ratio of the peak intensity (I) between $2\theta = 8^\circ$ and 43°, and P_o is the P for a randomly oriented specimen (JCPDS cards, No. 21-0139). The densities were measured using a Densitec density-measurements system (Metar sa, Matran, Switzerland). Fractured and polished microstructures of the samples in the cross-section direction of the pellets were analyzed on the scanning electron microscope (SEM) JEOL JSM-5800.

The TE characteristics of the samples, the electrical conductivity (σ), the Seebeck coefficient (S) and the thermal conductivity (κ), used to determine the figure of merit ZT, were analyzed in two different ways from room temperature up to about 627 °C. One set of TE characterizations was made using different instruments to measure the TE parameters (combined TE measurements-CM). The thermal diffusivity measurement was carried out by employing a commercial laser-flash apparatus (LFA, 427, Netzsch Gerätebau, Selb, Germany). The specific heat was determined using DSC (Netzsch) and the density was determined using Archimedes' principal. The κ was calculated using $\kappa(T) = \alpha(T)*c_p(T)*\rho(T)$, where κ is the thermal conductivity, α is the thermal diffusivity, c_p is the specific heat and ρ is the density of the material. Temperature-dependent S and σ measurements were carried out using a custom-built setup in a He atmosphere [41]. The measurement accuracy was estimated to be 8% for κ, 5% for σ and 5% for S, based on an intra-laboratory comparison, and the data analysis is described elsewhere [42]. The measurements were performed on the disc samples with a diameter of 10 mm and a height of about 2 mm, for the Seebeck coefficient S and the electrical conductivity σ in the direction perpendicular to the pressing direction, and for the thermal characteristics in a direction across the thickness of the disc (parallel to the pressing direction). In the case of the textured samples, the measurement in the direction perpendicular to the pressing direction is also an in-plane direction, coinciding with the a–b planes of the Ca349 compound, while the direction parallel to the pressing direction means a measurement across the thickness of the plate-like grains, so in the out-of-plain direction. The specimen's dimensionless figure of merit ZT was calculated according to the expression $ZT = S^2T/\rho(\kappa)$. The other set of measurements was made on a home-made Z-meter [43] based on the "Large ΔT method" in a vacuum of 10^{-2}–10^{-3} Pa on samples with a preferred height from 6 to 10 mm and a diameter of less than 12 mm, with a simultaneous measurement of S, σ and κ. With the Z-meter, the measurements were made on the same piece, a block with edges of around 6 mm, for selected samples in both directions, parallel and perpendicular to the applied pressure, which enabled an evaluation of the influence of the microstructural anisotropy (texturing) on the TE characteristics.

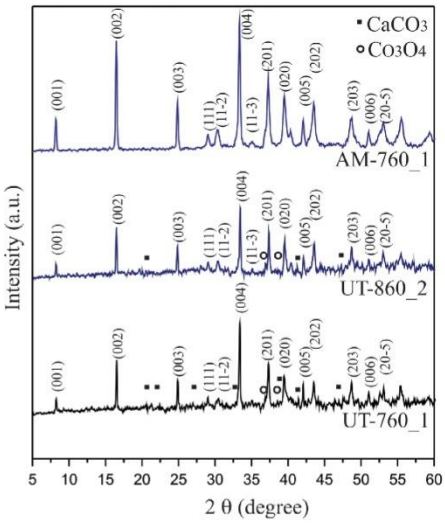


Fig. 1. The x-ray powder-diffraction patterns of the samples prepared from coarse, untreated (UT) and fine-grained attrition-milled (AM) powders of $CaCO_3$ and Co_3O_4, calcined at 760 °C or 860 °C for 12 h.

3. Results and discussion

3.1. XRD characterisation

The phase-composition analysis of the calcined samples using the XRD analysis showed a strong influence of the particle size of the $CaCO_3$ and the Co_3O_4 in the starting-powder mixtures on the formation of the $Ca_3Co_4O_9$ (Ca349) phase. With the mixtures of untreated (UT) powders, the pure Ca349 phase was not obtained, even after repeated calcinations at 760 °C, or also a higher temperature of 860 °C, and the presence of unreacted Co_3O_4 and especially $CaCO_3$ was detected. In contrast, the XRD of the pure Ca349 phase was obtained from a mixture of attrition-milled (AM) starting powders after just a single calcination at 760 °C (AM-760_1). The XRD patterns of the UT-760_1, the UT-860_2 and the AM-760_1 samples are presented in Fig. 1.

While in the sample AM-760_1 only peaks of the Ca349 phase are present (JCPDS 021-0139), the peaks of the $CaCO_3$ phase are still present even in the UT-860_2, and the intensity of the Ca349 peaks is also much lower. This showed that the quality of the starting powders has a key influence on the synthesis of the Ca349 phase and that the sluggishness reported for the formation reactions of the Ca349 phase [15] was likely a consequence of the coarse-grained starting powders.

3.2. Microstructure and processing

The microstructures of the UT and the AM samples calcined at 760 °C and 860 °C are given in Fig. 2. All the samples are

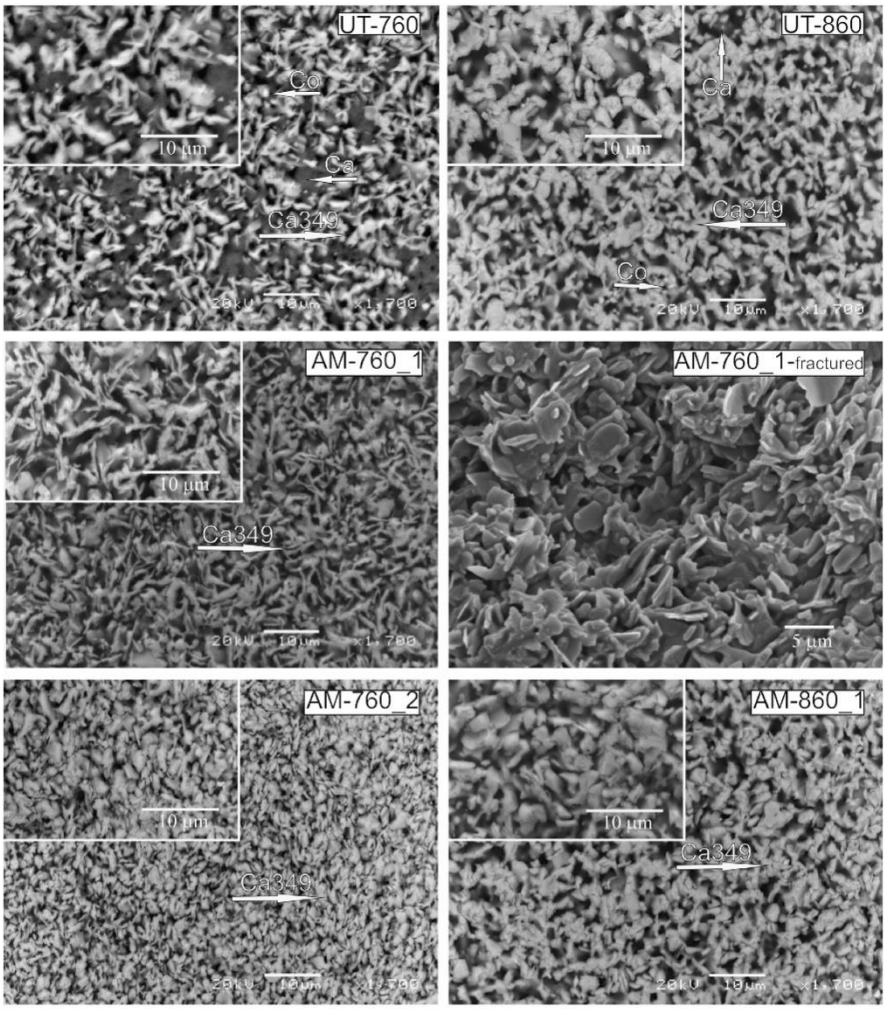


Fig. 2. SEM micrographs of polished and fractured surfaces of the $Ca_3Co_4O_9$ samples, prepared from untreated (UT) and attrition milled (AM) powders of $CaCO_3$ and Co_3O_4, calcined at 760 °C and 860 °C either once or twice (labelled _1 or_2, respectively).

highly porous with a density of only about 50% of theoretical (4.68 g/cm^3). In the UT samples, among the irregular-shaped, plate-like grains of the Ca349 phase, unreacted $CaCO_3$ and Co_3O_4 are present, but in smaller amounts at the higher calcination temperature. The SEM examinations supported by the EDXS analysis of the microstructure of the sample AM-760_1 confirmed the result of the XRD analysis, i.e., that already after the first calcination at 760 °C a single-phase Ca349 was obtained. Additional calcinations at the same or higher temperature of the samples AM-760_2 and AM-860_1, respectively, affected only the morphology of the plate-like Ca349 grains, which became thicker with more regular-shaped and rounded edges. After a single calcination at 760 °C the sample AM-760_1 had, from among all the calcined samples, the most distinct flake-like morphology of thin and irregular shaped grains with sharp edges. Due to the morphology of the Ca349 grains, precise measurements of the grain size are practically impossible. Hence, a reasonable estimation was made from a rough measurement of about 40 grains per sample, with clearly visible edges from the SEM image of a fractured surface. In the sample AM-760_1 the plate-like grains had a length in the range 1–3 µm, with a thickness in the range 0.1–0.2 µm. In the sample AM-860_ the grains had length in the range 2–3.5 µm and a thickness of approximately

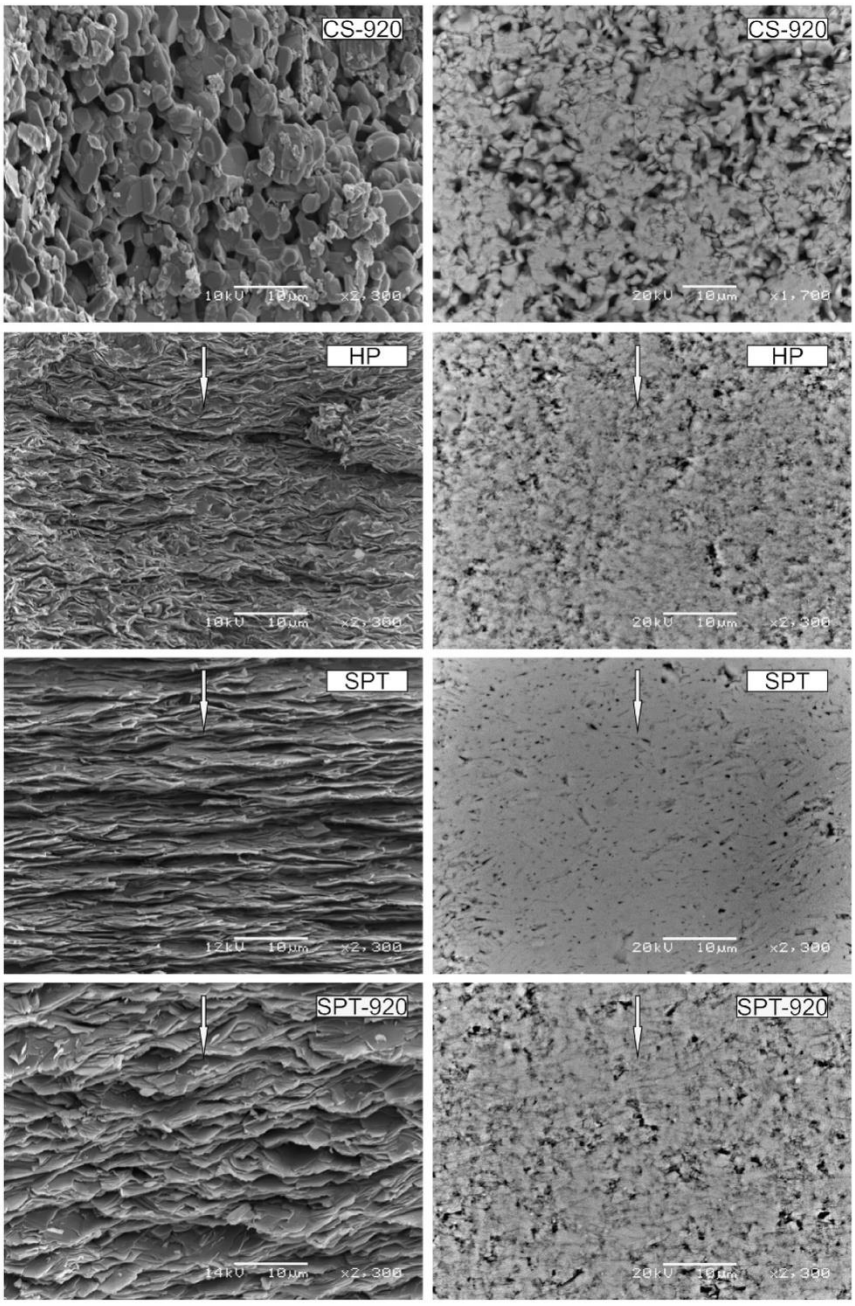


Fig. 3. SEM micrographs of fractured (left column) and polished (right column) surfaces of the $Ca_3Co_4O_9$ samples prepared by classic sintering at 920 °C (CS-920), hot pressing (HP), edge-free SPS of just compacted Ca349 powder (SPT) and the edge-free SPS of Ca349 ceramics already sintered at 920 °C (SPT-920). The arrow indicates the stress direction.

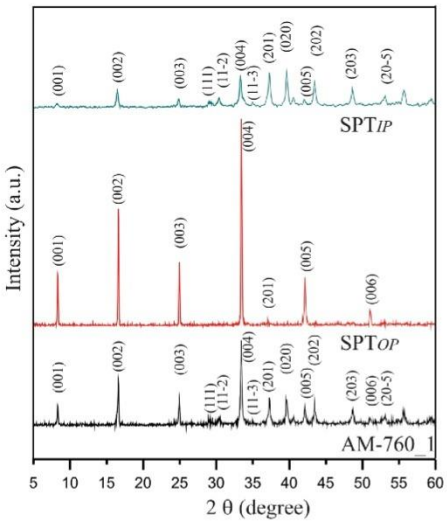


Fig. 4. The x-ray diffraction (XRD) patterns recorded on polished surfaces of the AM-760_1 sample in the parallel direction and the SPT sample in the parallel out-of-plane (*OP*) direction and the perpendicular in-plane (*IP*) direction.

0.7 μm. The finer grain size of the single-phase Ca349 powder is expected to enable the preparation of better Ca349 ceramics, which is also supported by the reports in the literature that fine-grained Ca349 ceramics had much better TE characteristics, i.e., higher ZT values [25,28]. Hence, for the subsequent preparation of the Ca349 ceramics using different processing methods, single-phase powders of Ca349 were prepared from the AM samples calcined at 760 °C for 12 h (AM-760_1).

The microstructures of the Ca349 ceramics prepared by different processing methods, i.e., classic sintering (CS), hot pressing (HP), free-edge spark-plasma sintering (SPT) and cold pressing (CP) are shown in Figs. 3 and 5. It is obvious that the type of processing had a significant influence on the microstructure development. The classically sintered sample at 920 °C for 20 hours had a high porosity and a density of about 60.2% of theoretical. The completely randomly oriented, plate-like grains of the Ca349 phase have a relatively uniform grain size with a length of around 3.7 μm and a thickness of approximately 0.8 μm. In comparison with the calcined sample AM-760_1 with a density of about 50%, the sintering of the sample CS-920 at 920 °C resulted in only a modest increase in the density. However, the grains of the Ca349 phase changed noticeably, not so much in regard to their length, but in terms of the shape and the thickness. With the hot-pressing at 800 °C for 16 hours the density of the sample HP reached 94% of

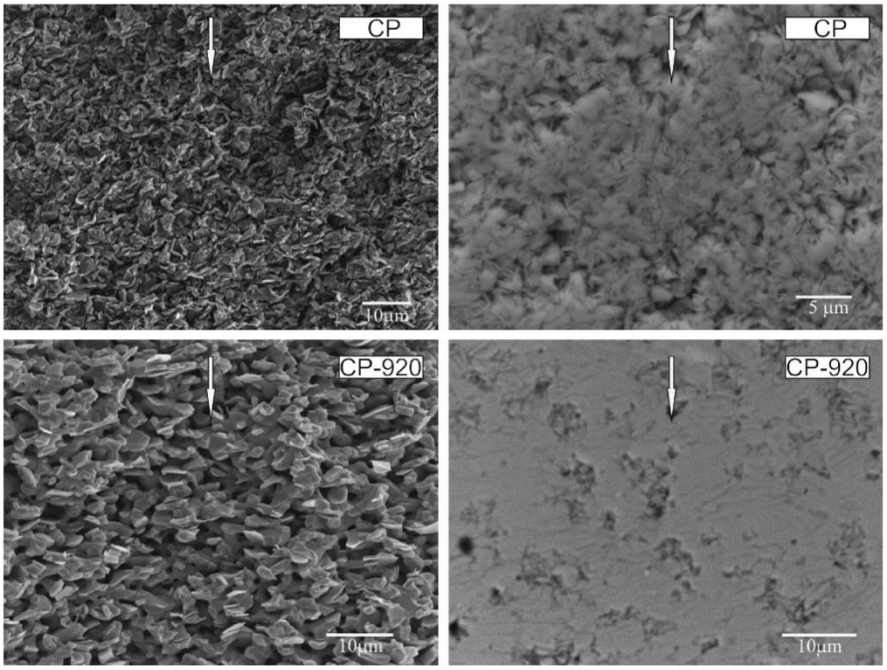


Fig. 5. Comparison of the SEM images of the fractured surfaces (left column) and the polished surfaces (right column) for the cold-pressed (CP) sample and cold-pressed sample with subsequent annealing at 920 °C (CP-920). The arrow indicates the stress direction.

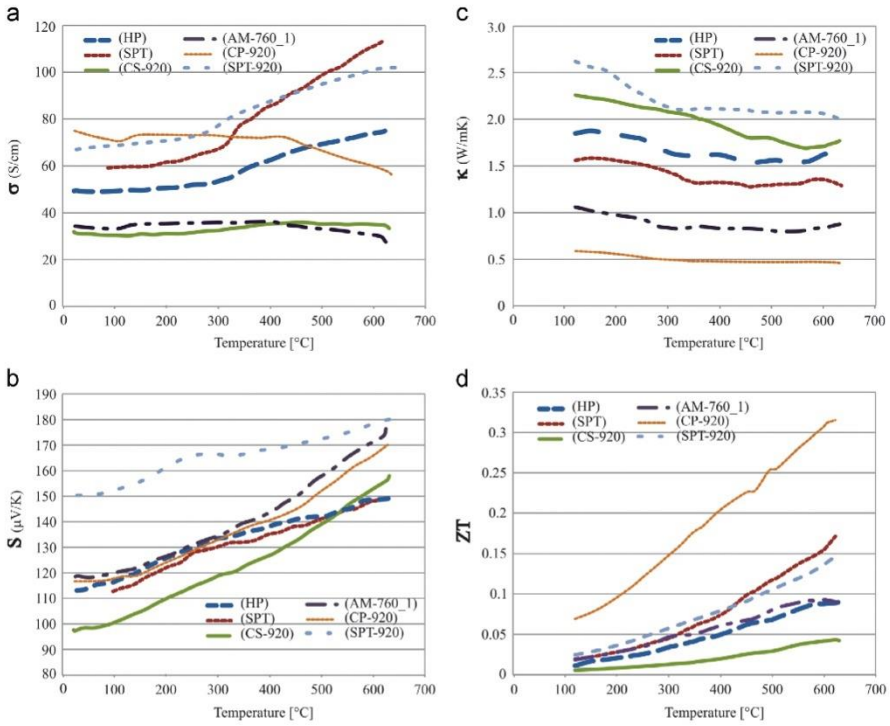


Fig. 6. Temperature dependence of the electrical conductivity σ, the Seebeck coefficient S, the thermal conductivity κ and the figure of merit ZT for the Ca349 samples prepared with different processing methods.

theoretical, (see Fig. 3) In the fractured microstructure the preferential alignment of the plate-like grains in the direction perpendicular to the applied stress is already evident, indicating quite high (f=0.77) texturing of the microstructure. The grains with irregular and sharp edges have a length of about 5 μm and a thickness of about 0.4 μm. The edge-free spark-plasma sintering (SPT) at 900 °C (2 minutes) of just the compacted pellet of the Ca349 powder resulted in a practically fully dense (99% of theoretical density) SPT sample, having perfectly aligned grains in the direction perpendicular to the applied stress and hence almost perfect texturing (f=0.99), which is clearly evident from the microstructures, as well as from the x-ray diffraction (XRD) patterns recorded on the polished surfaces, shown in Figs. 3 and 4, respectively. Very thin, about 0.1 μm, and sharp-edged, plate-like grains have a length from about 8 to 12 μm. With the edge-free spark-plasma sintering (SPT) at 900 °C (2 minutes) of the Ca349 pellet, which was pre-sintered at 920 °C for 2 hours, a highly dense and textured (f=0.91) sample of SPT-920 was also obtained; however, both of these characteristics were slightly reduced in comparison to the sample SPT made from the compacted-only Ca349 pellet. The difference is clear from a comparison of their microstructures, given in Fig. 3. The sample SPT-920 had a density of about 97% of theoretical and its sharp-edged, plate-like Ca349 grains with a greater thickness of about 0.3 μm have a shorter length of about 6.5 μm.

The classically sintered Ca349 ceramics have a high porosity caused by the random growth of the plate-like Ca349 grains in all directions, which inevitably leave empty spaces in between. Therefore, we considered that cold pressing of the sintered pellets of the Ca349 ceramics could increase their density due to the alignment of the grains and the microstructure texturing caused by possible breaking of the grains and perhaps even their 'gliding' during the cold deformation. Such cold processing of sintered pellets with a density of about 50% of theoretical is known to result in a highly dense (about 82% of theoretical) and textured microstructure for high Tc superconducting $(Bi,Pb)_2Sr_2Ca_2Cu_3O_{10}$ ceramics, which also have a pronounced plate-like morphology of the grains [44]. The microstructure of the sample prepared by cold pressing of the sample AM-760_1 is presented in Fig. 5. The density of the sample evidently increased in comparison to AM-760_1 (see Fig. 2): the measurements indicated from about 50% to 78% of the theoretical. However, no improvement in the texturing of the microstructure in general was obtained, only a local alignment of the Ca349

grains within randomly distributed areas. The morphology and size of the grains remained more or less the same as in the unprocessed starting sample AM-760_1, which could be expected in the absence of any subsequent thermal treatment. The free-edge cold pressing with subsequent annealing at 920 °C resulted in only modest texturing (f=0.21) and an increase in the density of the sample CP-920 to about 65% of theoretical. A long annealing of 20 hours at high temperature increased the initial thickness of the Ca349 grains from about 0.15 to about 0.3 μm and the length from about 2 to about 3.5 μm, while the sharp-edged, plate-like morphology remained. Interestingly, these changes in the grain size and the morphology are noticeably smaller than when a pellet from the AM-760_1 powder is sintered under the same heat-treatment regime (CS-920). Obviously, the grinded powder prepared from the AM-760_1 sample is more reactive, probably due to the irregular shape of the highly defected and strained structure of the Ca349 grains.

A microstructural analysis revealed that the type of processing method noticeably influenced the microstructure development in the Ca349 ceramics: the density, the shape and the thickness of the plate-like grains, and their alignment, which determines the degree of the microstructure texturing. All these microstructural features probably influenced the TE characteristics of the samples.

3.3. Thermoelectric properties

The TE characteristics of the Ca349 ceramic samples were measured in two different ways, either with the use of different instruments to assess all the electrical and thermal characteristics (σ, S, α and c_P) required to determine ZT (combined TE measurements – CM) or with a simultaneous measurement of σ, S and κ on the Z-meter. This is related to a possibility of preparing suitable samples for certain types of measurements and our aspiration to evaluate the influence of anisotropy. The preparation of the disc samples with a thickness of a few millimetres, which are proper for the CM measurements, is rather straightforward using any of the processing methods used in this work. However, for the Z-meter measurements, to determine the influence of anisotropy, taller samples are required, which is much more demanding, especially in the cases of the SPT and the HP processing methods.

The TE characteristics determined with the combined measurements (CM) for differently prepared samples are given in Fig. 6. The sample CS-920 showed a relatively constant electrical conductivity of approximately 33 S/cm with temperature (Fig. 6a). The electrical conductivity in the HP, SPT and SPT-920 samples is relatively constant up to a temperature of about 300 °C, i.e., 50 S/cm, 60 S/cm and 70 S/cm, respectively, while at higher temperatures a typical semiconducting behaviour is clearly evident. Hence, at 627 °C they had σ values of 75 S/cm, 115 S/cm and 102 S/cm, respectively. In contrast, the relatively constant electrical conductivities of the sample AM-760_1 of 35 S/cm and the sample CP-920 of 75 S/cm showed a transition to metallic behaviour at temperatures above approximately 420 °C, especially in the sample CP-920. The obtained conductivities of the samples closely correlate with their microstructures, i.e., a higher density and a higher degree of texturing resulted in a higher conductivity of the sample. This could be expected since in the highly textured samples the conductivity is measured in the in-plane direction, along the longest dimension of the plate like grains and in the direction with the least number of grain boundaries. According to the report of Bhattacharya et al. [45] the conductivity at room temperature of a single crystal of Ca349 is almost five times higher in the in-plane than in the out-of-plane direction. The sample SPT with the highest density and also the highest degree of texturing of the plate-like grains, also had the highest σ of 115 S/cm at 627 °C, comparable to the values reported in the literature [7–11,30,34,35,37,38,46]. The samples with a lower density and texturing, the SPT-920 and the HP, already had a lower conductivity, while it was much lower for the highly porous samples AM-760_1 and CS-920 with a completely random orientation of the plate-like Ca349 grains.

The temperature dependence of the Seebeck coefficient S in the temperature range from room temperature to approximately 630 °C is shown in Fig. 6b. The AM-760_1 sample showed a strong increase of S with temperature from 118 μV/K at room temperature to 174 μV/K at 627 °C. The sample has a high porosity, irregular-shaped and thin plate-like grains with sharp edges, which are randomly oriented (see Fig. 2). According to the Slater theory [47], the energy barriers at the grain boundaries are higher in a polycrystalline material with a smaller grain size, which results in enhanced scattering of the charge carriers. Seto [48] worked out that the relationship between the carrier concentration and the barrier height is reciprocal, i.e., a higher barrier means a lower carrier concentration. Accordingly, in the fine-grained ceramics only charge carriers with a higher energy can cross the grain boundaries, their number is reduced and they have a higher average energy. It is well known that such energy filtering results in a higher Seebeck coefficient S [49]. Only a slightly lower S in comparison to the AM-760_1 was found in the sample CP-920 – a sample that was prepared by cold pressing of the sample AM-760_1 and subsequent annealing at 920 °C for 20 hours. While both samples have a similar grain size, grains are already slightly aligned and more rounded in the sample CP-920, which also has the higher density. Very similar grain distribution to the sample AM-760_1, but with higher (however still low) density of 60% had the sample CS-920. Because of larger and much thicker plate-like grains with a more regular and rounded shape, it had a consistently lower S across the entire temperature range of the measurement in comparison to the AM-760_1, extending from 97 μV/K to 156 μV/K. In the CM the S is measured perpendicular to the pressing direction; hence, with increasing texturing of the microstructure it is more and more determined in the in-plane direction. This can affect the obtained value of S in subtle ways due to differences in the nature of the grain boundaries, caused by fine variations in the alignment of the grains at the grain boundary and also by the degree of the structural disorder within the individual plate-like grains (i.e., the mismatch between the substructures of the Ca349 phase) [25]. These microstructural and structural parameters are difficult for a comprehensive assessment of their influence on S and are certainly influenced by the entire history of

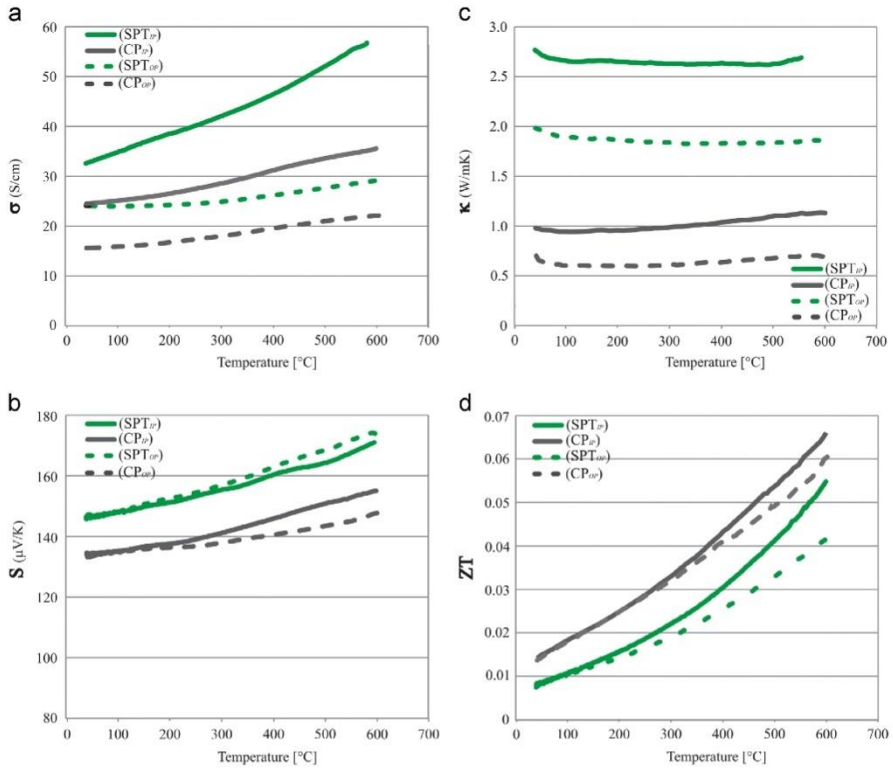


Fig. 7. Temperature dependence of the electrical conductivity σ, the Seebeck coefficient S, the thermal conductivity κ and the figure of merit ZT for the SPT and the CP samples of the Ca349 ceramics measured according to the applied pressure in parallel, i.e., in-plane (*IP*) and perpendicular, i.e. out-of-plane (*OP*) directions.

the samples' preparation. They are probably expressed in values of S obtained for the samples of the Ca349 ceramics with densities above 90% and high (but different) degrees of texturing (Fig. 3). Interestingly, the sample HP with the lowest density and degree of texturing and the sample SPT having both the highest, but with quite different lengths and thicknesses of the plate-like grains, had very similar S values across the entire temperature range of the measurement. However, the sample SPT-920 with microstructural parameters (density, grain size and shape, texturing) somewhere in between the HP and SPT samples had the highest S, ranging from 150 μV/K at room temperature to 180 μV/K at 627 °C. According to the literature, this value is among the highest reported for polycrystalline Ca349 ceramics [8–11,30,34,37,38].

The thermal conductivity κ of the studied samples is shown in Fig. 6c. The textured samples (HP, SPT-920 and SPT) with densities above 90% had some of the higher values of κ among the analyzed samples. The sample SPT with the highest density and the highest degree of texturing (Fig. 3), but also with much thinner grains, also had the lowest κ of approximately 1.45 W/mK. Between the other two samples with a similar degree of texturing and grain thickness, the HP and the SPT-920, a lower κ of 1.65 W/mK was observed for the samples HP with lower density. As expected, the sample AM-760_1 with the lowest density and random orientation of thin plate-like grains had a much lower κ of approximately 0.8 W/mK. The lowest κ of only 0.50 W/m, which to the best of our knowledge is among the lowest reported for Ca349-type ceramics [25,26,50], was obtained for the CP-920 sample, because of a relatively low density of 65% and relatively small and thin plate-like grains, which are already slightly textured. A surprisingly high κ of approximately 2 W/mK was observed for the sample CS-920 with a low density of 60% and a random orientation of the grains. However, in comparison to all the other samples it has significantly thicker and rounded plate-like grains, which are also much longer compared to the other samples with a random grain orientation, which probably results in less effective phonon scattering.

The dimensionless figure of merit ZT determined with CM for all the prepared materials is shown in Fig. 6d. The CP-920 sample showed the highest ZT across the whole temperature range of measurement with a remarkable value of 0.31 at 627 °C and, to the best of our knowledge, this ZT is one of the highest or even the highest value obtained for the un-doped Ca349 ceramics according to the literature [24,27,29]. It

should be noted this value is obtained with the combination of the in-plane σ and S with out-of-plane κ as in the most of other reports [6,8,9,16,17,24,26,29,31–33]. In comparison to them is excellent, however we would like to emphasise all such combined values (the majority of reports) are probably slightly overestimated due to the anisotropy of the samples. The sample was prepared using an original preparation method for the Ca349 ceramics of cold pressing, which had specific influence on the microstructure; The higher ZT value of the CP-920 in comparison to the other samples is a result of its relatively high electrical conductivity σ, medium values of the Seebeck coefficient S and the lowest thermal conductivity κ; such TE characteristics are certainly related to the distinct microstructure of the sample in regard to the morphology and size of the Ca349 grains, being also modestly oriented, which contributed to σ, while the low density goes with the low κ. The samples SPT and SPT-920 had similar ZT values, but much lower than the CP-920; while below 450 °C the sample SPT-920 °C had slightly higher ZT values, it is vice versa above this temperature so that at 627 °C the sample SPT had a ZT of 0.17 and the SPT-920 had a ZT of 0.15. For very different microstructures, which resulted either in higher σ and also higher κ in the samples HP or at lower σ also in lower κ in the sample AM-760_1, they had similar ZT values, lower than both of the SPT samples, especially above 350 °C, ranging from approximately 0.015 at 120 °C to approximately 0.09 at 627 °C. The lowest ZT, ranging from 0.01 to 0.04, was determined for the CS-920 sample, which could be expected from it having the lowest σ and S and among the highest κ of the analysed samples.

The results of the TE measurements using the Z-meter for selected textured samples in both directions, in-plane (IP) and out-of-plane (OP), are given in Fig. 7. In all the samples the electrical conductivity σ showed a semiconducting characteristic and increased with the temperature, which was more pronounced for the SPT sample with the highest density and degree of texturing in the in-plane direction, which also had the highest σ from 32 to 57 S/cm in the temperature range from 50 to 600 °C, respectively. In the out-of-plane direction the sample SPT already had a lower σ, ranging from 25 to 29 S/cm. The CP sample with the lower degree of texturing had, in the in-plane direction, a similar σ as the SPT_{OP} in the range from 25 to 35 S/cm, and, as expected, an even lower σ in the out-of-plane direction, ranging from 16 to 22 S/cm. However, the difference in σ between the in-plane and out-of-plane directions is slightly smaller for the CP samples with a lower degree of texturing than for the highly textured SPT samples. Despite the quite different σ, the SPT_{IP} and the SPT_{OP} (Fig. 7b) had a similar Seebeck coefficient S, ranging from 146 μV/K at 50 °C to 174 μV/K at 600 °C, which is obviously the consequence of the anisotropic geometry. Interestingly, the samples CP with a much lower density, degree of texturing and probably also a high concentration of stress defects due to cold pressing without subsequent annealing, with either a similar or lower σ, showed a noticeably lower S than the SPT samples in both directions. This could indicate the energy filtering effect [49, 51]. In addition, in the CP samples, at temperatures above 200 °C the S in the in-plane direction becomes progressively larger than in the out-of-plane direction, reaching a value of 156 μV/K at 600 °C vs. 147 μV/K of the out-of-plane direction. The obtained results clearly demonstrate the complex dependence of the Seebeck coefficient on the microstructural features in the Ca349 ceramics. The thermal conductivities κ of the samples SPT and CP in the in-plane and out-of-plane directions measured using the Z-meter are presented in Fig. 7c. As expected, the highly dense and textured samples SPT (Fig. 3) had, in the in-plane direction, a higher κ of 2.7 W/mK (for the single crystal a calculated κ of 3 W/mK is reported [5]) than in the out-of-plane direction (1.87 W/mK). Although the difference is quite large, an even lower κ could be expected for the out-of-plane direction. In the in-plane direction the length of the plate-like grains is approximately 10 μm and their thickness in the out-of-plane direction approximately 0.15 μm, which means that the number of grain boundaries per unit thickness is about 70-times larger in the out-of-plane than in the in-plane direction. In this view obviously the grain boundaries between the densely packed, plate-like Ca349 grains in out-of-plane direction relatively weakly affect the phonon scattering that is essential for a much larger reduction of κ. The same consideration about the influence of the grain boundaries could also be applied for the electrical conductivity σ of the SPT sample; while in the single crystal the value of σ is about five times lower in the out-of-plane than in the in-plane direction, while it is just 1.5 times lower in the SPT sample. Both κ values of the SPT sample are about three times higher in comparison to the κ values of the CP sample with a much lower density and degree of texturing (Fig. 5), being approximately 1 W/mK for the in-plane direction and just 0.6 W/mK in the out-of-plane direction. The obtained results indicate that a lower density with more or less randomly orientated plate-like grains can result in a much lower κ than could be achieved in fully dense and highly textured Ca349 ceramics. It is also clearly seen that the texturing has a much higher impact on the conductivities, electrical σ and thermal κ, than on the Seebeck coefficient S of the Ca349 ceramics, which coincides with the literature reports [27].

The values of the figure of merit ZT of the SPT and CP obtained from the measurements of the TE characteristics using the Z-meter are shown in Fig. 7d. The CP sample had, in both directions, similar ZT values and values higher than those of the SPT sample; in the in-plane direction from 0.015 at 50 °C to 0.066 at 600 °C and in the out-of-plane direction slightly lower above 250 °C, reaching 0.06 at 600 °C. For the SPT sample, the ZT values are slightly higher for the in-plane direction, from 0.008 to 0.055, in comparison to values from 0.008 to 0.041 in the out-of-plane direction. As the SPT sample had, for both directions, a higher S and a higher or at least similar σ, obviously the higher ZT values of the CP sample in both directions result from its much lower thermal conductivity.

4. Conclusions

The synthesis of the $Ca_3Co_4O_9$ (Ca349) phase from powders of $CaCO_3$ and Co_3O_4 using the classic ceramic procedure was

studied. We showed that with the use of fine starting powders the solid-state synthesis of the single-phase Ca349 is very simple, with a single calcination at 760 °C. Such ceramics are rather porous, with small and very thin plate-like grains of irregular shape, and with a surprisingly high ZT of 0.094 at 627 °C. We have shown that preserving such a fine, plate-like morphology with the minimum heat treatment at the lowest-possible temperatures is an important advantage for the preparation of Ca349 ceramics with better TE characteristics, as the results showed that at higher temperatures the plate-like grains become larger and much thicker, with a rounded shape, and the ceramics have a similarly low σ, but also a lower S and a much higher κ, all resulting in a noticeably lower ZT. Fine, plate-like ceramics can be further used as a material for the preparation of the starting Ca349 powder, for the processing of the Ca349 ceramics, or they can simply be processed.

Therefore, a comprehensive study using the same starting powder for the Ca349 was made, which gave an objective comparison about the influence of some already-reported processing methods (conventional sintering – CS, hot pressing – HP, free-edge spark-plasma sintering of a sintered pellet – SPT-920), some newly modified methods (free-edge SPS of a pellet from just-compacted powder – SPT) and novel processing methods, such as cold pressing of a sintered Ca349 pellet without post annealing (CP) and free-edge cold pressing of a sintered Ca349 pellet with post annealing (CP-920) on the microstructure, i.e., the density, size and morphology of the grains and texturing, and the TE characteristic of the Ca349 ceramic. Generally, it is considered that a high density and microstructure texturing are preferred for the enhancement of the TE characteristics. However, our results clearly revealed the limitations of such an approach. For a completely random orientation of plate-like grains and a high porosity, the Ca349 ceramics have a low thermal conductivity κ, but due to the limited connectivity among the grains, they also have a low electrical conductivity σ and a high Seebeck coefficient S. However, with increasing density, which for the plate-like morphology of the grains goes together with an increased degree of texturing, the σ is only high in the in-plane direction, the S is similar as for the porous samples, while the κ is increased a great deal for both directions, all resulting in only a slightly higher ZT than in the simply prepared sample with a very high porosity. Hence, we clearly showed that a compromise between the density and the degree of texturing gives the best TE characteristics. The original processing with free-edge cold pressing of the calcined single-phase Ca349 ceramics, and with a subsequent annealing, still resulted in highly porous ceramics (65% of t.d.), but already with slightly textured, small and thin, sharp-edged, plate-like grains, which resulted in a relatively high σ, a high S, and a very low κ (0.47 W/mK), all giving the highest ZT obtained in this work of 0.31 at 627 °C. This is one of the highest, if not the highest, reported ZT for polycrystalline Ca349 ceramics, to the best of our knowledge.

The hot pressing (HP), the free-edge SPS of the already-sintered pellet (SPT-920) and the novel free-edge SPS of a pellet from just-compacted powder of Ca349 (SPT) resulted in an increased degree of texturing, consequently, an increase in the density of the Ca349 ceramics from 94% of t.d. to 97% and to 99%, and finally in an increase in ZT from 0.09, to 0.14, and then to 0.17 at 627 °C. Certainly, the use of a pellet from compacted-only powder of the Ca349 phase in the SPS processing, as applied for the first time in this work, showed benefits in comparison to the typical practice of using already-sintered pellets, as the performance was about 13% better. Simultaneous measurements of the TE parameters on the Z-meter for the same block of sample in both directions, parallel and perpendicular to the applied stress, and a comparison between fully dense and textured Ca349 ceramics and highly porous Ca349 ceramics, gave additional support to previous findings and clearly showed the influence of density and microstructure anisotropy (texturing) on each TE parameter.

Our results showed that with a proper microstructure the TE characteristics of the Ca349 ceramics could be noticeably improved; however, for a major breakthrough in increasing the value of ZT, the electrical conductivity σ is too low, even in the favoured in-plane direction, and should be significantly increased by proper doping.

Acknowledgement

The authors acknowledge the financial support by the Slovenian Research Agency (Program Contract No. P2-0084, Project Grant L2-4192 and Young Researcher Program PR-03102).

References

[1] I. Terasaki, Y. Sasago, K. Uchinokura, Large thermoelectric power in $NaCo_2O_4$ single crystal, Phys. Rev. B 56 (1997) 12685–12687.

[2] D. Vengust, B. Jancar, A. Sestan, M.P. Svet, B. Budic, D. Suvorov, Chemical decomposition as a likely source of ambient and thermal instabilities of layered sodium cobaltate, Chem. Mater. 25 (2013) 4791–4797.

[3] M.L. Foo, T. Klimczuk, R.J. Cava, Hydration phase diagram for sodium cobalt oxide $Na_{0.3}CoO_2 \bullet yH_2O$, J. Mater. Res. Bull. 40 (2005) 665–669.

[4] A.C. Masset, C. Michel, A. Maignan, M. Hervieu, O. Toulemonde, F. Studer, B. Raveau, Misfit-layered cobaltite with an anisotropic giant magnetoresistance: $Ca_3Co_4O_9$, Phys. Rev. B 62 (2000) 166–175.

[5] M. Shikano, R. Funahashi, Electrical and thermal properties of single-crystalline $(Ca_2CoO_3)_{0.7}CoO_2$ with a $Ca_3Co_4O_9$ structure, Appl. Phys. Lett. 82 (2003) 1851–1853.

[6] S. Li, R. Funahashi, I. Matsubara, K. Ueno, S. Sodeoka, H. Yamada, Synthesis and thermoelectric properties of the new oxide materials $Ca_{3-x}Bi_xCo_4O_{9+\delta}$ $(0.0 < x < 0.75)$, Chem. Mater 12 (2000) 2424–7242.

[7] D. Kenfaui, D. Chateigner, M. Gomina, J.G. Noudem, Anisotropy of the mechanical and thermoelectric properties of hot-pressed single-layer and multilayer thick $Ca_3Co_4O_9$ Ceramics, Int. J. Appl. Ceram. Technol. 8 (2011) 214–226.

[8] C. Yuankui, C. Chuan, L. Xiang, Effect on the properties of different preparation process in Ca3Co4O9 thermoelectric material, 2010 International Conference on Electrical and Control Engineering-ICECE Wuhan, China, (2010) 4672-4676.

[9] R. Tian, R. Donelson, C.D. Ling, P.E.R. Blanchard, T. Zhang, D. Chu T.T. Tan, S. Li, Ga substitution and oxygen diffusion kinetics in $Ca_3Co_4O_{9+\delta}$-based thermoelectric oxides, J. Phys. Chem. 117 (2013) 13382–13387.

[10] D. Kenfau, D. Chateigner, M. Gomina, J.G. Noudem, Texture, mechanical and thermoelectric properties of $Ca_3Co_4O_9$ ceramics, J. Alloy and Compd 490 (2010) 427–429.

[11] D. Kenfaui, G. Bonnefont, D. Chateigner, G. Fantozzi, M. Gomina J.G. Noudem, $Ca_3Co_4O_9$ ceramics consolidated by SPS process: optimization of mechanical and thermoelectric properties, Mater. Res. Bull. 45 (2010) 1240–1249.

[12] H. Wang, X. Sun, X. Yan, D. Huo, X. Li, J.-G.- Li, X. Ding, Fabrication and thermoelectric properties of highly textured $Ca_9Co_{12}O_{28}$ ceramic, J. Alloy. Compd. 582 (2014) 294–298.

[13] G. Constantinescu, Sh Rasekh, M.A. Torres, P. Bosque, J.C. Diez M.A. Madre, A. Sotelo, Effect of Na doping on the $Ca_3Co_4O_9$ thermoelectric performance, Ceram. Int. 41 (2015) 897–903.

[14] G. Constantinescu, M.A. Madre, Sh Rasekh, M.A. Torres, J.C. Diez, A. Sotelo, Effect of Ga addition on Ca-deficient $Ca_3Co_4O_9$ thermoelectric materials, Ceram. Int. 40 (2014) 255–260.

[15] E. Woermann, A. Muan, Phase equilibria in the system Cao-cobalt oxide in air, J. Inorg. Nucl. Chem. 32 (1970) 1455–1459.

[16] N.V. Nong, C.J. Liu, M. Ohtaki, Improvement on the high temperature thermoelectric performance of Ga- doped misfit-layered $Ca_3Co_{4-x}Ga_xO_{9+\delta}$ (x = 0, 0.05, 0.1 and 0.2), J. Alloy. Compd. 509 (2010) 53–56.

[17] N.V. Nong, C.J. Liu, M. Ohtaki, High-temperature thermoelectric properties of late rare-earth-doped $Ca_3Co_4O_{9+\delta}$, J. Alloy. Compd. 509 (2011) 977–981.

[18] M. Mikami, N. Ando, R. Funahashi, The effect of Ag addition on electrical properties of the thermoelectric compound $Ca_3Co_4O_9$, J. Solid State Chem. 178 (2005) 2186–2190.

[19] J.C. Diez, M.A. Torres, Sh Rasekha, G. Constantinescu, M.A. Madre, A. Sotelo, Enhancement of $Ca_3Co_4O_9$ thermoelectric properties by Cr for Co substitution, Ceram. Int. 39 (2013) 6051–6056.

[20] H. Hao, L. Zhao, X. Hu, Microstructure and thermoelectric properties of Bi- and Cu- substituted $Ca_3Co_4O_9$ oxides, J. Mater. Sci. Technol. 25 (2009) 105–108.

[21] H. Nakatsugawa, H. M. Jeong and K. Nagasawa, Thermoelectric properties and crystal structure in Y doped Ca3Co4O9, In: prof. Il-H. Kim, editor, Proceedings of the 26th International Conference on Thermoelectrics-ICT, Jeju, Korea, (2007).

[22] Y. Huang, B. Zhao, S. Lin, R. Ang, W. Song, Y. Sun, Strengthening of thermoelectric performance via Ir doping in layered $Ca_3Co_4O_9$ System, J. Am. Ceram. Soc. 97 (2014) 798–804.

[23] G. Constantinescu, S.H. Rasekh, M.A. Torres, C. Chocarro, J.C. Diez, M. A. Madre, A. Sotelo, Influence of Ca substitution by Mg on the $Ca_3Co_4O_9$ performances, Bol. Soc. Esp. Cerám. V 53 (2014) 41–47.

[24] Y. Zhang, J. Zhang, Rapid reactive synthesis and sintering of textured $Ca_3Co_4O_9$ ceramics by spark plasma sintering, J. Mater. Process. Technol. 208 (2008) 70–74.

[25] S. Chen, X. Song, X. Chen, Y. Chen, E.J. Barbero, E.L. Thomas P.N. Barnes, Effect of precursor calcination temperature on the microstructure and thermoelectric properties of $Ca_3Co_4O_9$ ceramics, J. Sol-Gel Sci. Technol. 64 (2012) 627–636.

[26] Q. Xiaoling, Z. Lingke, W. Hui, L. Ping'an, L. Yanchun, Thermoelectric properties of $Ca_3Co_4O_9$ ceramics, J. Wuhan Univ. Technol. (2010) 287–290.

[27] N.Y. Wu, T.C. Holgate, N. Van Nong, N. Pryds, S. Linderoth, High temperature thermoelectric properties of $Ca_3Co_4O_{9+\delta}$ by autocombustion synthesis and spark plasma sintering, J. Eur. Ceram. Soc. 34 (2014) 925–931.

[28] M. Gunes, M. Ozenbas, Effect of grain size and porosity on phonon scattering enhancement of $Ca_3Co_4O_9$, J. Alloy. Compd. 626 (2015) 360–376.

[29] N. Prasoetsopha, S. Pinitsoontorn, V. Amornkitbamrung, Synthesis and thermoelectric properties of $Ca_3Co_4O_9$ prepared by simple thermal hydrodecomposition methods, Electron. Mater. Lett. 8 (2012) 305–308.

[30] M. Prevel, S. Lemonnier, Y. Klein, S. Hébert, D. Chateigner, B. Ouladdiaf, J.G. Noudem, Textured $Ca_3Co_4O_9$ thermoelectric oxides by thermo-forging process, J. Appl. Phys. 98 (2005) 93706–9.

[31] Y. Zhou, et al., Thermoelectric properties of highly grain-aligned and densified Co-based oxide ceramics, J. Appl. Phys. 93 (2003) 2653–2658.

[32] Y. Wang, Y. Sui, X. Wang, W. Su, X. Liu, Enhanced high temperature thermoelectric characteristics of transition metals doped $Ca_3Co_4O_9$ by cold high-pressure fabrication, J. Appl. Phys. 107 (2010) 033708-9.

[33] Y. Masuda, D. Nagahama, H. Itahara, T. Tani, W.S. Seo, K. Koumoto, Thermoelectric performance of Bi- and Na- subtituted $Ca_3Co_4O_9$ improved through ceramic texturing, J. Mater. Chem. 13 (2003) 1094–1099.

[34] Y. Zhang, J. Zhang, Q. Lu, Synthesis of highly textured $Ca_3Co_4O_9$ ceramics by spark plasma sintering, Ceram. Int. 33 (2007) 1305–1308.

[35] J.G. Noudem, D. Kenfaui, D. Chateigner, M. Gomina, Toward the enhancement of the thermoelectric properties of lamellar $Ca_3Co_4O_9$ by edge-free spark plasma texturing, Scripta Mater. 66 (2012) 258–260.

[36] M. Mikami, E. Guilmeau, R. Funahashi, Enhancement of electrical properties of the thermoelectric compound $Ca_3Co_4O_9$ through use of large-grained powder, J. Mater. Res. 20 (2005) 2491–2497.

[37] F. Delorme, C.F. Martin, P. Marudhachalam, D.O. Ovono, G. Guzman, Effect of Ca substitution by Sr on the thermoelectric properties of $Ca_3Co_4O_9$ ceramics, J. Alloy. Compd. 509 (2011) 2311–2315.

[38] R. Tian, T. Zhang, D. Chu, R. Donelson, L. Tao, S. Li, Enhancement of high temperature thermoelectric performance in Bi, Fe co-doped layered oxide-based material $Ca_3Co_4O_{9+y}$, J. Alloy. Compd. Vol. 615 (2014) 311–315.

[39] G. Xu, R. Funahashi, M. Shikano, I. Matsubara, Y. Zhou, Thermoelectric properties of Bi- and Na- substituted $Ca_3Co_4O_9$ system, Appl. Phys. Lett. 80 (2002) 3760–3762.

[40] F.K. Lotgering, Topotactical reactions with ferromagnetic oxides having hexagonal crystal structures-I, J. Nucl. Chem. 9 (1959) 113–123.

[41] J. de Boor, C. Stiewe, P. Ziolkowski, T. Dasgupta, G. Karpinski, E. Lenz, F. Edler, E. Mueller, High-temperature measurement of Seebeck coefficient and electrical conductivity, J. Electron. Mat. 42 (2013) 1711–1718.

[42] J. de Boor, E. Mueller, Data analysis for Seebeck coefficient measurements, Rev. Sci. Instrum. 84 (2013) 065102-9.

[43] S. Bernik, M. Pribošek, Construction and characteristics of a Z-meter setup for thermoelectric measurements of materials, In: Ž.A., Š.P., Š.I. editors, Proceedings of the 49th International conference on Microelectronics, Devices and Materials MIDEM Kranjska Gora, Slovenia, (2013) 121–6.

[44] J.-C. Grivel, X.P. Yang, A.B. Abrahamsen, Z. Han, N.H. Andersen, M. von Zimmermann, Influence of the initial Bi2223 phase content on microstructure development in Bi2223/Ag tapes, J. Phys. : Conf. Ser. 234 (2010) 022012-6.

[45] S. Bhattacharya, D.K. Aswal, A. Singh, C. Thinaharan, N. Kulkarni S.K. Gupta, J.V. Yakhmi, Anisotropic electrical transport studies of $Ca_3Co_4O_9$ single crystals grown by the flux method, J. Cryst. Growth 277 (2005) 246–251.

[46] N. Wu, T.C. Holgate, N. Van Nong, N. Pryds, S. Linderoth, High temperature thermoelectric properties of $Ca_3Co_4O_{9+\delta}$ by autocombustion synthesis and spark plasma sintering, J. Eur. Ceram. Soc. 34 (2014) 925–931.

[47] J.C. Slater, Barrier theory of the photoconductivity of lead sulfide, Phys. Rev. 103 (1956) 1631–1644.

[48] J.Y.W. Seto, The electrical properties of polycrystalline silicon films, J. Appl. Phys. 46 (1975) 5247–5254.

[49] J. Martin, L. Wang, L. Chen, G.S. Nolas, Enhanced Seebeck coefficient through energy-barrier scattering in PbTe nanoparticles, Phys. Rev. B 78 (2009) 11531–11535.

[50] C.H. Lim, S.M. Choi, W.S. Seo, High-temperature thermoelectric properties of the $Ca_{3-x}K_xCo_4O_9$ ($0 \leq x \geq 0.3$) system, J. Korean Phys. Soc. 57 (2010) 1054–1058.

[51] D. Narducci, E. Selezneva, G. Cerofolini, S. Frabboni, G. Ottaviani, Impact of energy filtering and carrier localization on the thermoelectric properties of granular semiconductors, J. Solid State Chem. 193 (2012) 19–25.

Electronic supplementary information (ESI) - **An insight about the agreement between the measurements using CM system and the Z-meter.**

Based on the Z-meter measurements we analysed the influence of microstructural anisotropy on the TE characteristics of the Ca349 ceramics. An insight about the agreement between the measurements using CM system and the Z-meter is illustrated with the effect of the type of measurement on the TE characteristics of the AM-760_1 sample, presented in Fig. S1. The sample AM-760_1 was selected because of its highly isotropic microstructure, with the least effect of the measuring direction on the obtained values and also the strong similarity in the microstructure between the thinner specimen for the CM measurement and the taller one for the Z-meter measurement. Hence, the smallest differences in the obtained TE parameters between both methods of measurement could be expected. Measurements of the sample with an anisotropic (i.e., textured) microstructure would give only larger differences in the TE values between both types of measurement. The comparison between the values obtained from the CM and the Z-meter measurements (Fig. S1) showed a reasonably good agreement within about ± 10%. The largest difference is obvious in the values of the Seebeck coefficient (S), with a much higher span of S with temperature in the case of the CM (120—175 μV/K) than in the Z-meter measurement (141—158 μV/K). It is well known that reliable measurements of S are very demanding [1,2,3].

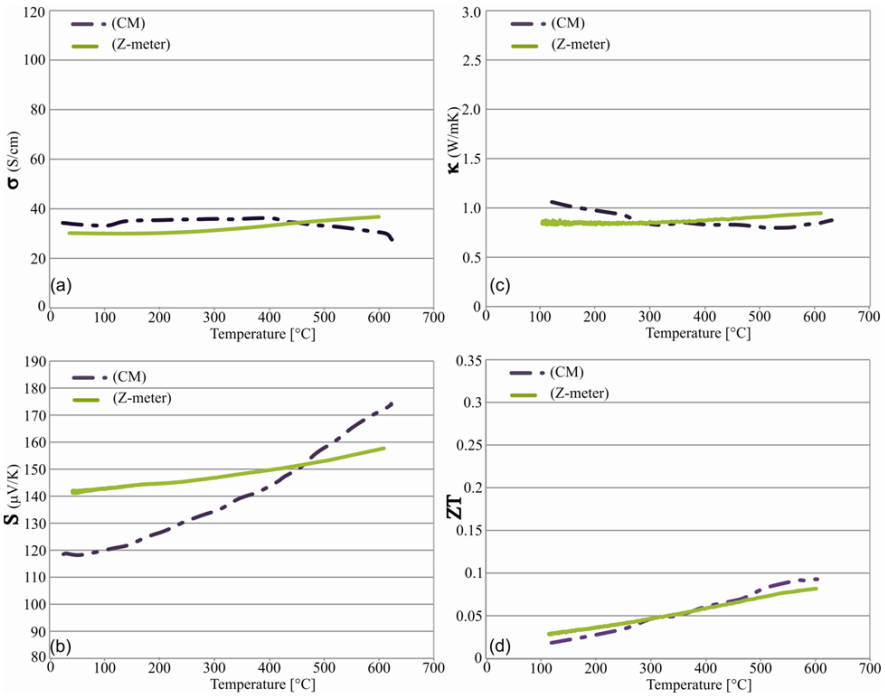


Figure S1: The TE characteristics of sample AM-760_1 determined by the CM system and the Z-meter.

References

[1] Beretta, P. Bruno, G. Lanzani, and M. Caironi, Rev. Sci. Instrum.86 (2015) 075104-5.
[2] H. Werheit, U. Kuhlmann, B. Herstell and W. Winkelbauer, J. Phys.: Conference Series 176 (2009) 012037-9.

Chapter 5

The Thermoelectric Compound $Ca_3Co_4O_9$ – Synthesis and Characteristics

In this chapter, a paper entitled "**The thermoelectric compound $Ca_3Co_4O_9$-Synthesis and characteristics**", by authors M. Presečnik and S. Bernik is presented.

The purpose of this work was to exploit the possibility to improve the classical ceramic solid state synthesis of the Ca349 compound by mechano-chemical (MC) treatment of the fine powder mixture of $CaCO_3$ and Co_3O_4. The formation of the Ca349 compound in the untreated and the MC treated powders was compared.

The MC treatment resulted in partial amorphization of the powder mixture without any formation of the Ca349 compound or even just enhancement of its formation compared to the untreated powder mixture. Absence of any reaction or just increased reactivity of the starting powder mixture triggered my curiosity to examine in more detail the MC treatment process and the influence of its processing parameters, which is presented in Chapter 6.

The Thermoelectric Compound $Ca_3Co_4O_9$ – Synthesis and Characteristics

Mojca Presečnik[a] and Slavko Bernik[a, b]

[a]*Jozef Stefan Institute, Department for Nanostructured Materials, Jamova cesta 39, 1000 Ljubljana, Slovenia*
[b]*Center of Excellence NAMASTE, Jamova cesta 39, 1000 Ljubljana, Slovenia*

Abstract. The synthesis of the $Ca_3Co_4O_9$ compound from starting powders of $CaCO_3$ and Co_3O_4 by mechanochemical alloying was studied. This mechanochemical treatment resulted only in an amorphisation of the powder mixture without any phase formation or an enhancement of its formation. The $Ca_3Co_4O_9$ phase formed in samples from untrteated and treated powder mixtures after sintering at 760°C, while traces of the Co_3O_4 were still present.

Keywords: thermoelectrics, oxides, $Ca_3Co_4O_9$, synthesis, characteristics
PACS: 60, 70, 80, 81

INTRODUCTION

Since the discovery of large thermoelectric power in $NaCo_2O_4$ single crystals in 1997 by Terasaki and coworkers [1] considerable attention has been given to research on thermoelectric oxide materials. They are very promising for applications in waste-heat recovery due to their high stability in an oxidizing atmosphere at elevated temperatures, low cost and atoxicity. As the use of single crystals has obvious drawbacks due to the difficult synthesis and the limitations in size and quantity, the focus has been on the development of polycrystalline materials. In the family of layered cobalt oxides the $Ca_3Co_4O_9$ compound showed good potential for further improvement of the thermoelectric characteristics via tailoring of its internal structure and the addition of certain dopants, which have a great influence on the thermal and electrical conductivity. The $Ca_3Co_4O_9$ compound has a mismatch layered structure, consisting of CdJ_2-type CoO_2 layers and the rock-salt- type Ca_2CoO_3 layer alternating in the direction of the c-axis. [2] According to phase equilibria studies in the Cao–CoO system the synthesis of the $Ca_3Co_4O_9$ compound from powders of $CaCO_3$ and Co_3O_4 is a very slow process due to the sluggishness of the solid-state reactions, which were not completed even after 6 weeks of firing at temperatures between 800 and 900°C with several intermediate grindings. [3] The $Ca_3Co_4O_9$ compound is stable up to 926°C when it decomposes into the CoO_{ss} (solid solution with CaO) and the $Ca_3Co_2O_6$ compound.[3] The $Ca_3Co_2O_6$ compound is also interesting as a thermoelectric material. In recent years several synthesis methods were used for the preparation of the $Ca_3Co_4O_9$ compound, such as conventional solid-state reactions, sol-gel, chemical co-precipitation, etc. Powder mixtures were sintered at temperatures between 700 and 900°C; besides pressureless sintering, hot-press sintering and spark plasma sintering were used as well.[4-9] The last two methods of sintering result in a significantly improved density of the samples and, especially for hot-pressing, also in strong texturing with alignment of the large platelet grains in the plane perpendicular to the stress direction, which all contributed to the improved thermoelectric properties of the $Ca_3Co_4O_9$ samples.

High-energy milling or mechanochemical alloying has been used for the solid-state synthesis of various complex oxides. [10] It was also successfully used in the case of compounds, the synthesis of which using conventional solid-state reactions is difficult, as in the case of the ferroelectric niobates [11,12], or even impossible, like in the case of multifferoic $BiMnO_3$ [13]. It is well known that mechanochemical reactions are promoted by the energy transferred from the milling bodies to the milling powder. This is influenced by numerous milling parameters, which define the process.[14]

In this work the possibility of preparing the $Ca_3Co_4O_9$ compound from starting powders of $CaCO_3$ and Co_3O_4 by mechanochemical synthesis was studied. The thermal characteristics of a stoichiometric powder mixture after mechanochemical activation for varying times were studied by differential thermal analysis (DTA), thermogravimetric analysis (TGA) and mass spectrometry (MS), while the phase composition was determined by x-ray diffraction analysis (XRD). Mechanochemically activated powders were pressed into pellets and sintered at different temperatures. The phase composition and microstructural characteristics of the sintered samples were analyzed using XRD and scanning electron microscopy (SEM), respectively. For comparison, samples from untreated powder mixtures were prepared and analyzed as well.

9th European Conference on Thermoelectrics
AIP Conf. Proc. 1449, 331-334 (2012); doi: 10.1063/1.4731564
© 2012 American Institute of Physics 978-0-7354-1048-0/$30.00

EXPERIMENTAL

A stoichiometric powder mixture for the $Ca_3Co_4O_9$ compound of $CaCO_3$ (Alfa Aesar Lot #G23W035, 99.5% metals basis) and Co_3O_4 (Alfa Aesar Lot #B29T027, 99.7% metals basis) in a molar ratio 9:4, respectively, were prepared by homogenization in an agate mortar in absolute ethanol media and subsequent drying. Prior to the preparation of the powder mixture the starting powders were attrition milled so that the mean particle size of the $CaCO_3$ was reduced from 2.5 μm to 0.45 μm powder and for Co_3O_4 from 1.5 μm to 0.4 μm. Batches of powder mixture with a weight of 3.5g were placed in the 80-ml tungsten-carbide milling bowl together with 23 tungsten-carbide balls with diameters of 10 mm for the mechanochemical treatment. This was carried out in a Fritsch Pulverisette 5 planetary mill with a supporting disc rotational speed of 300 or 360 rpm for different times of 5 h, 10 h, 15 h and 20 h (samples labeled MCx, where x is milling time). Such milling conditions gave a ball impact energy of 58 mJ/hit at 300 rpm and 83mJ/hit at 360 rpm, as calculated in accordance with the kinematic equation, which describe the velocity and the acceleration of the balls in the bowl of a planetary mill. [14]

The thermal characteristics of the treated powder mixture samples up to 1200°C were analyzed using differential thermal analysis (DTA), thermogravimetric analysis (TG) and mass spectrometry (MS) to follow the reactions, mass changes and released CO_2 with temperature. The study was performed in air with a heating rate of 10°C/min using a simultaneous thermal analysis instrument (STA) Netzsch Jupiter 449 coupled with a mass spectrometer (MS) 403C Aëoloss. For comparison the thermal behavior of the mechanochemically untreated powder mixture (B) was analyzed as well. The phase composition of the activated powders MCx was analyzed by x-ray diffraction analysis (XRD) using X'Pert PRO MPD (CuK_α, 2Θ range 5-80°). Disc samples with a diameter of 10 mm and a thickness of about 1 mm were uniaxially pressed with a pressure of 150MPa from activated MCx powder mixtures and also untreated mixture B and sintered in air at 760°C or 860°C for 12 and 20 hours. The density of the samples was determined by Archimedes' method. The phase composition of the samples was analyzed by XRD analysis. The microstructures in cross-section of the sintered discs were prepared by grinding and polishing. The microstructural characteristics of the sintered samples were analyzed using a scanning electron microscope (SEM) JEOL JSM-5800 equipped with an energy-dispersive x-ray spectrometer (EDXS) and a Link ISIS (Oxford Instruments) analytical system for qualitative and semi-quantitative analyses of the observed phases.

RESULTS AND DISCUSSION

The DTA/TG/MS data of the untreated (B) and mechanochemically treated for 10 hours (MC10) powder mixtures are presented in Fig. 1. Both powders showed very similar characteristics. A broad and shallow endothermic peak in the range from 720°C and 808°C indicates the formation of the $Ca_3Co_4O_9$, which is accompanied by the loss of CO_2. The decomposition of the $CaCO_3$ with the loss of CO_2 takes place at temperatures between 590°C and 780°C; it starts at a lower temperature and somehow provides the way for the formation of the $Ca_3Co_4O_9$ phase at about a 130°C higher temperature. In the case of the untreated powder B the total weight loss is about 19.7 wt.%; such a weight loss agrees with the reaction between $CaCO_3$ and Co_3O_4 and the formation of the $Ca_3Co_4O_9$ compound with all the cobalt in the 3+ state.

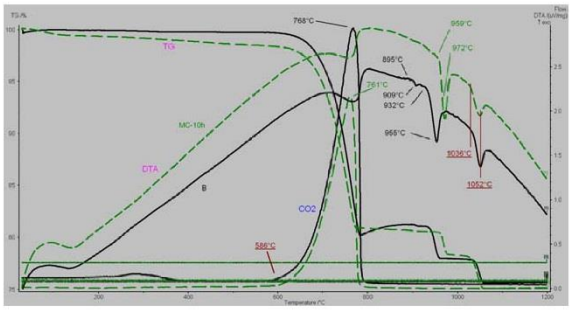


FIGURE 1. DTA/TG/MS(for CO_2) of the untreated (solid line) and mechanochemically treated for 10 hours (dashed line) of $CaCO_3$-Co_3O_4 powder mixtures.

However, in the mechanochemically treated powder MC10 the total weight loss is 18.6%, which indicates possible oxidation of the Co into a higher valence state of 4+ and hence the formation of the oxygen-enriched $Ca_3Co_4O_{9+\delta}$ compound. The results are in agreement with the previous reports.[4] Sharp endothermic peaks in the DTA patterns at temperatures above 900°C correspond to the decomposition reactions; the first one belongs to the decomposition of $Ca_3Co_4O_9$ into $Ca_3Co_2O_6$ and CoO_{ss} while the second indicates the further decomposition of $Ca_3Co_2O_6$ into CaO_{ss} and CoO_{ss}. It is interesting that the decomposition of the $Ca_3Co_4O_9$ compound in the mechanochemically treated sample starts at about a 30°C higher temperature than in the case of the untreated powder, which needs further examination. The same results of DTS/TG/MS analysis were also obtained in other mechanochemically treated powder mixtures prepared in this work. Such results, however, indicated that the mechanochemical treatment of the powder mixture did not result in the formation of the $Ca_3Co_4O_9$ and did not even enhance its formation.

The XRD analysis showed that the mechanochemical treatment of powder mixture resulted in a strong reduction of the characteristic XRD peaks of the $CaCO_3$ and Co_3O_4 after 5 hours and that a longer treatment had no noticeable effect. The results indicated that mechanochemical treatment resulted only in the amortization of the powder mixture without the formation of the $Ca_3Co_4O_9$ or any other compound.

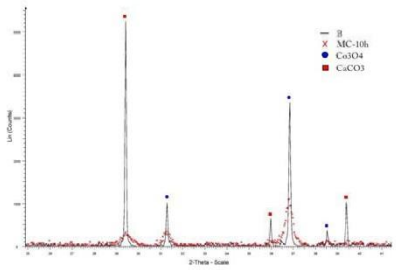


FIGURE 2. XRD patterns of untreated powder mixture of $CaCO_3$-Co_3O_4 (B) and powder mixture mechanochemically treated for 10 h (MC10).

The XRD analysis confirmed the formation of the $Ca_3Co_4O_9$ compound (JCPDF 23-0110) after sintering at 760°C in the sample prepared from the untreated powder mixture and in all samples prepared from mechanochemically treated powders. No significant difference in the XRD patterns of these samples was observed and in all the samples except the $Ca_3Co_4O_9$ compound only a trace of untreated Co_3O_4 was detected. The XRD patterns of all the samples were practically the same after sintering at 860°C for 12 hours; however after sintering for 20 hours at this temperature the appearance of the $Ca_3Co_2O_6$ compound was observed, which indicated partial decomposition of the $Ca_3Co_4O_9$ compound.

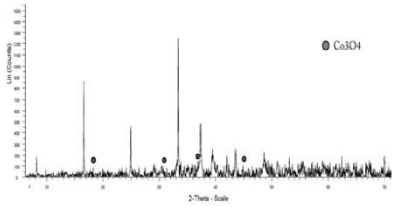


FIGURE 3. XRD pattern of the sample prepared from the untreated powder mixture and sintered at 760°C for 12 hours.

In Fig. 3 the microstructures of samples prepared from an untreated powder mixture (B) and a powder mixture mechanochemically treated for 10 hours (MC10), sintered at 760°C, are given. While in the sample B a uniformly distributed porosity and the plate-like morphology of the grains is evident, sample MC10 has a non-uniform density,

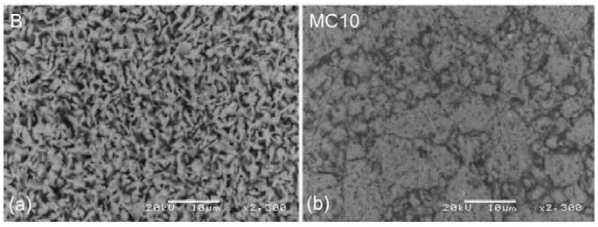


FIGURE 3. Microstructures of samples prepared from a) untreated powder mixture (B) and b) powder mixture mechanochemically for 10 hours (MC10), sintered at 760°C for 12 hours.

which indicated the presence of agglomerates in the mechanochemically treated powder mixture, and finer, plate-like grains. Such a microstructure was also observed in other sintered samples prepared from mechanochemically treated powder mixtures. After sintering at 860°C the microstructures of the samples had the same distinct characteristics, only the grain size increased. All the sintered samples had a low density of around 2.4 g/cm^3, regardless the treatment of the starting powder mixture and the sintering temperature.

CONCLUSIONS

The possibility to prepare the $Ca_3Co_4O_9$ compound from starting powders of $CaCO_3$ and Co_3O_4 by mechanochemical synthesis was studied. The results showed that the mechanochemical treatment resulted only in the amorphisation of the powder mixture, without the formation of any phase or even an enhancement of the $Ca_3Co_4O_9$ phase formation, which would show in a reduction of its formation temperature. The $Ca_3Co_4O_9$ phase was obtained after sintering at 760°C, both in samples from treated and untreated powder mixtures. Traces of Co_3O_4 were also present, even after sintering at 860°C.

ACKNOWLEDGMENTS

The financial support of the Slovenian Research Agency (Program Contract No. P2-0084-0106 and project grant L2-4192) is gratefully acknowledged.

REFERENCES

1. I. Terasaki, Y. Sasago and K. Uchinokura, *Phys. Rev. B* **56**, R12685-R12687 (1997).
2. A. C. Masset, C. Michel and A. Maignan, and K. Austin, *Appl. Phys. Letters* **85**, 2503-2504 (2004).
3. E. Woermann and A. Muan, *J. Inorg. Nucl. Chem.* **32**, 1455-1459 (1970).
4. P. Smaczynski, M. Sopicka-Lizer, K. Kozlowska and J. Plewa, *J. Electroceram.* **18**, 255-260 (2007).
5. D. Kenfaui, D. Chateigner, M. Gomina and J. G. Noudem, *J. Alloy. Comp.* **490**, 472-479 (2010).
6. M. Prevel, S. Lemmonier, Y. Klein, S. Hebert, D. Chateigner, B. Ouladdiaf and J. G. Noudem, *J. Appl. Phys.* **98**, 093706 (2005).
7. S. Fen and W. Yang, *J. Sol-Gel Sci. Technol.* **58**, 330-333 (2011).
8. S. Pinitsoontorn, N. Lerssongkram, A. Harnwunggmoung, K. Kurosaki and S. Yamanaka, *J. Alloy. Comp.* **503**, 431-435 (2010).
9. Y. Liu, Y. Lin, Z. Shi, C. W. Nan and Z. Shen, *J. Am. Ceram. Soc.* **88**, 1337-1340 (2005).
10. V. V. Zyryanov, *Russian Chemical Reviews* **77**, 105-135 (2008).
11. T. Rojac, M. Kosec, B. Malič and J. Holc, *Mater. Res. Bull.* **40**, 341-345 (2005).
12. J. Zhu, Z. Li, Z. Xu and X. Yao, *Ferroelectrics* **401**, 211-217 (2010).
13. Z. Branković, Z. Marinković Stojanović, L. Mančić, V. Vukotić, S. Bernik and G. Branković, *J. Eur. Ceram. Soc.* **30**, 277-281 (2010).
14. T. Rojac, M. Kosec, B. Malič and J. Holc, *J. Eur. Ceram. Soc.* **26**, 3711-3716 (2006).

Chapter 6

Influence of a Mechano-Chemical Treatment on the Synthesis and Characteristics of p-type Thermoelectric $Ca_3Co_4O_9$ Ceramics

In this chapter, a paper entitled "**Influence of a mechano-chemical treatment on the synthesis and characteristics of p-type thermoelectric $Ca_3Co_4O_9$ ceramics**", by authors M. Presečnik and S. Bernik is presented.

In this work the influence of the milling parameters, i.e. the amount of powder mixture and powder-to-milling balls ratio, ball-impact energy (Eb), ball impact frequency (υ_t) and cumulative energy (Ecum), on the mechano-chemical (MC) treatment of the fine powder mixture of $CaCO_3$ and Co_3O_4 was studied methodically in regard to the formation of the Ca349 compound and its TE characteristics.

The maximum ball-impact energy (Eb) of 283 mJ/hit obtained in the MC treatment of the fine powder mixture of $CaCO_3$ and Co_3O_4 was not sufficient for the formation of the Ca349 compound. It is known that in every system some critical minimum Eb should be exceeded for starting a reaction among reagents. However, the amorphisation of the MC-treated powder depends on the Ecum. Accordingly the MC treatment resulted in a fully amorphous starting mixture only when Ecum was around 2900 kJ/g, while at Ecum < 2300 kJ/g the powder was only partially amorphous and at Ecum > 3800 kJ/g the intensity of the XRD peaks of the starting reagents again started to increase. The completely amorphous powder mixture of $CaCO_3$ and Co_3O_4 showed increased reactivity in the TG analysis with the formation of the Ca349 compound at approximately 40 °C lower temperature than in the untreated one. The single-phase Ca349 ceramics was obtained with amorphous MC treated powder mixture already after 4 hours of calcination at 760 °C, which is three-times faster than in the case of fine untreated mixtures. The obtained Ca349 ceramics had fine grained and sharp-edged platelet grains of irregular shape and un-homogeneous microstructure with density of about 50%. With additional sintering at 920 °C the microstructure became highly homogeneous, its density increased to 72% while the morphology of the grains was largely preserved. Such Ca349 ceramics had, compared to the Ca349 ceramics from untreated powder mixture, slightly higher S, higher σ and lower κ, all contributing to an almost 2-times higher zT value of 0.10 at 600 °C.

Journal of Alloys and Compounds 686 (2016) 708–716

Contents lists available at ScienceDirect

Journal of Alloys and Compounds

journal homepage: http://www.elsevier.com/locate/jalcom

Influence of a mechano-chemical treatment on the synthesis and characteristics of p-type thermoelectric $Ca_3Co_4O_9$ ceramics

M. Presečnik [a, b, *], S. Bernik [a]

[a] Jožef Stefan Institute, Jamova cesta 39, 1000 Ljubljana, Slovenia
[b] Jožef Stefan International Postgraduate School, Jamova cesta 39, 1000 Ljubljana, Slovenia

ARTICLE INFO

Article history:
Received 14 January 2016
Received in revised form
22 April 2016
Accepted 7 June 2016
Available online 11 June 2016

Keywords:
$Ca_3Co_4O_9$
Oxide thermoelectric
Mechanochemical synthesis
Solid state synthesis
Thermoelectric properties

ABSTRACT

The influence of a mechano-chemical (MC) treatment on the formation of the Ca349 phase from a stoichiometric mixture of fine-grained $CaCO_3$ and Co_3O_4 powders, as well as the microstructural and thermoelectric characteristics of the Ca349 ceramics were studied. With an experimentally obtained maximum of 283 mJ/hit the critical ball-impact energy (Eb) required for the formation of the Ca349 compound was not obtained; however, the MC treatment resulted in complete amorphization and an enhanced reactivity of the starting-powder mixture. This enabled the preparation of single-phase Ca349 ceramics with an un-homogeneous microstructure and a density of 50% after only 4 h of calcination at 760 °C, while the untreated mixture required at least 12 h. Additional sintering at 920 °C resulted in a highly homogeneous and fine-grained microstructure for the Ca349 ceramics with a density of 72%, having an approximately two-times higher ZT of 0.10 at 600 °C in comparison to the previously reported values. Our study showed that the mechano-chemical treatment enhances the formation of the Ca349 phase at a low calcination temperature, which enables the preparation of Ca349 ceramics with a microstructure that leads to improved TE characteristics.

© 2016 Elsevier B.V. All rights reserved.

1. Introduction

Thermoelectric materials (TE) convert heat into electricity directly through the Seebeck effect. This unique property can be exploited with the help of power-generation devices, i.e., TE modules composed of p- and n-type TE materials, which provide the only viable route to harvesting waste heat energy by its direct conversion into electricity in an environmentally and economically friendly manner. The energy-conversion efficiency of the TE material is described using the dimensionless figure of merit $ZT = \sigma S^2 T/\kappa$, where σ is the electrical conductivity, S is the Seebeck coefficient, T is the absolute temperature and κ is the thermal conductivity. Since Terasaki et al. [1] reported that the transition-metal oxide Na_xCoO_4 shows a good thermoelectric performance, oxide TE materials are very promising for high-temperature applications, especially because they are in contrast to the otherwise much better, conventional TE alloys, cheaper, non-toxic and highly stable at elevated temperatures. While the practical application of Na_xCoO_4 is limited because of its poor humidity resistance and volatility [2,3], $Ca_3Co_4O_9$ (Ca349) is much more promising in this regard and simultaneously also suitable for further improvements in the TE properties. The TE properties of Ca349 ceramics are closely related to its complex misfit layered structure consisting of CdJ_2-type CoO_2 layers and the rock-salt-type Ca_2CoO_3 layer alternating in the direction of the c-axis [4], where CoO_2 sheets with strongly correlated electrons serve as electronic transport layers, while Ca_2CoO_3 misfit layers serve as phonon-scattering centres for reducing the thermal conductivity. The Ca349 single crystals showed a high Seebeck coefficient S of 240 μV/K and a high electrical conductivity σ of 434 S/cm, which are mostly responsible for the high ZT of 0.87 at 700 °C [5]; less credit goes to the relatively high thermal conductivity of 3 W/mK. On the other hand, the much more application-suitable polycrystalline Ca349 ceramic has, because of its complex microstructural features, much lower ZT values, which can vary significantly, depending on the preparation process. The un-doped Ca349 ceramics, conventionally prepared from the powder mixtures of $CaCO_3$ and CO_3O_4, with low densities around 65% of theoretical value, typically had reported ZT values about 0.07 at 700 °C [6], while for the highly textured Ca349 ceramics with densities above 90% prepared by the hot-pressing or

* Corresponding author. Jožef Stefan Institute, Jamova cesta 39, 1000 Ljubljana, Slovenia.
E-mail addresses: mojca.presecnik@ijs.si (M. Presečnik), slavko.bernik@ijs.si (S. Bernik).

http://dx.doi.org/10.1016/j.jallcom.2016.06.058
0925-8388/© 2016 Elsevier B.V. All rights reserved.

pressure of 200 MPa into pellets with diameters of 12 mm and heights of 3 mm and 12 mm, and sintered at 920 °C for 20 h (sample labeled UT-920 and MC-920). The phase composition of the Ca349 samples was checked using x-ray powder-diffraction analysis (XRD). Their densities were measured using a density-measurements system Densitec (Metar sa, Matran, Switzerland). The fractured and polished microstructures of the samples in the cross-sectional direction of the pellets were analysed on a scanning electron microscope (SEM) JEOL JSM-5800. From the SEM images of the fractured surfaces an average grain size was determined based on rough measurements of approximately 40 grains with clearly visible edges. The TE characterization of the samples with a height and diameter of 10 mm was performed in a vacuum of approximately $10^{-2} - 10^{-3}$ Pa using a Z-meter [45], which enables simultaneous measurement of S, σ and κ.

3. Results and discussion

The XRD analysis of the MC-prepared powders showed the strong influence of the milling parameters, i.e., the ball energies (Eb), the ball-impact frequencies (ν_t) and the cumulative energies (Ecum) used [31,44], which are given in Table 1. In MC1 the ball-impact energy was 196.4 mJ/hit and the ball-impact frequency was 3457 s^{-1}. After 2 h of milling the strongly reduced intensity and the broadening of the peaks of the $CaCO_3$ and Co_3O_4 indicate amorphization of the powder mixture, while longer milling times only resulted in sharper and more intense peaks of both starting components with no indication of the formation of the Ca349 phase (Fig. 1). By increasing the rate from 300 rpm to the maximum of 360 rpm, the Eb and ν_t increased to 283 mJ/hit and 4149 s^{-1}, respectively. According to the XRD patterns of the MC2 powder mixture, presented in Fig. 1, the $Ca_3Co_4O_9$ (Ca349) phase was not formed. The intensity of the peaks of the $CaCO_3$ and Co_3O_4 strongly decreased with broadening after 2 h of milling and the XRD patterns were similar for longer milling times. However, after 15 h of high-energy milling the peaks of the starting components disappeared, indicating that the powder was almost completely amorphous. Interestingly, after a longer milling of 20 h the peaks of the $CaCO_3$ and Co_3O_4 appeared again, like if an amorphous sample would be subjected to a modest heating and so recrystallize.

According to the literature and the models introduced by Burgio et al. [44] the changes of Eb and ν_t can lead to different reaction pathways and hence either to phase formation or just amorphous powder [44,46]. In the case that the reciprocal hindering of the balls is negligible, the number of balls in the milling vial affects only the ball-impact frequency ν_t [46,47], while the ball-impact energy Eb remains the same. We were prevented from incresing the rate above 360 rpm to gain a higher Eb. With a smaller number of balls in the vial we lowered the ball-impact frequency in MC3 by approximately 30% in comparison to MC1; nevertheless, the result after 15 h of milling was similar according to the XRD analysis (Fig. 2). The largest impact on the possibility of achieving phase formation and also on powder amorphization comes from Eb, while the ν_t and Ecum are less influential, based on the small differences between the MC1-15 and MC3-15 samples treated at the same Eb and different ν_t and Ecum. The obtained results also suggest that the energies used in our MC treatments were too low and the critical Eb (Eb_{Cr}) for the formation of the Ca349 phase was not reached. It is known that in each system some critical Eb needs to be exceeded to achieve a mechano-chemical reaction [44,46]; if the energies are lower than Eb_{Cr} the result is usually the amorphous phase, which is what more or less happened with our powder mixtures. However, for amorphization also some minimum cumulative critical energy $Ecum_{Cr}$ is required, which is milling-time dependent; for a certain stage of conversion to the amorphous phase the same amount of $Ecum_{Cr}$ is always needed, regardless of the Eb and ν_t [48–50]. According to our results the $Ecum_{Cr}$ should be around 2900 kJ/g. In the MC1 and MC3 samples the maximum obtained $Ecum_{Cr}$ was around 2200 kJ/g and the mixture was only partially amorphous, while in the MC2 the $Ecum_{Cr}$ of 2880 kJ/g resulted in a practically fully amorphous material. However, at an even higher Ecum of 3840 kJ/g the intensity of the peaks of the $CaCO_3$ and Co_3O_4 increased again. A similar phenomenon was reported by Zdujić et al. [26], where only an increase in the angular velocity of the planetary mill brought the relevant milling parameters above the critical value and resulted in the promotion of the phase formation and crystallinity. However, after resuming the lower milling intensity, the reverse process occurred, with a transition back to the amorphous matrix. In general, the Ecum governs the ratio between the crystalline and amorphous parts of the powder mixture. The lack of formation of the Ca349 phase, even with an extended milling time, indicated that in contrast to the cumulative process we had a so-called threshold process in which the result depends on whether or not the energy of some impact is sufficient to bring the relevant milling parameter above the critical value and not only the accumulated energy [51].

The maximum Eb that we were able to reach in our mechano-chemical processing study was still below the required Eb_{Cr} for the formation of the Ca349 phase. However, we obtained the highly amorphous powder mixture MC2-15 with much more homogeneously mixed reagents and probably a higher reactivity in comparison to the untreated mixture (UT), which could positively affect

Table 1
Parameters of the mechano-chemical processing calculated from the milling conditions.

Series (name)	Ball-impact energy Eb [mJ/hit]	Ball-impact frequency ν_t [s^{-1}]	Time [h]	Cumulative kinetic energy Ecum [kJ/g]
MC1			2	222.3
(300 rpm, 23 balls)			5	555.7
	196.4	3457.5	10	1111.5
Mater. – balls ratio			15	1667.2
1:54.4			20	2223
MC2			2	384.1
(360 rpm, 23 balls)			5	960.3
	282.8	4149	10	1920.6
Mater. – balls ratio			15	2881
1:54.4			20	3841.3
MC3			/	/
(300 rpm, 16 balls)			/	/
	196.4	2405.2	/	/
Mater. – balls ratio			15	1159.8
1:37.8			/	/

the SPS, ZT values of about 0.18 have been reported [7–9]. Recently, we reported that modestly textured Ca349 ceramics with a density of about 72% had ZT values of 0.31 at 627 °C [7]. Similar ZT values up to 0.29 were also reported for the sol-gel prepared un-doped Ca349 ceramics with fine, plate-like grains [10]. For the Ca349 ceramics with addition of various dopants, values of ZT up to 0.3 were also reported [11]. Such lower values of ZT in comparison to the single crystals are a consequence of the much lower electrical conductivity in the range 20–120 S/cm and also the lower Seebeck coefficient in the range 100–180 μV/K. The thermal conductivity in polycrystalline Ca349 ceramics is usually much lower and shows a strong dependence on the density and morphology of the grains; it can vary from 0.4 W/mK for fine-grained and highly porous ceramics to about 2 W/mK for a highly dense and perfectly textured one. However, even lowest values are still not enough to fully compensate for the loss in the other two TE properties [12–16]. Therefore, if properly influencing the grain size and distribution, their boundaries and the connectivity between them, and possibly also the Ca349 structure, there is a possibility of improving the TE characteristics of polycrystalline Ca349 ceramics.

According to phase-equilibria studies in the CaO–CoO system [17] the formation of the $Ca_3Co_4O_9$ phase is very sluggish, taking several weeks with intermediate grindings to obtain single-phase samples in the temperature range from 880 to 900 °C. The Ca349 phase is stable up to 926 °C, when it decomposes into the $Ca_3Co_2O_6$ (Ca326) and the CoO solid solution with CaO (CoOss). According to literature reports the Ca349 ceramic sintered with a classic ceramic procedure is usually prepared in two steps from $CaCO_3$ and Co_3O_4; with calcination at temperatures of 900–920 °C for around 24 h, followed by repeated annealing with intermediate grinding at 900–920 °C [11,13,17–21]. However, the sol-gel Pechini synthesis method from Ca- and Co-nitrates [10,22–24] and a thermal hydrodecomposition method of acetate salts [25] enable the preparation of fine-grained powders of single-phase Ca349 with shorter firing times and at much lower temperatures in the range from 650 to 800 °C. Pellets prepared from such powders were additionally sintered with temperatures at least 850 °C and higher [10,24].

The mechano-chemical (MC) treatment (i.e., high-energy milling) of starting-powder mixtures was shown to be very useful for the preparation of different materials, in some cases even enabling the synthesis of compounds that could not be prepared using a classic ceramic procedure; energy transfer from the milling bodies to the milled powder results in a decreasing particle size and hence an increased specific surface, crystal defects with plastic and elastic deformations, amorphization of the powders and chemical reactions [29]. All these features could also be beneficial for the synthesis of single-phase Ca349 ceramics and their TE properties. The MC method is also appropriate for large-scale production and is environmentally friendly.

The MC treatment is used in the preparation of a variety of materials, such as super-alloys, perovskites, niobates, titanates, silicides, TASTs, oxyselenides, etc., including thermoelectric materials [27–34]. While the MC treatment enables the synthesis of different compounds [35,36], it also failed in some cases [26]. The usual precursors in the MC synthesis of oxide ceramics are powders of oxides, hydroxides and carbonates, and their mixtures [37,38]. In the case of hydroxides and carbonates, high-energy milling could result in their decomposition and hence the enhanced reactivity of the mixture [39]. Also, according to the Hedvall effect [40–42] a disturbance in the structural stability caused by the high-energy milling increases the atomic mobility and reactivity of the crystalline matter. Apparently, high-energy milling results in very complex processes that are not yet completely clear; however, it is known that they contribute to mechanical activation, sometimes they lead to chemical changes, but in general they always change the physical properties of the material.

In this work we have continued our preliminary study of the MC treatment [43] with a more detailed analysis of the influence of the parameters of high-energy milling on the powder mixture of $CaCO_3$ and Co_3O_4, the synthesis of the Ca349 phase, and the microstructure and TE characteristics of the Ca349 ceramics. We clearly showed that the MC treatment results in the amorphization and enhanced reactivity of the starting powder mixture, which enable the synthesis of the pure Ca349 phase after a single calcination at the relatively low temperature of 760 °C in an approximately three-times-shorter time of 4 h than with an untreated mixture. A further heat treatment of the calcined samples from the MC-treated powder mixture led to a noticeably increased ZT value in comparison to literature reports for the pristine, non-textured Ca349 ceramics prepared using a classic ceramic solid-state synthesis, due to the development of the favourable fine-grained microstructure.

2. Experimental

Stoichiometric powder mixtures for the $Ca_3Co_4O_9$ compound of $CaCO_3$ (Alfa Aesar, stock #011403Lot #G23W035, 99.5% metals basis, 5 μm) and Co_3O_4 (Alfa Aesar, stock #45806, Lot #B29T027, 99.7% metals basis, 2–6 μm) in a molar ratio 9:4 were prepared by homogenization in a planetary mill in absolute ethanol media for 2 h and subsequent drying. Prior to the preparation of the mixture, both starting powders were attrition milled for 6 h to obtain fine powders. According to the laser-scattering particle-size distribution analysis using a Horiba LA-920 the starting particle size was effectively reduced from 2.5 μm to 0.46 μm for the $CaCO_3$ and from 1.38 μm to 0.36 μm for the Co_3O_4. For further studies either an untreated homogenized powder mixture was used (label UT) or mixtures of mechano-chemically treated (label MC) powder under different milling conditions with respect to the ball-impact frequencies (ν_t), ball-impact energies (Eb) and cumulative kinetic energies (Ecum). For all three series of MC treatments, batches of powder mixtures weighing 3.5 g were used. Each batch was dried at 180 °C to remove the air humidity and afterwards placed in an 80-ml tungsten-carbide milling vial together with either 23 (batches MC1 and MC2) or 16 (batch MC3) tungsten-carbide milling balls with a diameter of 10 mm. The MC treatment was performed in a Fritsch Pulverisette 5 planetary mill with a supporting-disc rotational speed of 300 rpm (batches MC1 and MC3) or 360 rpm (batch MC2) for various times from 2 to 20 h (samples labeled MCx-y, where y is the milling time in hours). The ball-impact frequencies (ν_t), the ball-impact energies (Eb) and the cumulative kinetic energies (Ecum) were calculated using corresponding kinematic equations, described elsewhere [31,44]. The thermal characteristics of the UT powders and of the MC-treated powders up to 1200 °C were analysed using differential thermal analysis (DTA), thermal-gravimetric analysis (TG) and mass spectrometry (MS) to follow the reactions, mass changes and released CO_2 with temperature, respectively. The study was performed in air with a heating rate of 10 °C/min using a simultaneous thermal analysis instrument, (STA) Netzsch Jupiter 449, coupled with a mass spectrometer (MS) 403C Aëoloss. The phase composition of the MCx-y activated powders was analysed by x-ray diffraction analysis (XRD) using an X'Pert PRO MPD (CuK_α, 2Θ range 5–80°).

The preparation of the Ca349 ceramics from the UT and the MC2-15 powder mixtures was further studied using the classic ceramic procedure. The powder mixtures were uniaxially pressed with a pressure of 200 MPa into pellets with diameters of 12 mm and thicknesses of 3 mm. The pellets were calcinated at either 600 °C for 2 h and 4 h (samples labeled 600-2/4 h) or at 760 °C for 2 h, 4 h and 12 h (sample labeling 760-2/4/12 h). The calcined samples were re-grinded in an agate mortar, pressed with a

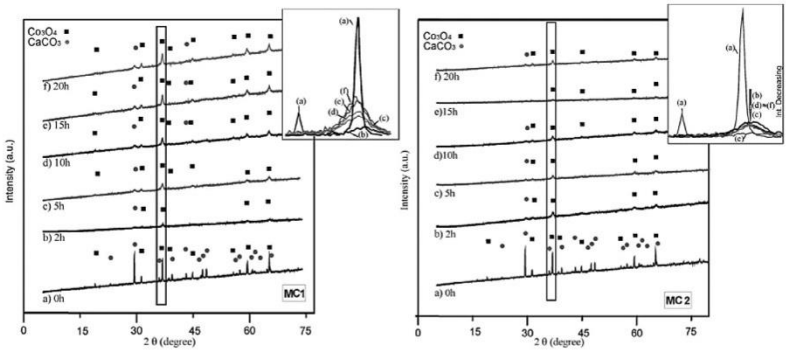


Fig. 1. The x-ray powder-diffraction patterns of series MC1 and MC2 for different milling durations.

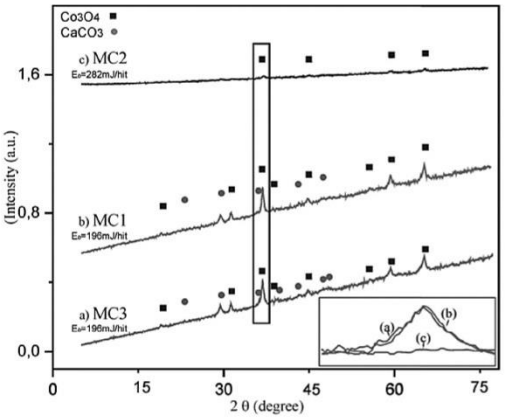


Fig. 2. X-ray powder-diffraction patterns comparison between the all three MC prepared series after 15 h of milling.

the formation of the Ca349 phase and consequently also its TE characteristics.

The results of the XRD analysis showed that after sintering at 600 °C for 2 h only the peaks of the $CaCO_3$ and Co_3O_4 occurred in the MC2-15 powder mixture and they became even stronger with a longer firing time; however, after 4 h of sintering, only in this sample, the peak of the Ca349 phase also weakly occurred (Fig. 3a).

After annealing at 760 °C for 2 h the formation of the Ca349 phase is clearly evident in both samples, in the MC2-15 sample and in the UT sample, while minor amounts of the starting reagents are still present (Fig. 3b). However, already after 4 h at 760 °C, the single-phase Ca349 was obtained in the mixture from the MC-treated powder, while in the case of the UT sample a longer time of 12 h was required. The results clearly showed that the MC-treated powder has a higher reactivity than the untreated powder.

The $Ca_3Co_4O_9$ phase forms in the reaction $9CaCO_3 + 4Co_3O_4 + O_2 \rightarrow 3Ca_3Co_4O_9 + 9CO_2$, assuming that all the cobalt in the resulting Ca349 phase is in the 3 + state, so that a theoretical weight loss due to the release of CO_2 would be 19.42%. In the case that the initial valence state of cobalt from the Co_3O_4, i.e., 2/3Co in 3 + and 1/3CO in 2+, would also be preserved in the Ca349 phase, the theoretical weight loss would be 21.15%. In order to follow the reaction of the Ca349 phase formation, the weight loss for the samples prepared from the UT and the MC2-15 powder mixtures of the attrition-milled reagents was checked at different calcination temperatures between 600 °C and 760 °C (Table 2). For comparison, also the weight loss of the mixture from the as-purchased original reagent powders of $CaCO_3$ and Co_3O_4 (OR) after calcination at

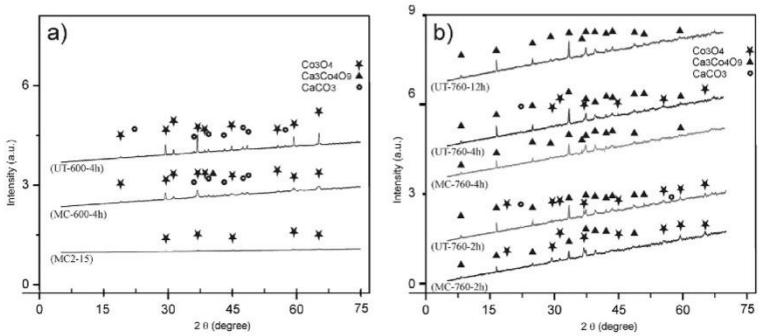


Fig. 3. X-ray diffraction patterns of the samples prepared from MC and UT powders, a) calcinated at 600 °C for 0 h and 4 h and at b) 760 °C for 2 h, 4 h and 12 h.

Table 2
Weight losses (in wt. %) after heat treatment of the samples from powder mixture of as-purchased, original reagents (OR), powder mixture from attrition-milled reagents (UT), and mechano-chemically activated powder mixture from attrition-milled reagents (MC2-15).

Calcination temperature [°C] time	600 2 h	600 4 h	760 2 h	760 4 h
Sample				
OR	/	0.36	/	/
UT	1.00	1.64	17.40	18.78
MC2-15	2.69	5.09	17.90	19.94

600 °C for 4 h is given. The much lower weight loss indicates the very poor reactivity of this mixture due to the coarse grain size of the reagents. While the use of the fine attrition-milled reagents (UT) evidently improved the reactivity of the powder mixture, it was additionally strongly enhanced by the mechano-chemical treatment; hence, after calcination at 600 °C for 4 h the weight loss in the MC2-15 sample was 5% and a sufficient amount of the Ca349 phase formed to be detected by the XRD analysis. At a higher temperature of 760 °C the weight loss is much greater after 2 h of calcination, indicating that this temperature is much more suitable for the formation of the Ca349 phase, which formed to a large degree in both powder mixtures. After 4 h of calcination the reaction of the Ca349 phase is completed only with the MC2-15 powder mixture, as indicated by the weight loss of 19.94%. Such a slightly higher weight loss than 19.42% also indicates that not all the Co^{2+} from the Co_3O_4 transformed into Co^{3+} in the Ca349 phase. In the case of UT the weight loss of 18.78% indicates an incomplete reaction and the presence of traces of the starting reagents, which is also confirmed by the XRD analysis.

The results of the DTA/TG/EG analyses of the powder mixtures are presented in Fig. 4. The TG analysis of the MC2-15 powder mixture with a weight loss of 19.9% showed good agreement with the weight loss obtained by weighing the sample after calcination at 760 °C for 4 h (Table 2). A slightly lower mass loss of 19.4 wt% was observed for the UT samples. In the DTA curve of the MC2-15 a broad endothermic peak, which could be associated with the formation of the Ca349 phase, started at approximately 432 °C and had a maximum at 706 °C. For the UT the beginning and the maximum of the endothermic peak were shifted to an almost 40 °C higher temperature. It is known that in the presence of the cobalt ion the decomposition of the $CaCO_3$ can start at low temperatures of approximately 400 °C [52]. The EG analysis clearly showed the release of CO_2 from the powder mixtures at temperatures above 550 °C; in the case of MC2-15 the maximum of the CO_2 peak was at 723 °C and with the UT at 761 °C. The results of the TG/DTA/EG analyses clearly confirm that the mechano-chemical treatment enhanced the reactivity of the powder mixture, which results in the formation of the $Ca_3Co_4O_9$ phase at an approximately 40 °C lower temperature than for the untreated mixture. The sharp endothermic peaks in the DTA patterns at temperatures above 900 °C correspond to the decomposition reactions: first, the $Ca_3Co_4O_9$ decomposes into $Ca_3Co_2O_6$ and CoO ss in the temperature range 917 °C–947 °C, followed by the decomposition of the $Ca_3Co_2O_6$ into CaO ss and CoO ss at temperatures between 1000 °C and 1023 °C.

The microstructures of the samples prepared from MC2-15 and UT powders, calcined at 760 °C for 4 and 12 h, are presented in Fig. 5. The samples have a high porosity with a density of only approximately 50% of theoretical. Such a low density resulted from the plate-like morphology of the Ca349 grains growing randomly in all directions, which inevitably leave empty spaces. The MC-760-4 h sample has the smallest and the thinnest plate-like grains with sharp edges, having a length in the range 0.2 μm–1.2 μm and a thickness up to 0.1 μm. The longer sintering time of 12 h resulted in slightly longer (0.3 μm–1.5 μm) and thicker (0.1 μm–0.2 μm) grains. In the polished microstructures of the MC samples areas of higher density can be observed, which resulted from the pronounced agglomeration of the mechano-chemically treated powder.

A much more homogeneous microstructure was obtained for the UT-760-12 h sample with a very distinct plate-like morphology of the grains, which is noticeably changed in comparison to the MC-760-12 h in terms of their shape and length. While all the grains are similar to the MC sample, i.e., very thin with a thickness of approximately 0.1 μm, they have an irregular shape with sharp edges and are almost three times longer, ranging from 1 μm to 3 μm.

The mechano-chemically activated powder mixture enabled the

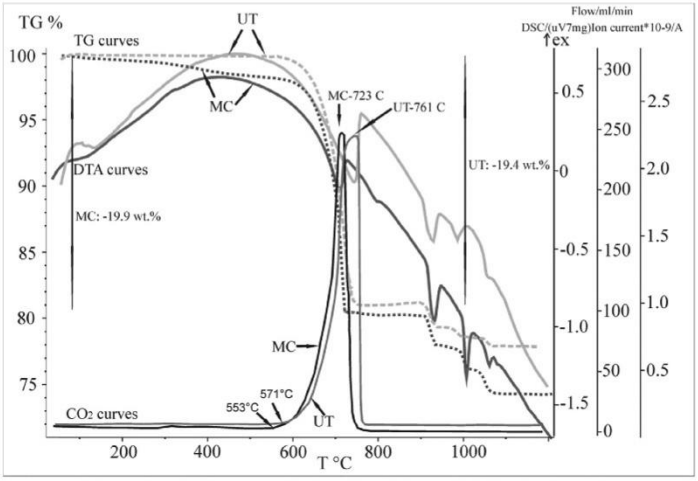


Fig. 4. DTA/TG/EG of the starting MC-treated and UT powders.

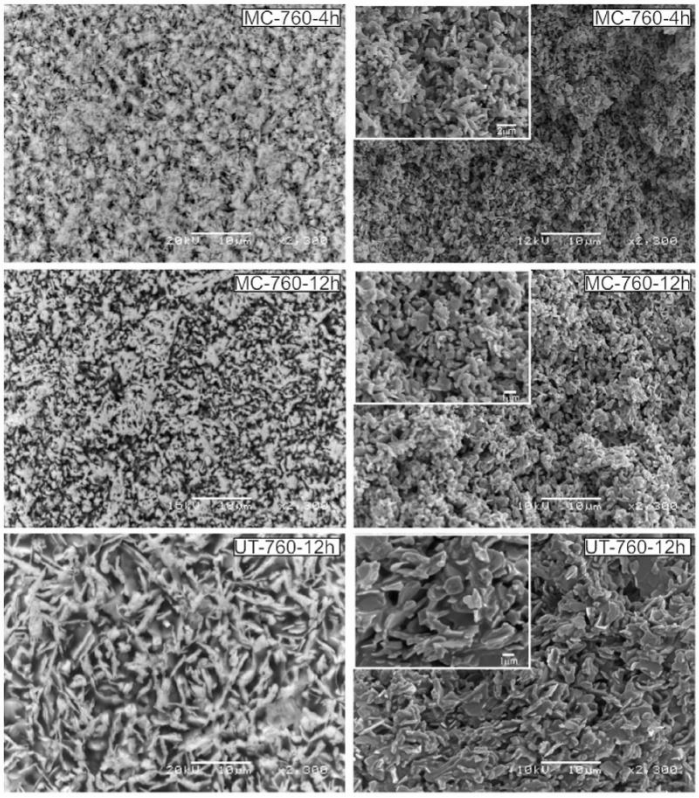


Fig. 5. SEM micrographs of polished (left) and fractured (right) surfaces of the $Ca_3Co_4O_9$ samples prepared from the MC2-15 and UT powder mixtures, calcined at 760 °C for 4 h and 12 h.

synthesis of single-phase Ca349 ceramics already after a calcination for 4 h at 760 °C; however, the microstructure is not homogeneous, even after a longer calcination of 12 h. According to reports, the finer grain size of the single-phase Ca349 powder is expected to allow the preparation of better Ca349 ceramics, with improved TE characteristics, i.e., higher ZT values [10,22]. Hence, the calcinated MC2-15 powders were reused for further processing at higher temperatures. The samples from the UT powders calcined at 760 °C for 12 h were also prepared for a comparison.

The microstructures of the Ca349 ceramics prepared from the calcined MC and UT powders and sintered at 920 °C for 20 h are presented in Fig. 6. Both samples had a relatively homogeneous microstructure and a uniform size of the randomly oriented plate-like grains. The MC-920 sample had a density of 72% and irregularly shaped grains with sharp edges, which are much smaller and thinner than in the UT-920 sample, with lengths from 0.5 to 2.5 μm and thicknesses from 0.1 to 0.3 μm. The UT-920 sample with the lower density of 60.2% had much larger grains with lengths ranging from 3 to 4 μm and also a much greater thickness of approximately 1 μm, while the plate-like grains also had much more rounded edges. The random orientation of the plate-like grains inevitably results in voids between them and hence ceramics with a low density; therefore, the longer the grains, the lower the density that could be expected. Based on the obtained results, the finer is the starting powder, the finer is the final microstructure of the Ca349 ceramics. However, due to powder agglomeration, additional intermediate grinding is needed for a homogeneous microstructure. The microstructural features observed in the Ca349 ceramics most probably influenced the TE characteristics of the samples as well.

The TE characteristics in the temperature range from approximately 40 °C–600 °C for the samples prepared from the UT and the MC powders are given in Fig. 7. In all the samples the electrical conductivity is generally slightly increasing with temperature. The highest σ of 44 S/cm at 600 °C was obtained for the sample prepared from the MC powder, sintered at 920 °C, and is among the highest reported for conventionally sintered Ca349 ceramics [12]. For comparison, the lower σ of 31 S/cm in the UT-920 sample was in very good agreement with other reports in the literature [13–16]. The obtained conductivities of those two samples closely correlate with their density, i.e., a higher density resulted in a higher conductivity of the sample. However, the influence of the grain morphology should also not be neglected. In our previous work we have shown that thin, irregular-shaped, plate-like grains with sharp edges are preferred, while thickening accompanied by rounding of their shapes results in reduced TE characteristics [7]. The microstructures of the MC-920 and the UT-920 (see Fig. 6) samples

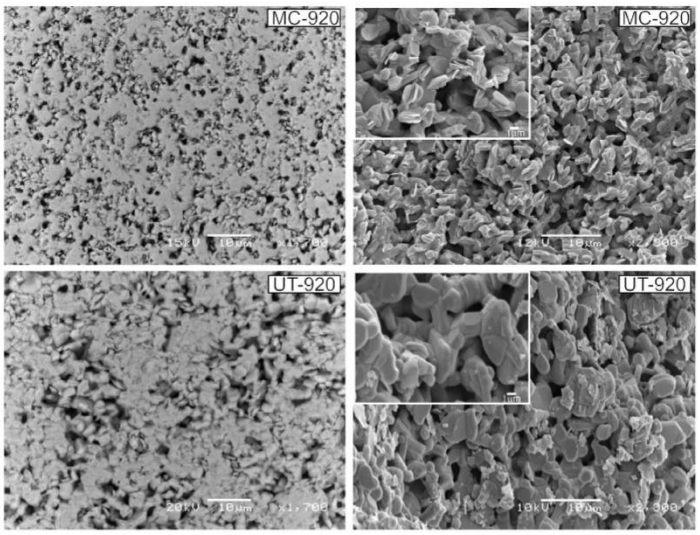


Fig. 6. SEM micrographs of polished and fractured surfaces of the $Ca_3Co_4O_9$ samples prepared from MC and UT powders, sintered at 920 °C for 20 h.

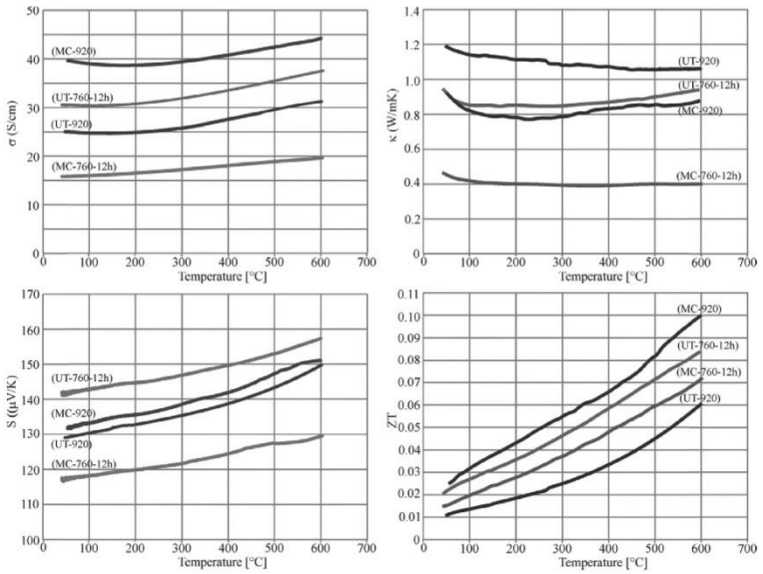


Fig. 7. Temperature dependence of electrical conductivity σ, Seebeck coefficient S, thermal conductivity κ and the figure of merit ZT for Ca349 samples prepared from UT and MC powders calcinated at 760 °C and sintered at 920 °C, respectively.

illustrate this perfectly. Furthermore, it is usually assumed that σ would be decreased by reducing the grain size due to an increased number of grain boundaries. However, this is not the case for the UT and the MC samples sintered at 920 °C, and could indicate an increased number of acceptor crystal defects and hence increased charge carriers concentration; it was recognized for the compounds with misfit layered structure that the charge carrier concentration is sensitive to the mechanical stress caused by the high-energy milling process [32]. A possible increase in the Co^{4+} ions caused by the charge transfer between the rock salt Ca_2CoO_3 layers with

Co^{3+}/Co^{2+} ions and the CdJ_2-type CoO_2 layers with Co^{3+}/Co^{4+} in order to preserve the charge neutrality of both layers, results in high concentration of mobile holes in the CoO_2 layer [53].

A very low conductivity σ in the range from 16 to 20 S/cm was obtained for the MC-760-12 h sample, which could be expected due to the very inhomogeneous microstructure and the large number of grain boundaries due to fine grains with a broad size distribution. For comparison, the UT-760-12 h sample performed much better in this regard, having much longer plate like grains, which can provide pathways with a lower resistivity.

The positive Seebeck coefficients of all the samples indicate a p-type electrical conductivity and are shown in Fig. 7. The UT-760-12 h sample with a low density and electrical conductivity showed the highest S, ranging from 142 to 157 μV/K. The MC-920 sample with a much smaller grain size had a lower S ranging from 131 to 151 μV/K. A similar S in the range from 129 to 150 μV/K was also observed for the sample UT-920, with a low density, having longer, thicker and more rounded grains. The smallest S, ranging from 117 to 130 μV/K, was observed for the MC-760-12 h sample with a high microstructural inhomogeneity and the least-developed plate-like morphology. The observed differences in S among the samples could be attributed to the complex influences of their microstructural features, including density, grain morphology, grain size and connectivity, the nature of the grain boundaries and also the mechanical stress in the grains, which can all affect the carrier concentration and their mobility [32,54–56]. However, the influence of the oxygen stoichiometry of the $Ca_3Co_4O_{9+d}$ compound, which is sensitive to the preparation conditions, and is known to affect the electrical conductivity and the Seebeck coefficient, could also not be excluded [57,58].

Surprisingly, the highest thermal conductivity κ ranging from 1.17 W/mK at approximately 40 °C to 1.06 W/mK at 600 °C was observed in the UT-920 sample with a rather low density and electrical conductivity. However, in comparison to all the other samples it has significantly thicker, longer and rounded plate-like grains, which probably results in less effective phonon scattering. The κ values for the UT-920 sample are in good agreement with reports in the literature [16,22]. As expected, the sample UT-760-12 h with a higher porosity and thin plate-like grains had a much lower κ of approximately 0.9 W/mK. However, an even lower κ of 0.87 W/mK was obtained in the MC-920 sample that still had a relatively low density, but the highest among the samples in this study. This could be mainly connected with its fine-grained, homogeneous microstructure (see Fig. 6), which increases the grain-boundary scattering. However, the influence of the defects, likely introduced by the mechano-chemical milling, should not be excluded, especially when explaining the difference between the more porous UT-760-12 h sample with the higher κ and the MC-920 sample, which actually had a lower κ. This low κ of the MC-920 sample is among the lowest reported for conventionally sintered samples with a random grain orientation and was previously achieved only in the case of sol-gel prepared samples [10]. As was anticipated, the lowest κ of 0.4 W/mK was observed in the MC-760-12 h sample because of the inhomogeneous microstructure of the fine, plate-like grains that were locally agglomerated.

Benefiting from the enhanced electrical conductivity and the very low thermal conductivity, the ZT value of the MC-920 sample significantly improved to 0.10 at 600 °C, as shown in Fig. 7, which is approximately two times higher in comparison to the highest ZT values reported in the literature for un-doped Ca349 ceramics prepared from $CaCO_3$ and Co_3O_4 powders using a classic ceramic procedure and sintering [6], and 40% higher than in the comparable UT-920 sample. A similar ZT of 0.08 was also measured for the UT-760-12 h sample, which confirms the importance of the small, thin, irregularly shaped, plate-like grains with sharp edges. The lowest ZT of 0.06 among the samples was measured for the UT-920 sample, which had the highest and the thickest, roundest and largest grains. The MC-760-12 h sample exhibited a ZT of 0.07; such a value was achieved because of its very low thermal conductivity, while the very low σ and S, due to the non-homogeneous microstructure, prevented it from being higher. Although the results clearly showed that the MC treatment can evidently improve the TE characteristics of the un-doped Ca349 ceramics prepared by the classic ceramic procedure and conventional sintering the obtained ZT values are still far away from the requirements of the application.

4. Conclusions

In this work the influence of a mechano-chemical (MC) treatment on the formation of the Ca349 phase from a stoichiometric mixture of fine-grained $CaCO_3$ and Co_3O_4 powders, the microstructural and the thermoelectric characteristics of the Ca349 ceramics was studied. The maximum ball-impact energy (Eb) of 283 mJ/hit obtained in this study was not sufficient for the synthesis of the Ca349 compound using high-energy milling. However, the MC treatment resulted in a completely amorphous mixture of $CaCO_3$ and Co_3O_4 powders. In such an activated powder mixture the reaction of the Ca349 phase formation started at an approximately 40 °C lower temperature in comparison to the untreated sample. Hence, with the MC powder mixture a single-phase Ca349 ceramic was obtained after only 4 h of calcination at 760 °C, while the untreated powder mixture required a three-times longer heat treatment. The calcined samples were fine-grained and highly porous with a density of 50% of theoretical. The MC samples had a particularly un-homogeneous microstructure, which caused a low electrical conductivity σ of 20 S/cm and a low Seebeck coefficient S of 130 μV/K, so that even with an extremely low thermal conductivity κ of 0.40 W/mK the sample had a ZT of 0.07 at 600 °C. However, additional sintering at 920 °C for 20 h of the calcined MC sample with intermediate grinding resulted in single-phase Ca349 ceramics with a density of 72% and a very homogeneous, fine-grained microstructure of randomly oriented, plate-like grains with a uniform size distribution, an irregular shape and sharp edges. Such a microstructure resulted in an enhanced σ of 44 S/cm, an S of 151 μV/K and a low κ of 0.87 W/mK, which all contributed to a significantly improved ZT value of 0.10 at 600 °C in comparison to the values reported in the literature for conventionally prepared Ca349 ceramics.

This study showed that a mechano-chemical treatment with high-energy milling increases the reactivity of the starting mixture of $CaCO_3$ and Co_3O_4 powders and enhances the formation of the fine-grained Ca349 phase at low calcination temperatures, thus enabling the preparation of Ca349 ceramics with improved TE characteristics.

Acknowledgements

The authors acknowledge the financial support by the Slovenian Research Agency (Program Contract No. P2-0084, Project Grant L2-4192 and Young Researcher Program PR-03102).

References

[1] I. Terasaki, Y. Sasago, K. Uchinokura, Large thermoelectric power in $NaCo_2O_4$ single crystal, Phys. Rev. B 56 (1997) 12685–12687.
[2] M. Ohtaki, Recent aspects of oxide thermoelectric materials for power generation from mid-to high temperature heat source, J. Ceram. Soc. Jpn. 119 (2011) 770–775.
[3] J.W. Fergus, Oxide materials for high temperature thermoelectric energy conversion, J. Eur. Ceram. Soc. 32 (2012) 525–540.
[4] A.C. Masset, C. Michel, A. Maignan, M. Herieu, O. Toulmonde, F. Studer, B. Raveau, J. Hajtmanek, Misfit-layered cobaltite with an anisotropic giant

magnetoresistance: $Ca_3Co_4O_9$, Phys. Rev. B 62 (2) (2000) 166–175.
[5] M. Shikano, R. Funahashi, Electrical and thermal properties of single-crystalline $(Ca_2CoO_3)_{0.7}CoO_2$ with a $Ca_3Co_4O_9$ structure, Appl. Phys. Lett. 82 (2003) 1851–1853.
[6] S. Li, R. Funahashi, I. Matsubara, K. Ueno, S. Sodeoka, H. Yamada, Synthesis and thermoelectric properties of the new oxide materials $Ca_{3-x}Bi_xCo_4O_{9-\delta}$ ($0.0 < x < 0.75$), Chem. Mater. 12 (2000) 2424–2427.
[7] M. Presečnik, J. de Boor, S. Bernik, Synthesis of single-phase $Ca_3Co_4O_9$ ceramics and their processing for microstructure-enhanced thermoelectric performance, Ceram. Int. 42 (2016) 7315–7327.
[8] Y. Masuda, D. Nagahama, H. Itahara, T. Tani, W.S. Seo, K. Koumoto, Thermoelectric performance of Bi- and Na-substituted $Ca_3Co_4O_9$ improved through ceramic texturing, J. Mater. Chem. 13 (2003) 1094–1099.
[9] F. Delorme, C. Fernandez Martin, P. Marudhachalam, D. Ovono Ovono, G. Guzman, Effect of Ca substitution by Sr on the thermoelectric properties of $Ca_3Co_4O_9$ ceramics, J. Alloys. Compd. 509 (2011) 2311–2315.
[10] M. Gunes, M. Ozenbas, Effect of grain size and porosity on phonon scattering enhancement of Ca3Co4O9, J. Alloy. Compd. 626 (2015) 360–376.
[11] N.V. Nong, C.J. Liu, M. Ohtaki, High-temperature thermoelectric properties of late rare-earth-doped $Ca3Co4O9+\delta$, J. Alloys Compd. 509 (2011) 977–981.
[12] G. Constantinescu, Sh. Rasekh, M.A. Torres, P. Bosque, J.C. Diez, M.A. Madre, A. Sotelo, Effect of Na doping on the $Ca_3Co_4O_9$ thermoelectric performance, Ceram. Int. 41 (2015) 897–903.
[13] D. Kenfaui, D. Chateigner, M. Gomina, J.G. Noudem, Anisotropy of the mechanical and thermoelectric properties of hot-pressed single-layer and multilayer thick $Ca_3Co_4O_9$ ceramics, Int. J. Appl. Ceram. Technol. 8 (1) (2011) 214–226.
[14] D. Kenfau, D. Chateigner, M. Gomina, J.G. Noudem, Texture, mechanical and thermoelectric properties of $Ca_3Co_4O_9$ ceramics, J. Alloy. Compd. 490 (2010) 427–429.
[15] D. Kenfaui, G. Bonnefont, D. Chateigner, G. Fantozzi, M. Gomina, J.G. Noudem, $Ca_3Co_4O_9$ ceramics consolidated by SPS process: optimisation of mechanical and thermoelectric properties, Mater. Res. Bull. 45 (2010) 1240–1249.
[16] H. Wang, X. Sun, X. Yan, D. Huo, X. Li, J.-G.- Li, X. Ding, Fabrication and thermoelectric properties of highly textured $Ca_9Co_{12}O_{28}$ ceramic, J. Alloy. Compd. 582 (2014) 294–298.
[17] E. Woermann, A. Muan, Phase equilibria in the system Cao-cobalt oxide in air, J. Inorg. Nucl. Chem. 32 (1970) 1455–1459.
[18] H. Hao, L. Zhao, X. Hu, Microstructure and thermoelectric properties of Bi- and Cu- substituted Ca3Co4O9 oxides, J. Mater. Sci. Technol. 25 (1) (2009) 105–108.
[19] H. Nakatsugawa, H.M. Jeong, K. Nagasawa, Thermoelectric properties and crystal structure in Y doped $Ca_3Co_4O_9$, in: H. Kim prof. II (Ed.), Proceedings of the 26th International Conference on Thermoelectrics, ICT, Jeju, Korea, 2007.
[20] Y. Huang, B. Zhao, S. Lin, R. Ang, W. Song, Y. Sun, Strengthening of thermoelectric performance via Ir doping in layered $Ca_3Co_4O_9$ system, J. Am. Ceram. Soc. 97 (3) (2014) 798–804.
[21] G. Constantinescu, S. Rasekh, M.A. Torres, C. Chocarro, J.C. Diez, M.A. Madre, A. Sotelo, Influence of Ca substitution by Mg on the $Ca_3Co_4O_9$ performances, Bol. Soc. Esp. Cerám. V. 53 (1) (2014) 41–47.
[22] S. Chen, X. Song, X. Chen, Y. Chen, E.J. Barbero, E.L. Thomas, P.N. Barnes, Effect of precursor calcination temperature on the microstructure and thermoelectric properties of $Ca_3Co_4O_9$ ceramics, J. Sol. Gel Sci. Technol. 64 (2012) 627–636.
[23] Q. Xiaoling, Z. Lingke, W. Hui, L. Ping'an, L. Yanchun, Thermoelectric properties of $Ca_3Co_4O_9$ ceramics, J. Wuhan. Univ. Technol. (2010) 287–290.
[24] N.Y. Wu, T.C. Holgate, N. Van Nong, N. Pryds, S. Linderoth, High temperature thermoelectric properties of $Ca_3Co_4O_{9+\delta}$ by auto-combustion synthesis and spark plasma sintering, J. Eur. Ceram. Soc. 34 (2014) 925–931.
[25] N. Prasoetsopha, S. Pinitsoontorn, V. Amornkitbamrung, Synthesis and thermoelectric properties of $Ca_3Co_4O_9$ prepared by simple thermal hydrodecomposition methods, Electron. Mater. Lett. 8 (3) (2012) 305–308.
[26] M. Zdujić, D. Poleti, Č. Jovalekić, L. Karanović, The evolution of structure induced by intensive milling in the system $2Bi_2O_3 + 3TiO_2$, J. Non Cryst. Solids 352 (2006) 3058–3068.
[27] S.K. Bux, M.T. Yeung, E.S. Toberer, G.J. Snyder, R.B. Kanerband, J.-P. Fleuriala, Mechanochemical synthesis and thermoelectric properties of high quality magnesium silicide, J. Mater. Chem. 21 (2011) 12259–12266.
[28] O. Falkenbach, A. Schmitz, T. Dankwort, G. Koch, L. Kienle, E. Mueller, S. Schlecht, Influence of mechanochemical syntheses and compacting methods on the thermoelectric properties of nanostructured $AgSnmSbTe_{2-m}$ (TAST-m), Semicond. Sci. Technol. 29 (2014), 124009 (9pp).
[29] V.V. Zyryanov, Mechanochemical synthesis of complex oxides, Russ. Chem. Rev. 77 (2) (2008) 105–135.
[30] J. Benjamin, Dispersion strengthened superalloys by mechanical alloying, Metall. Trans. (1970) 2943–2951.
[31] T. Rojac, M. Kosec, B. Malič, J. Holc, The application of a milling map in the mechanochemical synthesis of ceramics oxides, Mater. Res. Bull. 40 (2005) 341–345.
[32] F. Li, J.-F. Li, L.-D. Zhao, K. Xiang, Y. Liu, B.-P. Zhang, Y.-H. Lin, C.-W. Nan, H.-M. Zhu, Polycrystalline BiCuSeO oxide as a potential thermoelectric material, Energy Environ. Sci. 5 (2012) 7188–7195.
[33] B.D. Stojanovic, Mechanochemical synthesis of ceramic powders with perovskite structure, J. Mater. Process. Technol. 143–144 (2003) 78–81.
[34] K. Wieczorek-Ciurowa, P. Dulian, A. Nosal, J. Domagała, Effects of reagents' nature on mechanochemical synthesis of calcium titanate, J. Therm. Anal. Calorim. 101 (2010) 471–477.
[35] S.H. Ng, J.M. Xue, J. Wang, High temperature piezoelectric strontium bismuth titanate from mechanical activation of mixed oxides, Mater. Chem. Phys. 75 (2002) 131–135.
[36] M.H. Sim, J.M. Xue, J. Wang, Layer structured calcium bismuth titanate by mechanical activation, Mater. Lett. 58 (2004) 2032–2036.
[37] C. Gomez-Yanez, C. Benitez, H. Balmori-Ramirez, Mechanical activation of the synthesis reaction of $BaTiO_3$ from mixture of $BaCO_3$ and TiO_2 powders, Ceram. Int. 26 (2000) 271–277.
[38] V. Berbenni, A. Marini, Synthesis of $Sr_xBa_{(1-x)}TiO_3$ solid solutions from the mechanically activated system $BaCO_3$–$SrCO_3$–TiO_2, Z. Naturforsch. B 57 (8) (2002) 859–864.
[39] J. Liao, M. Senna, Mechanochemical dehydration and amorphization of hydroxides of Ca, Mg, Al on grinding with and without SiO_2, Solid State Ion. 66 (1993) 313–319.
[40] J.A. Hedvall, Solid State Chemistry: Whence, where and Whither, Elsevier, Amsterdam, 1966.
[41] P.D. Garn, T.S. Habash, A rigorous test of the Hedvall effect, J. Phys. Chem. 83 (2) (1979) 229–231.
[42] U. Seifert, S. Dietrich, Non-Markovian description of the Hedvall effect, Europhys. Lett. 3 (5) (1987) 593–600.
[43] M. Presečnik, S. Bernik, The Thermoelectric Compound $Ca_3Co_4O_9$ – Synthesis and Characteristics, AIP Publishing, Thessaloniki, 2011.
[44] N. Burgio, A. Iasonna, M. Magini, F. Padella, Mechanical alloying of the Fe–Zr system in different milling conditions, J. Phys. Colloq. 51 (C4) (1990) 265–271.
[45] S. Bernik, M. Pribošek, Construction and characteristics of a Z-meter setup for thermoelectric measurements of materials, in: Z.A., Š.P., Š.I (Eds.), Proceedings of the 49th International Conference on Microelectronics, Devices and Materials MIDEM Kranjska Gora, Slovenia, 2013, pp. 121–126.
[46] A. Iasonna, M. Magini, Power measurements during mechanical milling. An experimental way to investigate the energy transfer phenomena, Acta Mater. 44 (9) (1996) 1109–1117.
[47] M. Magini, N. Burgio, A. Iasonna, S. Martelli, F. Padella, E. Paradiso, Analysis of energy transfer in the mechanical alloying process in the collision regime, J. Mater. Synth. Process. 1 (3) (1993) 135–144.
[48] F. Delogu, G. Mulas, L. Schiffini, G. Cocco, Mechanical work and conversion degree in mechanically induced processes, Mater. Sci. Eng. A 382 (2004) 280–287.
[49] G. Cocco, F. Delogu, L. Schiffini, Toward a quantitative understanding of the mechanical alloying process, J. Mater. Synth. Process. 8 (3/4) (2000) 167–180.
[50] F. Delogu, L. Schiffini, G. Cocco, The invariant laws of the amorphization processes by mechanical alloying. I. Experimental findings, Philos. Mag. A 81 (8) (2001) 1917–1937.
[51] J. Alkebro, S. Begin-Colin, A. Mocellin, R. Warren, Modelling high-energy ball milling in the alumina-Yttria system, J. Solid State Chem. 164 (2002) 88–97.
[52] P. Smaczynski, M. Sopicka-Lizer, K. Kozlowska, J. Plewa, Low temperature synthesis of calcium cobalatites in a solid state reaction, J. Electroceram. 18 (2007) 255–260.
[53] G. Yang, Q. Ramasse, R.F. Klie, Direct measurement of charge transfer in thermoelectric $Ca_3Co_4O_9$, Phys. Rev. B 78 (2008), 153109–4.
[54] J.C. Slater, Barrier theory of the photoconductivity of lead sulphide, Phys. Rev. 103 (1956) 1631–1644.
[55] J.Y.W. Seto, The electrical properties of polycrystalline silicon films, J. Appl. Phys. 46 (1975) 5247–5254.
[56] J. Martin, L. Wang, L. Chen, G.S. Nolas, Enhanced Seebeck coefficient through energy-barrier scattering in PbTe nanoparticles, Phys. Rev. B 78 (2009) 11531–11535.
[57] M. Karppinen, H. Fjellvåg, T. Konno, Y. Morita, T. Motohashi, H. Yamauchi, Evidence for oxygen vacancies in misfit-layered calcium cobalt oxide, $[CoCa_2O_3]_qCoO_2$, Chem. Mater. 16 (2004) 2790–2793.
[58] M. Schrade, S. Casolo, P.J. Graham, C. Ulrich, S. Li, O.M. Løvvik, T.G. Finstad, T. Norby, Oxygen nonstoichiometry in $(Ca_2CoO_3)_{0.62}(CoO_2)$: a combined experimental and computational study, J. Phys. Chem. C 118 (2014) 18899–18907.

Chapter 7

Microstructural and Thermoelectric Properties of WO_3-Doped $Ca_3Co_4O_9$ Ceramics

In this chapter, a paper entitled "**Microstructural and thermoelectric properties of WO_3-doped $Ca_3Co_4O_9$ ceramics**", by authors M. Presečnik and S. Bernik is presented.

The purpose of this research was to synthesise the WO_3-doped Ca349 ceramics and to study the influence of doping with high-valence and heavy W^{6+} ion on the formation, phase composition, grain morphology, microstructure and thermoelectric properties (σ, S, κ and zT) in the temperature range from 40 to 615 °C. In the study reported in the literature only the influence of WO_3-doping on the electrical conductivity in the low-temperature range from 5 K to 350 K was examined.

Polycrystalline samples of the p-type $Ca_3Co_{4-x}W_xO_9$ ceramics for x=0, 0.02, 0.05 0.1 and 0.2, were prepared by the classic ceramic procedure using fine powders of $CaCO_3$, Co_3O_4 and WO_3, and sintering at 900 °C. The formation of single-phase solid solution with a composition of about $Ca_3Co_{3.88}W_{0.12}O_9$ was determined and confirmed that W^{6+} ions substitute the Co^{2+} in the Ca_2CoO_3 layers. For larger addition (x = 0.2) a Ca_3WO_6 secondary phase was detected in the samples even after several sintering and grinding cycles, while the composition of the solid solution remained the same. The result showed a much lower limit of WO_3-solid-solubility in the $Ca_3Co_{4-x}W_xO_9$ phase than reported previously ($0.4 < x < 0.5$). Doping with WO_3 resulted in more irregular-shaped, sharp-edged and thinner plate-like grains compared to the more rounded and thicker plate-like grains in the un-doped $Ca_3Co_4O_9$ ceramics. The TE characteristics of the $Ca_3Co_{4-x}W_xO_9$ ceramics were measured for the first time in the temperature range from 40 °C to 615 °C and in general showed, as expected, increased Seebeck coefficient (S), decreased thermal conductivity κ and unfortunately also decreased electrical conductivity(σ) in comparison to un-doped $Ca_3Co_4O_9$ ceramics. The decrease of κ was mainly attributed to the reduced lattice thermal conductivity κ_l, which accounts for about 95% of the total κ. The figure of merit zT of the samples decreased with the W-doping from 0.06 at 615 °C for the un-doped sample to 0.047 for the sample with the largest addition of WO_3 (x = 0.2).

ARTICLE IN PRESS

Ceramics International ∎ (∎∎∎∎) ∎∎∎–∎∎∎

Contents lists available at ScienceDirect

Ceramics International

journal homepage: www.elsevier.com/locate/ceramint

Microstructural and thermoelectric properties of WO_3-doped $Ca_3Co_4O_9$ ceramics

M. Presečnik [a,b,*], S. Bernik [a]

[a] Jožef Stefan Institute, Jamova cesta 39, 1000 Ljubljana, Slovenia
[b] Jožef Stefan International Postgraduate School, Jamova cesta 39, 1000 Ljubljana, Slovenia

ARTICLE INFO

Article history:
Received 13 June 2016
Accepted 18 July 2016

Keywords:
$Ca_3Co_4O_9$
WO_3-doping
Microstructure
Thermoelectric properties

ABSTRACT

WO_3-doped ceramics with the composition $Ca_3Co_{4-x}W_xO_9$ and x=0, 0.02, 0.05 0.1 and 0.2 were prepared by the classic ceramic procedure from fine oxide powders and sintering in air at 900 °C. The influence of the composition on the microstructure development and the thermoelectric characteristics in the temperature range from 40 °C to 615 °C was studied. The formation of a solid solution with the composition $Ca_3Co_{3.88}W_{0.12}O_9$ was determined and indicates a much lower limit of WO_3 solubility in the $Ca_3Co_4O_9$ than has been reported previously. Doping with WO_3 resulted in more irregularly shaped, sharp-edged and thinner plate-like grains in comparison to the grains in the un-doped $Ca_3Co_4O_9$ ceramics. The un-doped ceramics had an electrical conductivity σ of 31 S/cm, a Seebeck coefficient S of 147 μV/K and a thermal conductivity κ of 1.15 W/mK, giving a figure of merit ZT of 0.06 at 615 °C. The WO_3-doping decreased the electrical conductivity σ to 18 S/cm, increased the Seebeck coefficient to 157 μV/K and also decreased the thermal conductivity κ to 0.88 W/mK, resulting in an overall reduced ZT of 0.047 for the $Ca_3Co_{3.88}W_{0.12}O_9$ ceramics.

© 2016 Elsevier Ltd and Techna Group S.r.l. All rights reserved.

1. Introduction

Thermoelectric (TE) materials could play an important role in future energy-sustainable technologies; thermoelectric modules made from n- and p-type TE materials offer the only viable method for a direct conversion of thermal energy into electricity and hence the exploitation of waste heat, which makes up almost 70% of all primarily produced energy [1]. The TE characteristics of the materials are given by the dimensionless figure of merit ZT ($=S^2T/\rho\kappa$) [2]. In general, for a good TE material with a high value of ZT, a high thermopower S, a high electrical conductivity σ and a low thermal conductivity κ are required. However, in semiconductor materials the σ and the S are generally related to the carrier concentration and the mobility in opposite ways, and hence it is hard to optimize them simultaneously. An exception is the coexistence of a high S and a relatively high σ in single-crystal $Ca_3Co_4O_9$, makes it a promising p-type TE material [3–5]. Furthermore, in comparison to other layered cobalt oxides such as Na_xCoO_2 and $Bi_2Sr_2Co_2O_x$, the $Ca_3Co_4O_9$ is also considered to be more suitable due easier processing and better environmental stability up to high temperatures [6].

The $Ca_3Co_4O_9$ phase can also be described as $(Ca_2CoO_3)_{0.62}CoO_2$, which better expresses its structure composed of two subsystems stacking alternately along the c-axis: the rock-salt (RS)-type CaO–CoO–CaO layers and the CdI_2-type CoO_2 layers. The Ca_2CoO_3 is regarded as the charge reservoir to supply the charge carriers to the CoO_2 layers. The CoO_2 subsystem, in which the two-dimensional (2D) triangular lattice of Co-ions is formed by the network of an edge-sharing CoO_2 octahedral lattice, dominates the electronic structure and the carrier transport in the material. The two sub-lattices have the same a, c and β parameters, but they have a different b lattice parameter with the ratio between the b1 of Ca_2CoO_3 and the b2 of CoO_2 being 1.62, causing a misfit along the b-direction [7–9]. As a consequence of such a complex structure, various physical characteristics have also been observed, i.e., the low-temperature ferromagnetic (FIM) state, the incommensurate spin-density-wave (IC-SDW) ordering, the metal-insulator transition (MIT), and the spin-state transition (SST) for Co ions [10,11]. Also, the high ZT value for the oxide material of 0.87 at 700 °C for a single crystal [3] is one of the consequences. However, the use of single crystals for larger-scale applications is limited. Much more feasible is the use of polycrystalline ceramics, which unfortunately have inferior TE characteristics, despite many attempts to improve them using different processing methods, expressed for un-doped $Ca_3Co_4O_9$ in ZT values up to about 0.31 at 600–700 °C [12–16]. The addition of dopants was aimed at their substitution on either Ca-sites or Co-sites. In general, doping on Ca-sites only changes the carrier concentration of the system and

* Corresponding author.
E-mail address: mojca.presecnik@ijs.si (M. Presečnik).

http://dx.doi.org/10.1016/j.ceramint.2016.07.124
0272-8842/© 2016 Elsevier Ltd and Techna Group S.r.l. All rights reserved.

Please cite this article as: M. Presečnik, S. Bernik, Microstructural and thermoelectric properties of WO_3-doped $Ca_3Co_4O_9$ ceramics, Ceramics International (2016), http://dx.doi.org/10.1016/j.ceramint.2016.07.124

ARTICLE IN PRESS

has less influence on the band structure. In contrast, doping on Co-sites, especially in the CoO_2 layer, can cause a large change in the physical properties because the band structure and the transport mechanism are affected [5,17]. Doping with rare-earth elements (RE^{3+}) resulted in their substitution at the Ca-sites and, in general, decreased the electrical and thermal conductivities while increasing the Seebeck voltage (S) [18–25]. The substitution of Ca^{2+} with RE^{3+} is compensated by an increased share of Co^{2+} with respect to the Co^{3+} for preserving the charge neutrality of the Ca_2CoO_3 layers, which as a consequence affects the lower concentration of holes in the conducting CoO_2 layers. The highest ZT of 0.36 at 800 °C was reported for a Lu-doped $Ca_{2.8}Lu_{0.2}Co_4O_{9+\delta}$ sample [19]. Attempts at doping the Ca-sites were also made with the alkali (Na, K) elements [26,27], alkaline-earth metals Mg, Sr and Ba [28–30], and resulted in either just a slightly increased electrical conductivity σ and Seebeck coefficient S, or practically no change and a ZT value up to 0.22. Higher ZT values of 0.5 were obtained by doping with Ag, Ga, Sb, Pb and Bi. [26,31–34] For the substitutions at the Co-site mostly various transitional elements (Ti, Mn, Ni, Pt, Cu, Zn) were considered [35–41] and ZT values up to 0.28 were obtained. The results of these previous studies indicated that the doping/substitution of high-valence ions (i.e., 3^+ or 4^+) for the Ca- or Co-sites can increase S and decrease σ due to a decrease in the hole concentration, and also a reduced thermal conductivity by decreasing the lattice thermal conductivity. Fu et al. studied, in the temperature range from 5 to 350 K, the influence of Co substitution with 6+ ions of Cr, Mo and W on the structural, magnetic, transport and thermal properties of $Ca_3Co_{4-x}M_xO_9$ ceramics for x values from 0 to 0.5, sintered at 900 °C [40–42]. They found that Cr^{6+} substitutes Co^{4+} in the CoO_2 layers to a maximum amount of 0.3 (the limit of solid solubility); with increasing x the Seebeck voltage increased, the thermal conductivity k decreased due to a reduced lattice thermal conductivity k_l; however, a decrease in the electrical conductivity σ also prevented the enhancement of the ZT [42]. The Mo^{6+} substitutes Co in the CoO_2 layers, the solid solubility for x=0.4 (maximum doping) was not exceeded yet [40]. For x=0.1 the σ decreased and the S increased, while for $x > 0.1$ the σ increased and the S decreased; however, even for the largest x=0.4 the σ was still lower and the S still higher than for x=0. The thermal conductivity was not reported. In the case of W^{6+} the authors reported [41] that it substitutes Co in the Ca_2CoO_3 layers with the solubility limit being in the range $0.4 < x < 0.5$, resulting in a decreased electrical conductivity σ with increasing W-doping, so that for x=4 the conductivity was about 4-times lower than for x=0. The valence of W is higher than the average valence of Co ions (generally 2+, 3+ or 4+); hence, the substitution of W to Co can be considered as electron-doping, which will decrease the carrier concentration (i.e., the concentration of holes) in the system. They also considered the oxygen non-stoichiometry, which always exists in the $Ca_3Co_4O_9$ system and would increase with W-doping based on the valence equilibrium, causing a decrease in the carrier concentration. However, with regard to the same sample-preparation conditions, the authors concluded that the variation in the oxygen non-stoichiometry is minor in the studied series of samples. They did not report the other TE characteristics.

In this work W-doped ceramics with the composition $Ca_3Co_{4-x}W_xO_9$ for x=0, 0.02, 0.05, 0.1 and 0.2 were prepared by the classic ceramic procedure from oxide powders and sintering at 900 °C. The influence of W-doping on the phase composition, grain morphology, microstructure and thermoelectric properties (σ, S, κ and ZT) in the temperature range from 40 to 615 °C was studied.

2. Experimental

Samples of $Ca_3Co_{4-x}W_xO_9$ with x=0, 0.02, 0.05, 0.1 and 0.2 were prepared using a classic ceramic procedure from powders of $CaCO_3$ (Alfa Aesar, stock #011403Lot #G23W035, 99.5% metals basis, 5 μm), Co_3O_4 (Alfa Aesar, stock #45806, Lot #B29T027, 99.7% metals basis, 2–6 μm) and WO_3 (Inframat Advanced Materials, stock #74N-0812, 99.9% purity, ~40 nm). The $CaCO_3$ and the Co_3O_4 were attrition milled for 6 h to obtain fine powders with an average grain size of 0.45 μm and 0.36 μm, respectively. The mixtures of $CaCO_3$, Co_3O_4 and WO_3 were homogenised for 2 h in a planetary mill with absolute ethanol, dried and uniaxially pressed using a pressure of 250 MPa into pellets with a diameter of 12 mm and a height of 12 mm. The samples were sintered four times at 900 °C for 20 h in air with intermediate grindings in the agate mortar.

The phase composition of the samples and the formation of the $Ca_3Co_4O_9$ phase were analysed after each sintering using X-ray diffraction (XRD) analysis (X'PertPRO MPD, Cu-Kα, 2Θ range 5–80°). Their densities were measured using a density-measurements system Densitec (Metar sa, Matran, Switzerland). The microstructures of the fractured and polished cross-sections of the samples were analysed using a JEOL JSM-5800 scanning electron microscope (SEM) equipped with an energy-dispersive x-ray spectrometer (EDXS) and an Oxford Instruments Link Isis software system for the compositional analysis of the phases. From the SEM images of the fractured surfaces an average grain size was determined based on rough measurements of approximately 40 grains with clearly visible edges per sample. The TE characteristics were measured on samples with diameters and heights of approximately 9 mm in a vacuum of 10^{-2} to 10^{-3} Pa using a Z-metre [43], which enables simultaneous measurements of the Seebeck voltage (S), the electrical (σ) and the thermal conductivity (κ) up to a maximum temperature of 650 °C.

3. Results and discussion

3.1. XRD characterisation

The XRD patterns of the $Ca_3Co_{4-x}W_xO_9$ samples for x=0, 0.02, 0.05, 0.1 after the 2nd sintering and for x=0.2 after the 4th sintering at 900 °C are shown in Fig. 1. In the samples with $x \leq 0.1$ only the $Ca_3Co_4O_9$ phase (Ca349) was observed (JCPDF 21-139). In the sample with x=0.2 a secondary Ca_3WO_6 phase (JCPDF 22-0541) was also detected. Its amount decreased with additional grinding and sintering cycles; however, some Ca_3WO_6 phase was still detected even after the 4th sintering at 900 °C. In the XRD patterns of all the samples the (001) peaks are strongly expressed and dominate in comparison to the other (*hkl*) peaks, which results from the distinctive plate-like morphology of the grains unavoidably causing their spontaneous alignment in the powder while being set into the holder for the XRD analysis. In the inset of Fig. 1 a (004) peak is given in detail and its shift to a higher 2Θ angle is clearly evident with the addition of WO_3 to the sample, indicating the incorporation of W into the $Ca_3Co_4O_9$ phase with the formation of a solid solution. While the shift to a higher angle in the XRD pattern is attributed to the substitution of smaller ions, the shift to a lower angle is indicative of the substitution of larger ions [40,44]. The ionic radii are 0.745 Å for Co^{2-}, 0.545 Å for Co^{3+}, 0.53 Å for Co^{4+} and 0.6 Å for W^{6+} [45]. Hence, the shift to a higher angle in the XRD patterns indicates that W probably substitutes the Co^{2+} in the Ca_2CoO_3 layers of the $Ca_3Co_4O_9$ phase. It is known that Co ions in the Ca_2CoO_3 layers can have a valence of 2+/3+ and in the CoO_2 layers, 3+/4+[46]. The result is consistent with a previous study [41].

Please cite this article as: M. Presečnik, S. Bernik, Microstructural and thermoelectric properties of WO_3-doped $Ca_3Co_4O_9$ ceramics, Ceramics International (2016), http://dx.doi.org/10.1016/j.ceramint.2016.07.124

ARTICLE IN PRESS

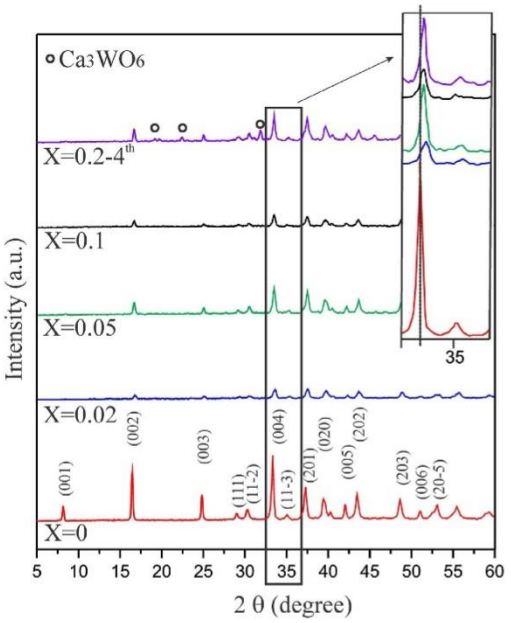


Fig. 1. X-ray powder-diffraction patterns of $Ca_3Co_{4-x}W_xO_9$ samples ($0 \le x \le 0.2$). The inset shows the shift of the (004) peaks with the variation of the W-doping concentration.

3.2. Microstructural characteristics

The microstructures of the $Ca_3Co_{4-x}W_xO_9$ samples ($0 \le x \le 0.2$) sintered two times at 900 °C are given in Fig. 2. All the samples have relatively similar microstructures composed of randomly oriented plate-like grains of the $Ca_3Co_4O_9$ phase with the length being in the range 1–5 μm. However, in the un-doped sample ($x=0$) the plate-like grains are more rounded with a thickness of about 1 μm, while with an increasing amount of WO_3 the grains are getting more irregularly shaped, sharp edged and with a lower thickness, ranging from about 0.2 μm to about 1 μm. This can in some way also indicate a larger disorder in the layered structure of the $Ca_3Co_4O_9$ phase containing W, which can, together with the grain morphology, effect the reduced intensity of the peaks in the XRD patterns of doped samples in comparison to the un-doped one. The random growth and consequently the random orientation of the plate-like grains (no texturing) inevitably resulted in the relatively isotropic and highly porous microstructures of the samples. In contrast, the polished microstructures of the samples (Fig. 2, right column) showed a similar porosity in all the samples, with the measurements showing an increase in the density from 60% for an un-doped sample to 70% for the WO_3-doped samples. The additional two sinterings (the 3rd and the 4th) of the samples with intermediate grindings resulted in only a slightly increased thickness of the grains in all the samples, while the density remained the same. From the SEM backscattered-electron (BE) images of the polished microstructures it is evident that the samples with $x \le 0.1$ are single phase, while in the sample with $x=0.2$ a brighter secondary phase is also present, which was determined using EDS analysis to be Ca_3WO_6. The results of the EDXS analysis for the $Ca_3Co_{4-x}W_xO_9$ matrix phase in the samples after two sinterings at 900 °C, normalized for 7 cations per formula unit, indicated the contents of W in the samples in the amounts 0.02, 0.05, 0.09 and 0.10 (standard deviation within ± 15%), which for most of the samples corresponded well with their starting compositions for the x values. After additional sintering at 900 °C similar values for the content of W were detected by EDXS analysis in the samples with $x \le 0.1$, while in the sample with $x=0.2$ it increased to about 0.12. In contrast to the previous report [41] that the solubility limit of W in $Ca_3Co_{4-x}W_xO_9$ is in the range $0.4 < x < 0.5$, our results indicate a lower solubility limit, below 0.2.

3.3. Thermoelectric properties

The results of the thermoelectric measurements in the temperature range from 40 °C to 615 °C, i.e., the electrical conductivity (σ), the Seebeck voltage (S) and the thermal conductivity (κ), and the obtained ZT values, are graphically presented in Fig. 3. The electrical conductivity σ of all the samples showed a slight increase with the temperature. However, it can also be observed that in general the conductivity of the $Ca_3Co_{4-x}W_xO_9$ samples is lower for a higher x. The un-doped sample had a σ of 31 S/cm at 615 °C, whereas in the doped samples the value decreased with the increasing addition of WO_3 from 24 S/cm for $x=0.02$–18 S/cm for $x=0.2$. The result indicated that the incorporation of the W^{6+} with the formation of the $Ca_3Co_{4-x}W_xO_9$-type solid solution most probably decreased the charge-carrier concentration, which was to be expected. The Ca_3CoO_9 phase is a p-type conductor with holes as the major charge carrier. The preferential conduction paths are the CoO_2 layers in which the charge-carrier concentration is determined by the ratio between Co^{4+} and Co^{3+} and is affected by the charge coupling with the neighbouring Ca_2CoO_3 layers containing Co^{2+}/Co^{3-} to ensure a local charge neutrality [46–49]. Accordingly, the incorporation of the W^{6+} into the Ca_2CoO_3 layers results in their surplus charge, and to preserve the local charge neutrality the share of the Co^{3+} in neighbouring CoO_2 layers has to be increased at the expense of the Co^{4+} (i.e., reduce the Co^{4+}/Co^{3+} ratio), which results in a reduced hole concentration and hence a lower electrical conductivity.

The positive Seebeck coefficients S confirmed the p-type of the $Ca_3Co_{4-x}W_xO_9$ samples ($0 \le x \le 0.2$), as shown in Fig. 3. In general, the sample with a lower electrical conductivity σ showed a higher S. Accordingly, the samples doped with $x=0.2$ and 0.1 showed a similar S with values at 615 °C of 157 μV/K and 154 μV/K, respectively, and the un-doped sample ($x=0$) of about 148 μV/K. While they showed similar σ, the sample with $x=0.02$ had an S of 151 μV/K and the sample with $x=0.05$, the lowest among all the samples, of 145 μV/K. The observed differences in S among the samples are rather small, i.e., below 10%. In general they could be attributed to the influence of WO_3 doping on the charge-carrier concentration; however, other factors, difficult to assess, including fine microstructural differences, also likely had an effect on the obtained S values.

The thermal conductivity κ of the $Ca_3Co_{4-x}W_xO_9$ samples ($0 \le x \le 0.2$) similarly decreased with the increasing temperature. In general, κ can be expressed as $\kappa=\kappa_L+\kappa_E$, where κ_L is the lattice thermal conductivity and κ_E is an electronic thermal conductivity. The value for κ_E can be estimated from the Wiedemann-Franz law given by the equation $\kappa_e=L\sigma T$, where L is the Lorenz number $=2.45 \times 10^{-8}$ W Q K^{-2} [50]. The calculated values showed that κ_E accounted just for about 5%, while the main contribution to the κ of the samples came from the κ_L, as would be expected for the semiconducting oxide ceramics. The un-doped sample had the highest κ in the range from 1.15 W/mK at 40 °C to 1.08 W/mK at 615 °C (Fig. 3). With increasing W-doping up to $x=0.1$ the κ of the $Ca_3Co_{4-x}W_xO_9$ samples decreased to values in the range from 1.03 W/mK to 0.88 W/mK. However, the sample with $x=0.2$

Please cite this article as: M. Presečnik, S. Bernik, Microstructural and thermoelectric properties of WO_3-doped $Ca_3Co_4O_9$ ceramics, Ceramics International (2016), http://dx.doi.org/10.1016/j.ceramint.2016.07.124

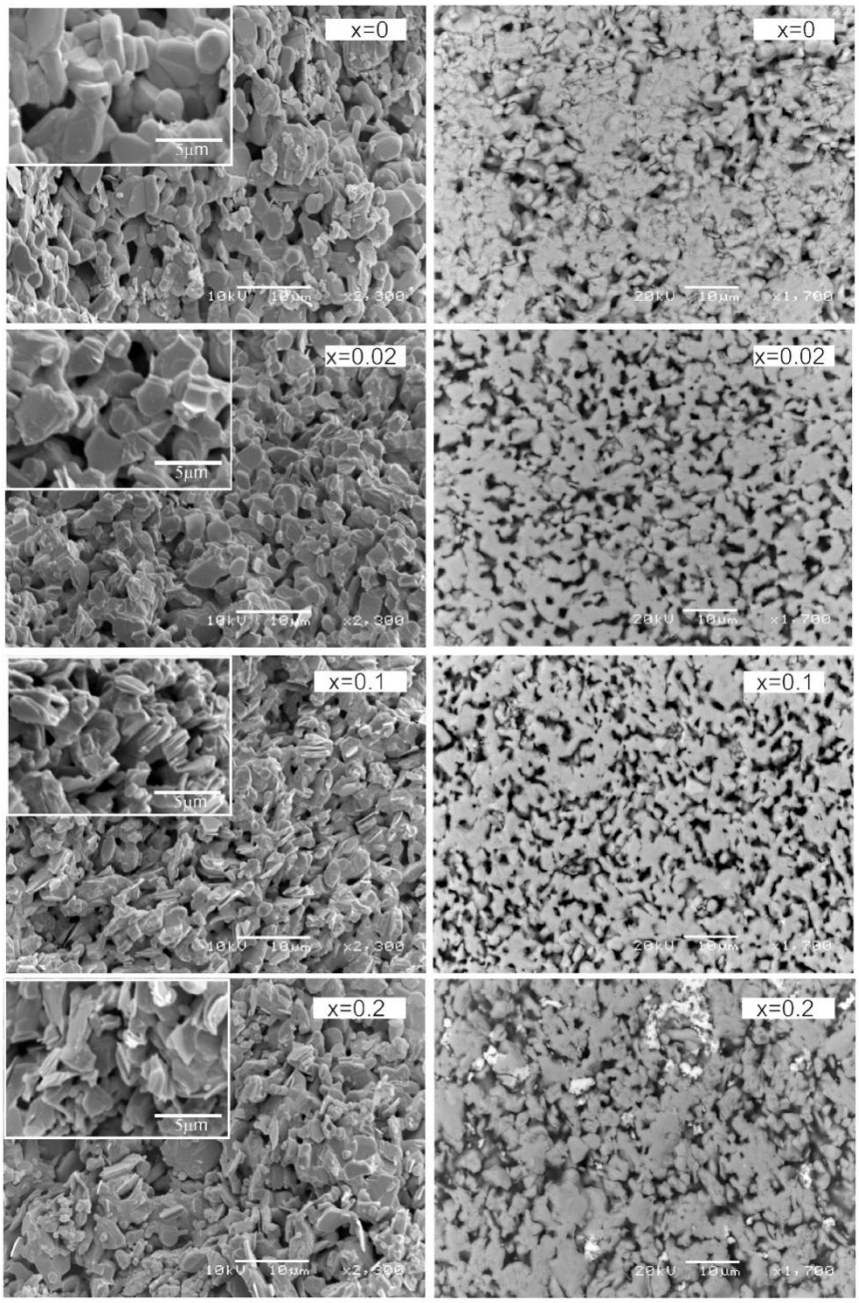


Fig. 2. SEM micrographs of fractured and polished surfaces of the $Ca_3Co_{4-x}W_xO_9$ samples ($0 \leq x \leq 0.2$) prepared by classic sintering at 900 °C for two times. The degree of irregularly shaped grains with sharp edges is increasing with the W-content.

Please cite this article as: M. Presečnik, S. Bernik, Microstructural and thermoelectric properties of WO_3-doped $Ca_3Co_4O_9$ ceramics, Ceramics International (2016), http://dx.doi.org/10.1016/j.ceramint.2016.07.124

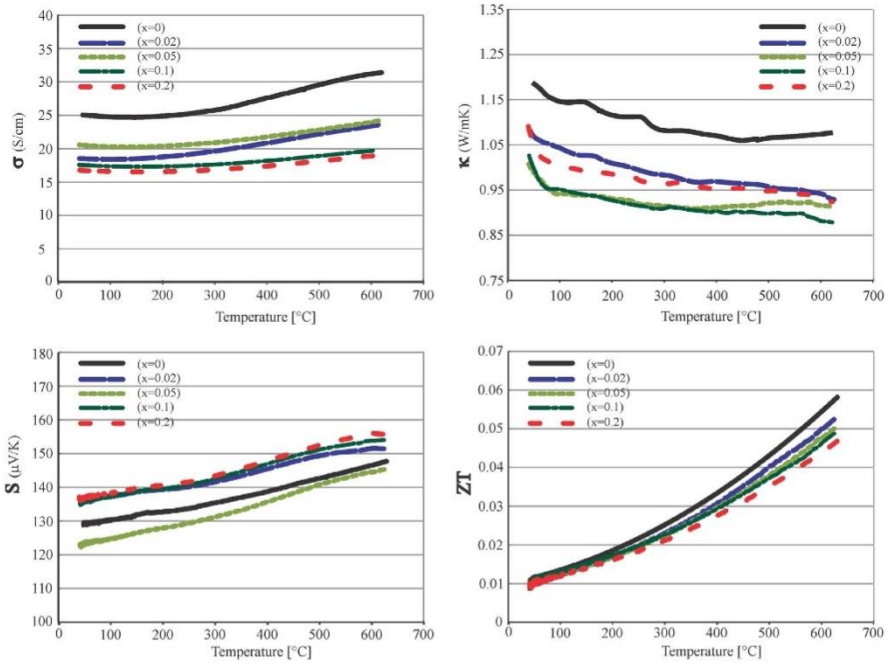


Fig. 3. Temperature dependence of the electrical conductivity σ, the Seebeck coefficient S, the total thermal conductivity κ and the figure of merit ZT for the single-phase $Ca_3Co_{4-x}W_xO_9$ samples ($0 \le x \le 0.2$).

already showed a higher κ in the range from 1.08 W/mK to 0.93 W/mK, similar to the sample with the lowest addition of WO_3 for x=0.02. The results indicate that W-doping reduced the lattice thermal conductivity κ_L of the samples. The incorporation of the W into the Ca_2CoO_3 layers affects their structural parameters [41], i.e., b_1 and c decrease significantly with increasing W-doping, which contributes to an increased mismatch with the CoO_2 layers for enhanced phonon scattering and hence a reduced lattice thermal conductivity κ_L. An increase of κ in the sample with the highest addition of WO_3 (x=0.2) could result from the presence of the secondary phase in this sample.

Combining the electrical and thermal transport properties, the values of the dimensionless figure of merit ZT for the samples as shown in Fig. 3 were obtained. The ZT of the $Ca_3Co_{4-x}W_xO_9$ ($0 \le x \le 0.2$) samples showed a very similar increasing trend with the temperature, while the values are lower with higher additions of WO_3. Accordingly, at 615 °C the ZT values were in the range from 0.06 for the un-doped sample (x=0) to 0.047 for the x=0.2 sample.

4. Conclusions

Polycrystalline samples of the p-type $Ca_3Co_{4-x}W_xO_9$ ceramics for $0 \le x \le 0.2$ were prepared by the classic ceramic procedure using fine powders of $CaCO_3$, Co_3O_4 and WO_3, and sintering at 900 °C. The single-phase $Ca_3Co_{4-x}W_xO_9$ ceramics were obtained for additions of WO_3 up to x=0.1, while for a larger addition (x=0.2) a Ca_3WO_6 secondary phase was detected in the samples even after four grindings and sintering cycles. The results confirmed the formation of the $Ca_3Co_{4-x}W_xO_9$ solid solution with the incorporation of W into the Ca_2CoO_3 layers of the $Ca_3Co_4O_9$ phase; however, in contrast to the previous report of the solubility limit being in the range $0.4 < x < 0.5$ [41], a much lower limit was determined in the range $0.1 < x < 0.2$. The highest amount of W equal to 0.12 was detected in the sample with the largest addition of WO_3 (x=0.2), sintered 4 times at 900 °C with intermediate grindings. While in the un-doped samples the plate-like grains were more rounded, doping with WO_3 resulted in more irregularly shaped, shape-edged and thinner plate-like grains of the $Ca_3Co_{4-x}W_xO_9$ phase. The thermoelectric characteristics of the samples were measured in the temperature range from 40 °C to 615 °C. In general, the electrical conductivity decreased with WO_3 doping from 31 S/cm at 615 °C in the un-doped sample to 18 S/cm in the sample for x=0.2. Accordingly, the sample for x=0.2 had the highest Seebeck voltage of 157 μV/K, the un-doped sample, 148 μV/K, and the lowest value of 145 μV/K was for the sample with x=0.05. Doping with WO_3 resulted in a decrease of the thermal conductivity κ from 1.15 W/mK for the un-doped sample to the lowest value of 0.88 W/K in the sample with x=0.1. The electronic thermal conductivity κ_E was determined to contribute only about 5% to the total thermal conductivity κ. Hence, its reduction could be attributed mainly to the reduced lattice thermal conductivity κ_L of the $Ca_3Co_{4-x}W_xO_9$ solid solution due to enhanced phonon scattering, caused by an increased mismatch between the sub-structural units, the Ca_2CoO_3 containing W and CoO_2. The figure of merit ZT for the samples decreased with the W-doping from 0.06 at 615 °C for the un-doped sample to 0.047 for the sample with largest addition of WO_3 (x=0.2).

Please cite this article as: M. Presečnik, S. Bernik, Microstructural and thermoelectric properties of WO_3-doped $Ca_3Co_4O_9$ ceramics, Ceramics International (2016), http://dx.doi.org/10.1016/j.ceramint.2016.07.124

ARTICLE IN PRESS

Acknowledgements

The authors acknowledge the financial support by the Slovenian Research Agency (Program Contract no. P2-0084, Project Grant L2-4192 and Young Researcher Program PR-03102).

References

[1] M. Ito, D. Furumoto, Effects of mechanical and Ag addition on thermoelectric properties of $Na_xCo_2O_9$, Scr. Mater. 55 (2006) 533–536.
[2] Y. Nishikubo, S. Nakano, K. Kudo, M. Nohara, Enhanced thermoelectric properties by Ir doping of $PtSb_2$ with pyrite structure, Appl. Phys. Lett. 100 (2012) 252104.
[3] M. Shikano, R. Funahashi, Electrical and thermal properties of single-crystalline $(Ca_2CoO_3)_{0.7}CoO_2$ with a $Ca_3Co_4O_9$ structure, Appl. Phys. Lett. 82 (2003) 1851–1853.
[4] S. Pinitsoontorn, N. Lerssongkram, A. Harnwunggmoung, K. Kurosaki, S. Yamanaka, Synthesis, mechanical and magnetic properties of transition metals-doped $Ca_3Co_{3.8}M_{0.2}O_9$, J. Alloy. Compd. 503 (2010) 431–435.
[5] Y. Wang, L. Xu, Y. Sui, X. Wang, J. Cheng, W. Su, Enhanced electron correlation in rare-earth doped $Ca_3Co_4O_9$, Appl. Phys. Lett. 97 (2010) 062114.
[6] I. Terasaki, Y. Sasago, K. Uchinokura, Large thermoelectric power in $NaCo_2O_4$ single crystal, Phys. Rev. B 56 (1997) 12685–12687.
[7] A.C. Masset, C. Michel, A. Maignan, M. Hervieu, O. Toulemonde, F. Studer, B. Raveau, J. Hejtmanek, Misfit-layered cobaltite with an anisotropic giant magnetoresistance: $Ca_3Co_4O_9$, Phys. Rev. B 62 (1) (2000) 166–175.
[8] W. Koshibae, K. Tsutsui, S. Maekawa, Thermopower in cobalt oxides, Phys. Rev. B 62 (11) (2000) 6869–6872.
[9] Y. Miyataki, M. Onoda, T. Oku, M. Kikuchi, Y. Ishii, Y. Ono, Y. Morii, T. Kajitani, Modulated structure of the thermoelectric compound $[Ca_2CoO_3]_{0.62}CoO_2$, J. Phys. Soc. Jpn. 71 (2) (2002) 491–497.
[10] Y. Huang, B. Zhao, R. Ang, S. Lin, Z. Huang, S. Tan, Y. Liu, W. Song, Y. Sun, Enhanced thermoelectric performance and room-temperature spin-state transition of Co^{4+} ions in the $Ca_3Co_{4-x}Rh_xO_9$ system, J. Phys. Chem. C. 117 (2013) 11459–11470.
[11] P. Limelette, V. Hardy, P. Auban-Senzier, D. J'erome, D. Flahaut, S. H'ebert, R. Fr 'esard, Ch Simon, J. Noudem, A. Maignan, Strongly correlated properties of the thermoelectric cobalt oxide $Ca_3Co_4O_9$, Phys. Rev. B 71 (2005) 233108.
[12] M. Presečnik, J. de Boor, S. Bernik, Synthesis of single-phase $Ca_3Co_4O_9$ ceramics and their processing for a microstructure-enhanced thermoelectric performance, Ceram. Int. 42 (2016) 7315–7327.
[13] T. Yin, D. Liu, Y. Ou, F. Ma, S. Xie, J.-F. Li, J. Li, Nanocrystalline thermoelectric $Ca_3Co_4O_9$ ceramics by sol-gel based electrospinning and spark plasma sintering, J. Phys. Chem. C 114 (2010) 10061–10065.
[14] S. Chen, X. Song, X. Chen, Y. Chen, E.J. Barbero, E.L. Thomas, P.N. Barnes, Effect of precursor calcination temperature on the microstructure and thermoelectric properties of $Ca_3Co_4O_9$ ceramics, J. Sol–gel Sci. Technol. 64 (2012) 627–636.
[15] J.G. Noudem, D. Kenfaui, D. Chateigner, M. Gomina, Toward the enhancement of the thermoelectric properties of lamellar $Ca_3Co_4O_9$ by edge-free spark plasma texturing, Scr. Mater. 66 (2012) 258–260.
[16] Y. Zhou, et al., Thermoelectric properties of highly grain-aligned and densified Co-based oxide ceramics, J. Appl. Phys. 93 (2003) 2653–2658.
[17] R. Asahi, J. Sugiyama, T. Tani, Electronic structure of misfit-layered calcium cobaltite, Phys. Rev. B 66 (2002) 155103.
[18] N.V. Nong, N. Pryds, S. Linderoth, M. Ohtaki, Enhancement of the thermoelectric performance of (p-) type layered oxide $Ca_3Co_4O_{9-\delta}$ through heavy doping and metallic nanoinclusions, Adv. Mater. 23 (2011) 2484–2490.
[19] N.V. Nong, C.-J. Liu, M. Ohtaki, High-temperature thermoelectric properties of late rare earth-doped $Ca_3Co_4O_{9+\delta}$, J. Alloy. Compd. 509 (2011) 977–981.
[20] D. Wang, L. Chena, Q. Yao, J. Li, High-temperature thermoelectric properties of $Ca_3Co_4O_{9-\delta}$ with Eu substitution, Solid State Commun. 129 (2004) 615–618.
[21] S. Butt, Y.-C. Liu, J.-L. Lan, K. Shehzad, B. Zhan, Y. Lin, C.-W. Nan, High-temperature thermoelectric properties of La and Fe co-doped Ca–Co–O misfit-layered cobaltites consolidated by spark plasma sintering, J. Alloy. Compd. 588 (2014) 277–283.
[22] H.Q. Liu, X.B. Zhao, F. Liu, Y. Song, Q. Sun, T.J. Zhu, F.P. Wang, Effect of Gd-doping on thermoelectric properties of $Ca_3Co_4O_{9+\delta}$ ceramics, J. Mater. Sci. 43 (2008) 6933–6937.
[23] H.Q. Liu, Y. Song, S.N. Zhang, X.B. Zhao, F.P. Wang, Thermoelectric properties of $Ca_3XY_xCo_4O_{9+\delta}$ ceramics, J. Phys. Chem. Solids 70 (2009) 600–603.
[24] S. Rasekh, G. Constantinescu, M.A. Torres, J.C. Diez, M.A. Madre, A. Sotelo, Thermoelectric properties of rare earth doped $Ca_{3-x}RE_xCo_4O_9$ (RE = Dy, Er, Gd, and Tb; x=0, 0.01, 0.03, and 0.05), J. Electroceram. 32 (2014) 376–382.
[25] M. Prevel, O. Perez, J.G. Noudem, Bulk textured $Ca_{2.5}(RE)_{0.5}Co_4O_9$ (RE: Pr, Nd, Eu, Dy and Yb) thermoelectric oxides by sinter-forging, Solid State Sci. 9 (2007) 231–235.
[26] G. Xu, R. Funahashi, M. Shikano, I. Matsubara, Y. Zhou, Thermoelectric properties of the Bi- and Na- substituted $Ca_3Co_4O_9$ system, Appl. Phys. Lett. 80 (20) (2002) 3760–3762.
[27] C.-H. Lim, S.-M. Choi, W.-S. Seo, High-temperature thermoelectric properties of the $Ca_{3-x}K_xCo_4O_9$ ($0 \le x \ge 0.3$) system, J. Korean Phys. Soc. 57 (4) (2010) 1054–1058.
[28] F. Delorme, C.F. Martin, P. Marudhachalam, D.O. Ovono, G. Guzman, Effect of Ca substitution by Sr on the thermoelectric properties of $Ca_3Co_4O_9$ ceramics, J. Alloy. Compd. 509 (2011) 2311–2315.
[29] F.P. Zhang, Q.M. Lu, J.X. Zhang, Synthesis and high temperature thermoelectric properties of $Ba_xAg_yCa_{3-x-y}Co_4O_9$ compounds, J. Alloy. Compd. 484 (2009) 550–554.
[30] G. Constantinescu, Sh. Rasekh, M.A. Torres, C. Chocarro, J.C. Diez, M.A. Madre, A. Sotelo, Influence of Ca substitution by Mg on the $Ca_3Co_4O_9$ performances, Bol. Soc. Esp. Cerám. 53 (1) (2014) 41–47.
[31] Y. Wang, Y. Sui, J. Cheng, X. Wang, W. Su, Comparison of the high temperature thermoelectric properties for Ag-doped and Ag-added $Ca_3Co_4O_9$, J. Alloy. Compd. 477 (2009) 817–821.
[32] G. Constantinescu, M.A. Madre, Sh Rasekh, M.A. Torres, J.C. Diez, A. Sotelo, Effect of Ga addition on Ca-deficient $Ca_3Co_4O_y$ thermoelectric materials, Ceram. Int. 40 (2014) 6255–6260.
[33] S. Demirel, E. Altin, E. Oza, S. Altin, A. Bayri, An enhancement ZT and spin state transition of $Ca_3Co_4O_9$ with Pb doping, J. Alloy. Compd. 627 (2015) 430–437.
[34] S. Demirel, M.A. Aksan, S. Altin, Low temperature electrical and thermal transport properties of the $Ca_{3-x}Sb_xCo_4O_9$ system, J. Mater. Sci.: Mater. Electron. 23 (2012) 2251–2256.
[35] S. Pinitsoontorn, N. Lerssongkram, N. Keawprak, V. Amornkitbamrung, Thermoelectric properties of Transition metals-doped $Ca_3Co_{3.8}M_{0.2}O_{9-d}$ (M = CO, CR, FE, NI, CU and Zn), J. Mater. Sci: Mater. Electron. 23 (2012) 1050–1056.
[36] L. Xua, F. Li, Y. Wang, High-temperature transport and thermoelectric properties of $Ca_3Co_{4-x}Ti_xO_9$, J. Alloy. Compd. 501 (2010) 115–119.
[37] Y. Huang, B. Zhao, S. Lin, R. Ang, W. Song, Y. Sun, Strengthening of thermoelectric performance via Ir doping in layered $Ca_3Co_4O_9$ system, J. Am. Ceram. Soc. 97 (3) (2014) 798–804.
[38] Y. Huang, B. Zhao, S. Lin, R. Ang, Y. Sun, Structure and transport properties in $Ca_3Co_{4-x}M_xO_9$ (M = Re and Pt) ceramics, Ceram. Int. 40 (2014) 10545–10550.
[39] D. Li, X.Y. Qin, Y.J. Gu, J. Zhang, The effect of Mn substitution on thermoelectric properties of $Ca_3Mn_xCo_4K_xO_9$ at low temperatures, Solid State Commun. 134 (2005) 235–238.
[40] Y. Fu, B. Zhao, Y. Huang, J. Yang, J. Dai, M. Zhou, Y. Sun, Spin-glass and spin-fluctuation in Mo-doped $Ca_3Co_4O_9$ system, Solid State Commun. 151 (2011) 933–937.
[41] Y. Fu, B. Zhao, Y. Huang, J. Dai, Y. Sun, Enhanced electrical correlation in the W-doped cobaltite $Ca_3Co_4O_9$ ceramics, Phys. B 414 (2013) 16–20.
[42] Y. Fu, S. Lin, Y. Huang, R. Shi, B. Zhao, Cr^{6-} ion doping effects in layered $Ca_3Co_4O_9$ system, J. Alloy. Compd. 613 (2014) 87–92.
[43] S. Bernik, M. Pribošek, Construction and characteristics of a Z-meter setup for thermoelectric measurements of materials, in: Andrej Žemva, Polona Šorli, Iztok Šorli (Eds.), Proceedings of the 49th International conference on Microelectronics, Devices and Materials MIDEM Kranjska Gora, Slovenia, 2013, pp. 121–126.
[44] N. Prasoetsopha, S. Pinitsoontorn, T. Kamwanna, V. Amornkitbamrung, K. Kurosaki, Y. Ohishi, H. Muta, S. Yamanaka, The effect of Cr substitution on the structure and properties of misfit-layered $Ca_3Co_{4-x}Cr_xO_{9+d}$ thermoelectric oxides, J. Alloy. Compd. 588 (2014) 199–205.
[45] R.D. Shannon, Revised effective ionic radii and systematic studies of interatomic distances in halides and chaleogenides, Acta Cryst. A32 (1976) 751.
[46] K. Nagasawa, S. D.-Minaud, N. Preux, A. Rolle, P. Roussel, H. Nakatsugawa, O. Mentré, $Ca_3Co_4O_{9-\delta}$, a thermoelectric material for SOFC cathode, Chem. Mater. 21 (2009) 4738–4745.
[47] M. Schrade, T. Norby, T.G. Finstad, Hall effect measurements on thermoelectric $Ca_3Co_4O_9$: on how to determine the charge carrier concentration in strongly correlated misfit cobaltites, J. Appl. Phys. 117 (2015) 205103.
[48] M. Karppinen, H. Fjellvåg, T. Konno, Y. Morita, T. Motohashi, H. Yamauchi, Evidence for oxygen vacancies in misfit-layered calcium cobalt oxide, $[CoCa_2O_3]_qCoO_2$, Chem. Mater. 16 (2004) 2790–2793.
[49] G. Yang, Q. Ramasse, R.F. Klie, Direct measurement of charge transfer in thermoelectric $Ca_3Co_4O_9$, Phys. Rev. B 78 (2008) 153109.
[50] K. Seeger, Semiconductor Physics: An Introduction, 9th Ed., Springer-Verlag, Berlin Heidelberg New York 2004, p. 76.

Please cite this article as: M. Presečnik, S. Bernik, Microstructural and thermoelectric properties of WO_3-doped $Ca_3Co_4O_9$ ceramics, Ceramics International (2016), http://dx.doi.org/10.1016/j.ceramint.2016.07.124

Chapter 8

Conclusions

The main topic of the PhD research presented in the dissertation was the development of the p-type thermoelectric ceramics based on the $Ca_3Co_4O_9$ (Ca349) compound with microstructurally enhanced thermoelectric (TE) characteristics. The classical ceramic solid-state synthesis from the powders of $CaCO_3$ and Co_3O_4 was studied in regard to the characteristics of the starting powders and by the mechano-chemical treatment of the starting powder mixture in order to optimise the formation of the single-phase Ca349 compound with preferred fine grain morphology. Furthermore, by using such fine single-phase Ca349 material, the influence of different processing methods on the microstructure development and consequently TE properties of the Ca349 ceramics was analysed to gain knowledge and understanding about the possibilities and ways to enhance TE characteristics by the microstructural optimisation. Finally, the influence of the selected dopant on the formation of the Ca349 compound, microstructure and TE characteristics of the Ca349 ceramics was also studied.

Studies showed that in classical ceramic solid state synthesis the characteristics of the starting powders of $CaCO_3$ and Co_3O_4 strongly effect the formation and grain morphology of the Ca349 compound. In the case of relatively coarse-grained starting powders with average grain size of a few micrometres the formation of the Ca349 compound was sluggish; even after several calcinations at temperature of 920 °C for about 20 hours with intermediate grindings some secondary phases (i.e. starting reagents) were still present and the platelet Ca349 grains were more rounded and thicker. However, with the use of fine-grained starting powders with average size of about 0.4 μm a single phase Ca349 compound with fine plate-like morphology of thin irregular shaped grains was obtained after single calcination at 760 °C for 12 hours. Such high porous Ca349 ceramics with completely random orientation of grains had surprisingly high zT of 0.09 at 627 ^{0}C with σ of 35 S/cm, the S of 175 μV/K, and κ of 0.8 W/mK. The TE characteristics with about 50% higher zT value compared to the literature reports clearly showed that a single-step synthesis at the lowest possible temperature, which leads to the preferred fine plate-like grain morphology of the single-phase Ca349 compound, is beneficial. Such single-phase Ca349 material turned out to be advantageous in the further preparation of the Ca349 ceramics using different processing methods.

In a further attempt to improve the solid state synthesis of the Ca349 compound the mechano-chemical treatment of the fine starting powder mixture of $CaCO_3$ and Co_3O_4 was studied with detailed analysis about the influence of the milling parameters. It showed that maximum ball impact energy (Eb) of 283 kJ/hit obtained in our work was still below critical Eb required for

phase-formation reaction and hence no Ca349 phase was detected in the samples. However, MC treatment resulted in a fully amorphous starting mixture at proper cumulative energy Ecum around 2900 kJ/g, while at Ecum < 2300 kJ/g the powder was only partially amorphous and at Ecum > 3800 kJ/g the intensity of the XRD peaks of the starting reagents again started to increase. Fully amorphous MC treated powder had enhanced reactivity and enabled preparation of the single-phase Ca349 compound only after single calcination at 760 °C for 4 hours, 3 times faster time than with an untreated powder mixture. The obtained Ca349 ceramics was highly inhomogeneous and porous (50% of theoretical density) with completely random orientation of very fine and thin plate-like grains of irregular shape. After sintering at 920 °C homogeneous Ca349 ceramics with a density increased to 72% was obtained, while the fine-grained microstructure was still preserved, which resulted in increased zT value of 0.10 at 600 °C.

In the study of microstructural optimisation for enhanced TE characteristics of the Ca349 ceramics, a single-phase Ca349 material prepared by calcination at 760 °C was further on processed using different processing methods, which resulted in microstructural diversity in regard to the degree of texturing and density, and also grain morphology. Besides in literature already studied processing methods (conventional sintering – CS, hot pressing – HP, free-edge spark-plasma sintering of a sintered pellet – SPT-920), newly modified method (free-edge SPS of a pellet from just-compacted powder – SPT) and also novel processing methods (cold pressing of a calcined Ca349 pellet without post annealing – CP and free-edge cold pressing of a calcined Ca349 pellet with post annealing – CP-920) were studied. In contrary to general consideration that fully textured and dense Ca349 ceramics is required for enhanced TE properties and high zT, my study showed the limitations of such an approach. The classically prepared just calcined Ca349 ceramics with high porosity (density below 60%) and at completely random orientation of the plate-like grains had low σ, high S and also very low κ, resulting in a relatively high zT of 0.09 at 600 °C. In highly textured and dense (> 90%) Ca349 ceramics prepared by much more equipment and processing demanding methods the σ was significantly improved only in the in-plane direction, the S was similar while κ was greatly increased in both directions, in-plane and out-of-plane. Compared to the highly porous Ca349 ceramics the κ of the highly textured ceramics increased with increasing density even up to 3-times. Accordingly, with the degree of texturing (f) the density of the Ca349 ceramics, prepared by the HP, the SPS and the SPT methods, increased from 94% (f=0.77) to 97% (f=0.91) and to 99% (f=0.99) while the zT increased only from 0.09, to 0.14, and to 0.17, respectively. However, with the original processing method of the free-edge cold pressing of calcined Ca349 pellet with post annealing (CP-920) modestly textured and still porous Ca349 ceramics (65% density) was obtained having a relatively high σ, high S and very low κ (0.47 W/mK). Such TE parameters obtained with combined method resulted in the highest zT obtained in this work of 0.31 at about 600 °C, which is to the best our knowledge the highest zT value reported for pristine Ca349 ceramics. Simultaneous measurements of the TE parameters on the same block of highly porous Ca349 ceramics and also perfectly textured Ca349 ceramics in both directions (in-plane and out-of-plane) gave additional support to these findings clearly showing the influence of density and microstructure anisotropy (texturing) on each TE parameter. Results clearly revealed that a proper degree of texturing with

some optimal porosity could play a key role in microstructural enhancement of the zT, ensuring still high σ and low κ.

Polycrystalline samples of the p-type $Ca_3Co_{4-x}W_xO_9$ ceramics for $0 \leq x \leq 0.2$ were prepared by the classic ceramic procedure using fine powders of $CaCO_3$, Co_3O_4 and WO_3, and sintering at 900 °C. The influence of high valence and heavy W^{6+} ions on the formation of the $Ca_3Co_{4-x}W_xO_9$ solid solution, phase composition, grain morphology, microstructure and thermoelectric properties was studied in the temperature range from 40 to 615 °C for the first time. The single-phase $Ca_3Co_{4-x}W_xO_9$ ceramics were obtained for additions of WO_3 up to x = 0.1, while for larger additions a Ca_3WO_6 secondary phase was detected in the samples even after several cycles of sintering with intermediate grindings. The much lower solubility limit in the range $0.1 < x < 0.2$ was determined contrary to the previously reported one ($0.4 < x < 0.5$). However, the results did confirm the previous findings that solid solution is indeed formed by the incorporation of the W^{6+} to the Co^{2+} sites in the Ca_2CoO_3 layers of the $Ca_3Co_4O_9$ phase. Doping with WO_3 resulted in more irregularly shaped, shape-edged and thinner plate-like grains of the $Ca_3Co_{4-x}W_xO_9$ phase compared to the undoped samples. In general, in comparison to the undoped Ca349 ceramics, the WO_3 doping as expected resulted in the increase of S and noticeable decrease of κ from 1.15 W/mK to 0.88 W/mK, and unfortunately also in decrease of σ. As the contribution of the electronic thermal conductivity was determined to be only 5%, the main reduction was attributed to the lattice thermal conductivity due to enhanced phonon scattering. In overall, the WO_3-doping resulted in a decreased zT value of the $Ca_3Co_{3.88}W_{0.12}O_9$ ceramics compared to the pristine one.

The results of my PhD research clearly showed the possibilities to optimise the classical ceramic solid-state synthesis of the Ca349 compound and the possibilities for further microstructure related enhancements of the TE characteristics and zT value of the p-type Ca349 ceramics. Fine, highly reactive starting powders of $CaCO_3$ and Co_3O_4 are required, enabling formation of a single phase Ca349 compound in a single calcination step at the lowest possible temperature, which is also the condition to obtain the preferred fine and thin plate-like morphology of the Ca349 grains. In further processing of the Ca349 ceramics the fine-grained morphology has to be preserved, while the degree of texturing and consequently porosity has to be such, that obtained microstructure supports high electrical conductivity and low thermal conductivity. The Seebeck coefficient showed to be relatively microstructure independent. Hence, again lower temperatures and shorter sintering times are preferred. However, the results also indicated limits in enhancing the zT solely by tailoring the microstructure. For a major breakthrough in increasing the zT of the Ca349 ceramics, while having favourable microstructure for low thermal conductivity (κ), their electrical conductivity (σ) will have to be increased significantly, which can be achieved only by proper doping not affecting (decreasing) too much the Seebeck coefficient (S).

References

1. S. B. Riffat, X. Ma, "Thermoelectrics: a review of present and potential applications," *Appl. Therm. Eng.*, vol. 23, pp. 913–935, 2003.
2. G. H. Rinehart, "Design characteristics and fabrication of radioisotope heat sources for space missions," *Prog. Nucl. Energy*, vol. 39, no. 3–4, pp. 305–319, 2001.
3. I. Terasaki, "Thermal conductivity and thermoelectric power of semiconductors," in *Comprehensive Semiconductor Science and Technology 1*, P. Bhattacharya, R. Fornari and H. Kamimura, ed., Elsevier, 2011. http://dx.doi.org/10.1016/B978-0-44-453153-7.00070-5.
4. M. S. Dresselhaus, G. Chen, M. Y. Tang, R. Yang, H. Lee, D. Wang, Z. Ren, J.-P. Fleurial and P. Gogna, "New directions for low-dimensional thermoelectric materials," *Adv. Mater.*, vol. 19, pp. 1043-1053, 2007.
5. T. M. Tritt and M. A. Subramanian, "Thermoelectric Materials, Phenomena, and Applications: A Bird's Eye View," *MRS Bull.*, vol. 31, pp. 188-194, 2005.
6. S. M. Kauzlarich, S. R. Brown and G. J. Snyder, "Zintl phases for thermoelectric devices," *Dalton T.*, pp. 2099-2107, 2007.
7. G. J. Snyder , E. S. Toberer , "Complex thermoelectric materials," *Nat. Mater.*, vol. 7, pp. 105 – 114, 2008.
8. N. Wu, S. Linderoth, N. Pryds, and N. Van Nong, "Development and Processing of p-type Oxide Thermoelectric Materials," Department of Energy Conversion and Storage, Technical University of Denmark, Risø, Denmark, 2014.
9. T. J. Seebeck, "Magnetic polarization of metals and minerals," *Abhandlungen der Deutschen Akademi der Wissenschafren zu Berlin*, vol. 265, pp. 1822-1823.
10. D. M. Rowe, "Introduction," in *CRC Handbook of Thermoelectrics*, D. M. Rowe, Ed., CRC Boca Raton, 1995.
11. J. Martin, T. Tritt, and C. Uher, "High temperature Seebeck coefficient metrology," *J. Appl. Phys.*, vol. 108, pp. 121101-12pp., 2010.
12. D. M. Rowe,"General principles and basic considerations" in *Thermoelectrics handbook: Macro to nano*, D. M. Rowe, Ed., CRC Press Boca Raton, 2006.
13. A. F. Ioffe, "Semiconductor Thermoelements and Thermoelectric Cooling," *Infosearch*, London, 1957.
14. W. Thomson, "On a mechanical theory of thermo-electric currents," *Proc. R. Soc. Edinburgh*, pp. 91–98, 1851.
15. A. Polozine, S. Sirotinskaya, L. Schaeffer, "History of Development of Thermoelectric Materials for Electric Power Generation and Criteria of their Quality," *Mater. Res.*, vol. 17, no. 5, pp. 1260-1267, 2014.
16. A.F. Ioffe, "Semiconductor Thermocouples," Academy of science of the USSR, Moskva- Leningrad, 1960.
17. I. Terasaki, "Thermal conductivity and thermoelectric power of semiconductors," in *Comprehensive Semiconductor Science and Technology 1*, P. Bhattacharya, R. Fornari and H. Kamimura, ed., Elsevier, 2011. http://dx.doi.org/10.1016/B978-0-44-453153-7.00070-5.

18. M. Bachmann, M. Czerner, S. Edalati-Boostan and C. Heiliger, "Ab initio calculations of phonon transport in ZnO and ZnS," *Eur. Phys. J. B*, vol. 85, no. 146/1, pp.9, 2012.
19. A. Li, "With reference to the history of using semiconductors in thermoelectricity," *J. Thermoelectricity*, vol. 4, no.12/7, pp. 7-10, 2002.
20. R. Venkatasubramanian, E. Siivola, T. Colpitts and B. O'Quinn, "Thin-film thermoelectric devices with high room-temperature figures of merit," *Nature*, vol. 413, no. 6856, pp. 597-602, 2001, http:// dx.doi.org/10.1038/35098012. PMid:11595940
21. McCormick, "Thermoelectric Material the Best at Converting Heat Waste to Electricity. Evanston," McCormick School of Engineering and Applied Science, 2012. [Online]. Available: http://www.mccormick.northwestern.edu/news/articles/2012/09/vinayak-dravid-thermoelectric-materialworld- record.html. [Accessed in: 13 07 2016].
22. W.H. Chen, C. Y. Liao, C. I. Hung and W. L. Huang, "Experimental study on thermoelectric modules for power generation at various operating conditions," *Energy*, vol. 45, no.1, pp. 874-881, 2012.
23. M. Cutler, J. F. Leavy and R. L. Fitzpatrick, "Electronic transport in semimetallic cerium sulphide," *Phys. Rev.*, vol. 133, pp. A1143–A1152, 1964.
24. C. M. Bhandari and D. M. Rowe, "Optimisation of carrier concentration," in *CRC Handbook of Thermoelectrics*, D. M. Rowe, Ed., CRC Boca Raton, 1995.
25. K. Koumoto, I. Terasaki and R. Funahashi, "Complex oxide materials for potential thermoelectric applications," *Mater. Res. Soc. Bull.*, vol. 31, pp. 206–210, 2006.
26. G. J. Snyder, T. Caillat and J.-P. Fleurial, "Thermoelectric transport and magnetic properties of the polaron semiconductor $Fe_xCr_{3-x}Se_4$, *Phys. Rev. B*, vol. 62, pp. 10185-10193, 2000.
27. G. A. Slack, "The thermal conductivity of non-metallic crystals," *Solid State Phys.*, vol. 34, pp.1-70, 1979.
28. J. S. Tse, D. D. Klug, "Recent trends for desighn and optimization of thermoelectric materials - A theoretical perspective" in *Thermoelectrics handbook: Macro to nano*, D. M. Rowe, Ed., CRC Press Boca Raton, 2006.
29. G. A. Slack, "New materials and performance limits for thermoelectric cooling" in *CRC Handbook of Thermoelectrics*, D. M. Rowe, Ed., CRC Boca Raton, 1995.
30. X. Zhang, L.-D. Zhao, "Thermoelectric materials: Energy conversion between heat and electricity," *J. Materiomics* 1, pp. 92-105, 2015.
31. L.D. Zhao, V.P. Dravid, M.G. Kanatzidis, "The panoscopic approach to high performance thermoelectrics," *Energy Environ. Sci.*, vol. 7, pp. 251-68, 2014. doi:10.1039/C3EE43099E
32. K.F. Hsu, S. Loo, F. Guo, W. Chen, J.S. Dyck, C. Uher, T. Hogan, E.K. Polychroniadis, M. G. Kanatzidis, "Cubic $AgPb_{(m)}SbTe_{(2+m)}$: bulk thermoelectric materials with high figure of merit," *Science*, vol. 303, pp. 818-821, 2004.
33. Y.Z. Pei, X.Y. Shi, A. LaLonde, H. Wang, L.D. Chen, G.J. Snyder, "Convergence of electronic bands for high performance bulk thermoelectrics," *Nature*, vol. 473, pp. 66-69, 2011.
34. K. Biswas, J. He, I.D. Blum, C.I. Wu, T.P. Hogan, D.N. Seidman, V.P. Dravid, M.G. Kanatzidis, "High-performance bulk thermoelectrics with all-scale hierarchical architectures," *Nature*, vol. 489, no. 7416, pp.:414-418, 2012.

35. L.D. Zhao, S.H. Lo, Y.S. Zhang, H. Sun, G.J. Tan, C. Uher, C. Wolverton, V.P. Dravid, M.G. Kanatzidis, "Ultralow thermal conductivity and high thermoelectric figure of merit in SnSe crystals," *Nature*, vol. 508, pp. 373-378, 2014.
36. J. He, Y. Liu, R. Funahashi, "Oxide thermoelectrics: The challenges, progress and outlook," *J. Mater. Res.*, vol. 26, no. 15, pp. 1762-1772, 2001.
37. A. Nag and V. Shubha, "Oxide Thermoelectric Materials: A Structure–Property Relationship," *J. Electron. Mater.*, vol. 43, no. 4, pp. 962-977, 2014. [Online]. Doi: 10.1007/s11664-014-3024-6.
38. I. Terasaki, Y. Sasago and K. Uchinokura, "Large thermoelectric power in $NaCo_2O_4$ single crystal," *Phys. Rev. B,* vol. 56, pp. 12685-12687, 1997.
39. M. Ohtaki, T. Tsubota, K. Eguchi, and H. Arai, "High temperature thermoelectric properties of $(Zn_{1-x}Al_x)O$," *J. Appl. Phys.*, vol. 79, no. 3, pp.1816-1818, 1996.
40. M. Ohtaki, K. Araki, and K. Yamamoto, "High Thermoelectric Performance of Dually Doped ZnO Ceramics," *J. Electron. Mater.*, vol. 38, no. 7, pp.1234-1238, 2009.
41. D. F. Morgan and D. A. Wright, "Electrical properties of single crystals of antimony-doped stannic oxide," *Brit. J. Appl. Phys.*, vol. 17, pp. 337-340, 1966.
42. T. Tsubota, T. Ohno, N. Shiraishi, Y. Miyazaki, "Thermoelectric properties of $Sn_{1-x-y}Ti_ySb_xO_2$ceramics," *J. Alloy. Compd.*, vol. 463, pp. 288–293, 2008.
43. D. Berardan, E. Guilmeau, A. Maignan, B. Raveau, "In_2O_3:Ge, a promising n-type thermoelectric oxide composite," *Solid State Commun.*, vol. 146, pp. 97–101, 2008.
44. M. Ohtaki, and R. Hayashi, "Enhanced thermoelectric performance of nanostructured ZnO: A possibility of selective phonon scattering and carrier energy filtering by nanovoid structure", in *Proceedings of the 25th International Conference on Thermoelectrics*, Vienna, Austria, IEEE, 2006.
45. H. Ohta, W.-S. Seo, and K. Koumoto, "Thermoelectric properties of homologous compounds in the ZnO-In_2O_3 system," *J. Am. Ceram. Soc.*, vol. 79, no. 2193, pp. 2193-2196, 1996.
46. L. D. Zhao, D. Berardan, Y. L. Pei, C. Byl, L. Pinsard-Gaudart, and N. Dragoe, "$Bi_{1-x}Sr_xCuSeO$ oxyselenides as promising thermoelectric materials," *Appl. Phys. Lett.*, vol. 97, no. 9, pp. 092118-3pp., 2010.
47. Y. Liu, L.-D. Zhao, Y. Liu, J. Lan, W. Xu, F. Li, B.-P. Zhang, D. Berardan, N. Dragoe, Y.-H. Lin, C.-W. Nan, J.-F. Li, and H. Zhu, "Remarkable enhancement in thermoelectric performance of BiCuSeO by Cu deficiencies," *J. Am. Chem. Soc.*, vol. 133, no. 50, pp. 20112–20115, 2011.
48. J. Sui, J. Li, J. He, Y.-L. Pei, D. Berardan, H. Wu, N. Dragoe, W. Cai, and L.-D. Zhao, "Texturation boosts the thermoelectric performance of BiCuSeO oxyselenides," *Energy Environ. Sci.*, vol. 6, no. 10, pp. 2916-2920, 2013.
49. J. Li, J. Sui, Y. Pei, C. Barreteau, D. Berardan, N. Dragoe, W. Cai, J. He, and L.-D. Zhao, "A high thermoelectric figure of merit ZT > 1 in Ba heavily doped BiCuSeO oxyselenides," *Energy Environ. Sci.*, vol. 5, no. 9, pp. 8543-8547, 2012.
50. B. Zhang, J. Wang, T. Zou, S. Zhang, X. Yaer, N. Ding, C. Liu, L. Miao, Y. Li and Y. Wu, "High thermoelectric performance of Nb-doped $SrTiO_3$ bulk materials with different doping levels," *J. Mater. Chem. C*, vol. 3, pp. 11406-11411, 2015.
51. K. Hyoung Lee, Y. Mune; H. Ohta, K. Koumoto, Thermal stability of giant thermopower in $SrTiO_3/SrTi_{0.8}Nb_{0.2}O_3$

superlattices at 900 K," in *Proceedings of the 6th European conference on thermoelectrics*, Paris, France, 2008.
52. L. Zhang, T. Tosho, N. Okinaka, and T. Akiyama, "Thermoelectric Properties of Combustion-Synthesized Lanthanum-Doped Strontium Titanate," *Mater. Trans.*, vol. 48, no. 5, pp. 1079–1083, 2007.
53. K. Koumoto, Y. Wang, R. Zhang, A. Osuga, and R. Funahashi, "Oxide Thermoelectric Materials: A Nanostructuring Approach," *Ann. Rev. Mater. Res.*, vol. 40. pp. 363–394, 2010.
54. J. Lan, Y.-H. Lin, H. Fang, A. Mei, C . Nan, Y. Liu, S. Xu, and M. Peters, "High- Temperature Thermoelectric Behaviors of Fine-Grained Gd-Doped $CaMnO_3$ Ceramics," J. *Am. Ceram. Soc.*, vol. 93, no. 8, pp. 2121–2124, 2010.
55. S. Populoh, M. Trottmann, M. H. Aguire, and A. Eidenkaff, "Nanostructured Nb-substituted $CaMnO_3$ n-type thermoelectric material prepared in a continuous process by ultrasonic spray combustion," *J. Mater. Res.*, vol. 26, no. 15, pp. 1947–1952, 2011.
56. Y. Wang, Y. Sui, and W. Su, "High temperature thermoelectric characteristics of $Ca_{0.9}R_{0.1}MnO_3$ (R=La,Pr, . . . ,Yb…)," *J. Appl. Phys.*, vol. 104, pp. 093703 -7pp., 2008.
57. L. Bocher, M. H. Aguirre, D. Logvinovich, A. Shkabko, R. Robert, M. Trottmann, and A. Weidenkaff, "$CaMn_{1-x}$ Nb_xO_3 ($x \leq 0.08$) Perovskite-Type Phases As Promising New High-Temperature n-Type Thermoelectric Materials," *Inorg. Chem.*, vol. 47, pp. 8077-8085, 2008.
58. R. Funahashi, I. Matsubara, H. Ikuta, T. Takeuchi, U. Mizutani and S. Sodeoka, "An Oxide Single Crystal with High Thermoelectric Performance in Air," *Jpn. J. Appl. Phys.*, vol. 39, pp. L 1127–L 1129, 2000.
59. K. Koumoto, I. Terasaki, T. Kajitani, M. Ohtaka, R. Funahashi, "Oxide thermoelectrics" in *Thermoelectrics handbook: Macro to nano*, D. M. Rowe, Ed., CRC Press Boca Raton, 2006.
60. W. Koshibae, K. Tsutsui, and S. Maekawa, "Thermopower in cobalt oxides," *Phys. Rev. B*, vol. 62, no. 11, pp. 6869-6872, 2000.
61. Y. Wang, N. S. Rogado, R. J. Cava & N. P. Ong, "Spin entropy as the likely source of enhanced thermopower in $Na_xCo_2O_4$," *Nature* ,vol. 423 , no. 22, pp. 425-428, 2003.
62. K. Fujita T. Mochida and K. Nakamura, "High-Temperature Thermoelectric Properties of $Na_xCoO_{2-\delta}$ Single Crystals," *Jpn. J. Appl. Phys.*, vol. 40, pp. 4644–4647, 2001.
63. Y. Miyazaki, S. Yousuke, O. Mitsuko, I. Yoshinobu, M. Yukio and K. Tsuyoshi, "Modulated Structure of Misfit Layered Cobalt Oxide $[(Ca_{0.9}0Bi_{0.10})_2(Co_{0.95}Bi_{0.05})O_3]pCoO_2$," *Jpn. J. Appl. Phys.*, vol. 43, no. 9A, pp. 6252–6258, 2004.
64. H. Leligny, D. Grebille, O. Pe´rez, A.C. Masset, M. Hervieu, and B. Raveau, "A five-dimensional structural investigation of the misfit layer compound $[Bi_{0.87}SrO_2]_2[CoO_2]_{1.82}$," *Acta Cryst.*, vol. B 56, pp. 173-182, 2000.
65. J.-M. Tarascon, R. Ramesh, P. Barboux, M.S. Hedge, G.W. Hull, L.H. Greene, M. Giroud, Y. LePage, W.R. McKinnon, J.V. Waszcak, and L.F. Schneemeyer, "New non-superconducting layered Bi-oxide phases of formula $Bi_2M_3Co_2O_y$ containing Co instead of Cu," *Solid State Commun.*, vol. 71, no. 8, pp. 663-668, 1989.
66. Y. Miyazaki, K. Kudo, M. Akoshima, Y. Ono, Y. Koike and T. Kajtani, "Low-Temperature Thermoelectric Properties of the Composite Crystal $[Ca_2CoO_{3.34}]_{0.614}[CoO_2]$, *Jpn. J. Appl. Phys.*, vol. 39, no. 6A/2, pp. L 531–L 533, 2000.

67. Y. Miyazaki, T. Miura, M. Onoda, M. Uchida, Y. Ishii, Y. Ono, Y. Morii and T. Kajitani, "Modulated Structure of Misfit-Layered Cobalt Oxide $[Ca_2(Co_{0.65}Cu_{0.35})_2O_4]_{0.63}CoO_2$," *Jpn. J. Appl. Phys.*, vol. 42, pp. 7467–7473, 2003.
68. E. Woermann and A. Muan, "Phase equilibria in the system Cao-cobalt oxide in air," *J. Inorg. Nucl. Chem.*, vol. 32, pp. 1455-1459, 1970.
69. S. Li, R. Funahashi, I. Matsubara, K. Ueno and H. Yamada, "High temperature thermoelectric properties of oxide $Ca_9Co_{12}O_{28}$," *Mater. Chem.*, vol. 9, pp. 1659–1660, 1999.
70. A. C. Masset, C. Michel, A. Maignan, M. Hervieu, O. Toulemonde, F. Studer, and B. Raveau, "Misfit-layered cobaltite with an anisotropic giant magnetoresistance: $Ca_3Co_4O_9$," *Phys. Rev. B*, vol. 62, no. 1, pp. 166-175, 2000.
71. M. Shikano, R. Funahashi, "Electrical and thermal properties of single-crystalline $(Ca_2CoO_3)_{0.7}CoO_2$ with a $Ca_3Co_4O_9$ structure," *Appl. Phys. Lett.*, vol. 82, pp. 1851–1853, 2003.
72. P. Limelette, V. Hardy, P. Auban-Senzier, D. Jrome, D. Flahaut, S. Hbert, R. Frsard, Ch. Simon, J. Noudem, and A. Maignan, "Strongly correlated properties of the thermoelectric cobalt oxide $Ca_3Co_4O_9$," *Phys. Rev. B*, vol. 71, pp. 233108 -4pp, 2005.
73. M. Ihns, "Structural engineering of $Ca_3Co_4O_9$ thermoelectric thin films," Faculty of Science and Technology, University of Twente, Enschede, Nederland, 2013
74. T. Wu, T.A. Tyson, H. Chen, J. Bai, H. Wang, and C. Jaye, "A structural change in $Ca_3Co_4O_9$ associated with enhanced thermoelectric properties," *J. Phys.: Condensed Matter*, vol. 24, pp. 455602 -7pp, 2012.
75. A. Satake, H. Tanaka, T. Ohkawa, T. Fujii, and I. Terasaki, "Thermal conductivity of the thermoelectric layered cobalt oxides measured by the Harman method," *J.Appl. Phys.*, vol. 96, pp. 931-933, 2004. doi: 10.1063/1.1753070
76. D. Kenfaui, D. Chateigner, M. Gomina, and J. G. Noudem, "Anisotropy of the mechanical and thermoelectric properties of hot-pressed single-layer and multilayer thick $Ca_3Co_4O_9$ Ceramics," *Int. J. Appl. Ceram. Technol.*, vol. 8, pp. 214–226, 2011.
77. S. Chen, X. Song, X. Chen, Y. Chen, E. J. Barbero, E. L. Thomas, P.N. Barnes, "Effect of precursor calcination temperature on the microstructure and thermoelectric properties of $Ca_3Co_4O_9$ ceramics," *J. Sol-Gel Sci. Techn.*, vol. 64, pp. 627-636, 2012.
78. N. Y. Wu, T.C. Holgate, N. Van Nong, N. Pryds, S. Linderoth, "High temperature thermoelectric properties of $Ca_3Co_4O_{9+\delta}$ by auto-combustion synthesis and spark plasma sintering," J. Eur. Ceram. Soc., vol. 34, pp. 925-931, 2014.
79. M. Gunes, M. Ozenbas, "Effect of grain size and porosity on phonon scattering enhancement of $Ca_3Co_4O_9$," *J. Alloy. Compd.*, vol. 626, pp. 360-376, 2015.
80. N. Prasoetsopha, S. Pinitsoontorn and V. Amornkitbamrung, "Synthesis and thermoelectric properties of $Ca_3Co_4O_9$ prepared by simple thermal hydro-decomposition methods, Electron. Mater. Lett., vol. 8, pp. 305-308, 2012.
81. L. Zhang, G.H. Liu, Y.B. Li, J.R. Xu, X.B. Zhu, Y.P. Sun, "Simple chemical solution deposition of $Ca_3Co_4O_9$ films directly on Si substrates," *Mater. Lett.*, vol. 62, pp. 1322–1324, 2008.
82. J. C. Diez, M. A. Torres, Sh. Rasekha, G. Constantinescu, M. A. Madre, A. Sotelo, "Enhancement of

$Ca_3Co_4O_9$, thermoelectric properties by Cr for Co substitution," *Ceram. Int.*, vol. 39, pp. 6051–6056, 2013.
83. S. Li, R. Funahashi, I. Matsubara, K. Ueno, S. Sodeoka, H. Yamada, "Synthesis and thermoelectric properties of the new oxide materials $Ca_{3-x}Bi_xCo_4O_{9+\delta}$ ($0.0 < x < 0.75$)," *Chem. Mater.*, vol. 12, pp. 2424–2427, 2000.
84. V. V. Boldyrev, "Mechanochemistry and sonochemistry", *Ultrasononics Sonochemistry*, vol. 2, no. 2, pp. S143–S144, 1995.
85. V. V. Boldyrev, "Mechanochemistry and mechanical activation of solids," *Russ. Chem. Reviews*, vol. 75, no. 3, pp. 177–189, 2006.
86. V.V. Zyryanov, "Mechanochemical synthesis of complex oxides," *Russ. Chem. Rev.*, vol. 77, no. 2, pp. 105- 135, 2008.
87. Z. M. Stanojević, Z. Branković, Z. Jagličić, M. Jagodič, L. Mančić, S. Bernik, A. Rečnik, G. Branković, "Structural and magnetic properties of nanocrystalline bismuth manganite obtained by mechanochemical synthesis," *J. Nanopart. Res.*, vol. 13, no. 8, pp. 3431-3439, 2011. : doi:10.1007/s11051-011-0265-7
88. F. Li, J.-F. Li, L.-D. Zhao, K. Xiang, Y. Liu, B.-P. Zhang, Y.-H. Lin, C.-W. Nan and H.-M. Zhu, "Polycrystalline BiCuSeO oxide as a potential thermoelectric material," *Energy Environ. Sci.*, vol. 5, pp. 7188-7195, 2012.
89. S. Bhattacharya, D. K. Aswal, A. Singh, C. Thinaharan, N. Kulkarni, S. K. Gupta, J. V. Yakhmi, "Anisotropic electrical transport studies of $Ca_3Co_4O_9$ single crystals grown by the flux method," *J. Cryst. Growth.*, vol. 277, pp. 246-251, 2005.
90. E. Guilmeau, R. Funahashi, M. Mikami, K. Chong, and D. Chateigner, "Thermoelectric properties–texture relationship in highly oriented $Ca_3Co_4O_9$ composites," *Appl. Phys. Lett.*, vol. 85, pp. 1490-1492, 2004. ; doi: 10.1063/1.1785286
91. M. Mikami, E. Guilmeau, R. Funahashi, K. Chong, D. Chateigner, "Enhancement of electrical properties of the thermoelectric compound $Ca_3Co_4O_9$ through use of large-grained powder," *J. Mater. Res.*, vol. 20, no. 9, pp. 2491-2497, 2005.
92. Y. Zhou, I. Matsubara, S. Horii, T. Takeuchi, R. Funahashi, M. Shikano, J.I. Shimoyama, K. Kishio, W. Shin, N. Izu, N. Murayama., "Thermoelectric properties of highly grain-aligned and densified Co-based oxide ceramics," *J. Appl. Phys.*, vol. 93, pp. 2653-2658, 2003.
93. Y. Wang, Y. Sui, X. Wang, W. Su, X. Liu, "Enhanced high temperature thermoelectric characteristics of transition metals doped $Ca_3Co_4O_9$ by cold high-pressure fabrication, *J. Appl. Phys.*, vol. 107, pp. 033708-9pp., 2010.
94. Y. Masuda, D. Nagahama, H. Itahara, T. Tani, W. S. Seo, and K. Koumoto, "Thermoelectric performance of Bi- and Na-subtituted $Ca_3Co_4O_9$ improved through ceramic texturing," *J. Mater. Chem.*, vol. 13, pp. 1094-1099, 2003.
95. Y. Zhang, J. Zhang, Q. Lu, "Synthesis of highly textured $Ca_3Co_4O_9$ ceramics by spark plasma sintering," *Ceram. Int.*, vol. 33, pp. 1305–1308, 2007.
96. J. G. Noudem, D. Kenfaui, D. Chateigner and M. Gomina, "Toward the enhancement of the thermoelectric properties of lamellar $Ca_3Co_4O_9$ by edge-free spark plasma texturing," *Scripta Mater.*, vol. 66, pp. 258–260, 2012.
97. D. Kenfau, D. Chateigner, M. Gomina, J. G. Noudem, "Texture, mechanical and thermoelectric properties of $Ca_3Co_4O_9$ ceramics," *J. Alloy and Compd.*, vol. 490, pp. 427-429, 2010.

98. Y. Wang, L. Xu, Y. Sui, X. Wang, J. Cheng, W. Su, "Enhanced electron correlation in rare-earth doped $Ca_3Co_4O_9$," *Appl. Phys. Lett.*, vol. 97, pp. 062114-3pp., 2010.
99. R. Asahi, J. Sugiyama, and T. Tani, "Electronic structure of misfit-layered calcium cobaltite," *Phys. Rev. B*, vol. 66, pp. 155103-7pp., 2002.
100. N. V. Nong, N. Pryds , S. Linderoth, and M. Ohtaki, "Enhancement of the thermoelectric performance of p - type layered oxide Ca3Co4O9+δ through heavy doping and metallic nanoinclusions," Adv. Mater., vol. 23, pp. 2484–2490, 2011.
101. N.V. Nong, C.-J. Liu, M. Ohtaki, "High-temperature thermoelectric properties of late rare earth-doped $Ca_3Co_4O_{9+I}$," *J. Alloy. Compd.*, vol. 509, pp. 977–981, 2011.
102. C.-H. Lim, S.-M. Choi and W.-S. Seo, "High-temperature thermoelectric properties of the $Ca_{3-x}K_xCo_4O_9$ ($0 \le x \le 0.3$) system," *J. Korean Phys. Soc.*, vol. 57, no. 4, pp. 1054-1058, 2010.
103. F. Delorme, C. F. Martin, P. Marudhachalam, D. O. Ovono, G. Guzman, "Effect of Ca substitution by Sr on the thermoelectric properties of $Ca_3Co_4O_9$ ceramics," *J. Alloy. Compd.*, vol. 509, pp. 2311–2315, 2011.
104. S. Pinitsoontorn, N. Lerssongkram, N. Keawprak, V. Amornkitbamrung, "Thermoelectric properties of transition metals-doped $Ca_3Co_{3.8}M_{0.2}O_{9+d}$ (M = Co, Cr, Fe, Ni, Cu and Zn)," *J. Mater. Sci.: Mater. Electron.*, vol. 23, pp. 1050–1056, 2012.
105. Y. Huang, B. Zhao, S. Lin, R. Ang, Y. Sun, "Structure and transport properties in $Ca_3Co_{4-x}M_xO_9$ (M=Re and Pt) ceramics," *Ceram. Int.*, vol. 40, pp. 10545–10550, 2014.
106. Y. Fu, B. Zhao, Y. Huang, J. Dai, Y. Sun, "Enhanced electrical correlation in the W-doped cobaltite $Ca_3Co_4O_9$ ceramics," *Physica B*, vol. 414, pp.16–20, 2013.
107. S. Demirel, E. Altin, E. Oza, S. Altin, A. Bayri, "An enhancement ZT and spin state transition of $Ca_3Co_4O_9$ with Pb doping," *J. Alloy. Compd.*, vol. 627, pp. 430–437, 2015.
108. S. Demirel, M. A. Aksan, S. Altin, "Low temperature electrical and thermal transport properties of the $Ca_{3-x}Sb_xCo_4O_9$ system," *J. Mater. Sci.: Mater Electron*, vol. 23, pp. 2251-2256, 2012.
109. Y. Fu, B. Zhao, Y. Huang, J. Yang, J. Dai, M. Zhou, Y. Sun, "Spin-glass and spin-fluctuation in Mo-doped $Ca_3Co_4O_9$ system," *Solid State Commun.*, vol. 151, pp. 933–937, 2011.
110. A. R. West, "Preparative methods," in *Solid state chemistry and its applications*, A.R. West, Ed., John Wiley and Sons, 1984.
111. V. V. Boldyrev, K. Tkáčová, "Mechanochemistry of solids: Past, present, and prospects," *J. Mater. Synth. Process.*, vol. 8, no. 3/4, pp. 121–132, 2000.
112. E. Gaffet, F. Bernard, J. C. Niepce, F. Charlot, C. Gras, G. Le Caër, J. L. Guichard, P. Delcroix, A. Mocellin, O. Tillement, "Some recent developments in mechanical activation and mechanosynthesis," *J. Mater. Chem.*, vol.9, pp. 305–314, 1999.
113. T. Rojac, M. Kosec, B. Malič and J. Holc, "The application of a milling map in the mechanochemical synthesis of ceramics oxides," *Mater. Res. Bull.*, vol. 40, pp. 341-345, 2005.
114. T. Rojac, "Mehanokemijska sinteza $NaNbO_3$," Univerza v Ljubljani, Ljubljana, Slovenija, 2007.
115. N. Burgio, A. Iasonna, M. Magini, S. Martelli, F. Padella, "Mechanical alloying of the Fe-Zr system, Correlation between input energy and end products," *Nuovo cimento*, vol. 13D, no. 4, pp. 459–476, 1990.

116. M. Magini, N. Burgio, A. Iasonna, S. Martelli, F. Padella, E. Paradiso, "Analysis of energy transfer in the mechanical alloying process in the collision regime," *J. Mater. Synth. Proc.*, vol. 1, no. 3, pp. 135-144, 1993.
117. M. Magini, A. Iasonna, "Energy transfer in mechanical alloying," *Mater. Trans. JIM*, vol. 36, no. 2, pp. 123—133, 1994.
118. A. Iasonna, M. Magini, "Power measurements during mechanical milling. An experimental way to investigate the energy transfer phenomena," *Acta Mater.*, vol. 44, no. 9, pp. 1109-1117, 1996.
119. M. Magini, C. Colella, A. Iasonna, F. Padella, "Power measurements during mechanical milling – II. The case of "single path cumulative" solid state reaction," *Acta Metall.*, vol. 46, no. 8, pp. 2841–2850, 1998.
120. M. Magini, A. Iasonna, F. Padella, "Ball milling: An experimental support to the energy transfer evaluated by the collision model," *Scripta Mater.*, vol. 43, no. 1, pp. 13–19, 1996.
121. M. Pentimalli, M. Bellusci and F. Padella, "High energy ball milling as a general tool for nanomaterials synthesis and processing," in *Handbook of Mechanical Nanostructuring,* 2 Volume set, M. Aliofkhazraei, Ed., John Wiley and Sons, 2015.[Online].Available:https://books.google.si/books?id=swQxBgAAQBAJ&pg=PA654&lpg=PA654&dq=cumulative+milling+energy&source=bl&ots=zsT96nnjyr&sig=1YD9SZyL8DYYWvEyiaMZCaLRWXg&hl=sl&sa=X&ved=0ahUKEwilwfOo_pDPAhXC2SwKHS2XAIQQ6AEIUzAI#v=onepage&q=cumulative&f=false.
122. Murty, B. S., Mohan Rao, M. and Ranganathan, S., "Milling maps and amorphization during mechanical alloying," *Acta Metall. Mater.*, vol. 43, no. 6, pp. 2443–2450, 1995.
123. O. Guillon, J. Gonzalez-Julian, B. Dargatz, T. Kessel, G. Schierning, J. Räthel and M. Herrmann, "Field-Assisted Sintering Technology/ Spark Plasma Sintering: Mechanisms, Materials, and Technology Developments," *Adv. Eng. Mater.*, vol. 16, no.7, pp. 830-848, 2014.

Bibliography

Journal Articles related to the Thesis

Presečnik, M., de Boor J., Bernik, S., "Synthesis of single-phase $Ca_3Co_4O_9$ ceramics and their processing for a microstructure-enhanced thermoelectric performance," *Ceram. Int.*, vol. 42, no. 6, pp. 7315-7327, 2016.

Presečnik, M., Bernik, S., "The thermoelectric compound $Ca_3CO_4O_9$ - synthesis and characteristics, "*AIP conf. proc.*, vol. 1449, pp. 331-334, 2012.

Presečnik, M., Bernik, S., "Influence of a mechano-chemical treatment on the synthesis and characteristics of p-type thermoelectric $Ca_3Co_4O_9$, *J. Alloy. Compd.*, vol. 686, pp. 708-716, 2016.

Presečnik, M., Bernik, S., "Microstructural and thermoelectric properties of WO_3-doped $Ca_3Co_4O_9$ ceramics, "*Ceram. Int.*, vol. 42, no. 14, pp. 16103-16108, 2016.

Other Journal Articles

Rudež, R., Markowski, P., Presečnik, M., Košir, M., Dziedzic, A., Bernik, S., "Development of thick-film thermoelectric microgenerators based on p-type $Ca_3Co_4O_9$ and n-type $(ZnO)_5In_2O_3$ legs," *Ceram. Int.*, no. 10, part A, pp. 13201-13209. 2015.

Conference Paper

Presečnik, M., Rečnik, A., Dražić, G., Bernik, S., "Preliminary study of the stability of thermoelectric $Ca_3Co_4O_9$-based ceramics," in *Conference proceedings of* 51th *International Conference on Microelectronics, Devices and Materials and the Workshop on Terahertz and Microwave Systems*, Bled, Slovenia: MIDEM - Society for Microelectronics, Electronic Components and Materials, pp. 215-220, 2015.

Presečnik, M., Bernik, S., "Effect of processing methods on the microstructural development and thermoelectric properties of $Ca_3Co_4O_9$," in *proceedings of the 50th International Conference on Microelectronics, Devices and Materials*, Ljubljana, Slovenia: MIDEM - Society for Microelectronics, Electronic Components and Materials, pp. 209-214, 2014.

Bernik, S., Presečnik, M., Košir, M.," The role of microstructure in the enhancement of the thermoelectric characteristics of oxide ceramics," in *Conference program* of the 35th International Conference on Thermoelectrics & the 1st Asian Conference on Themmodynamics, (ICT/ACT 2016),Wuhan, China, 2016.

Presečnik, M., Bernik, S., "Microstructural and thermoelectric characteristics of Ca_3Co4O_9 prepared by different fabrication methods," in the *program and abstract book* of *9th Young researchers' day,* Ljubljana, Slovenija: Jožef Stefan Institute, 2015.

Presečnik, M., Daneu, N., Rečnik, A., Bernik, S., "Synthesis and stability of the thermoelectric $Ca_3Co_4O_9$-based ceramics," in *Book of abstracts of the 34th Annual International Conference on Thermoelectrics, (ICT 2015) and 13th European Conference on Thermoelectrics, (ECT 2015)*, Dresden, Germany:), Dresden, Germany, International Thermoelectric society and European Thermoelectric society, 2015.

Presečnik, M., Bernik, S., "Microstructural and thermoelectric characteristics of WO_3 - doped $Ca_3Co_4O_9$," in *Program and the book of abstracts of the 3CSCS-2015, 3rd Conference of the Serbian Ceramic Society*, Belgrade, Serbia: Institute for Multidisciplinary Research, University of Belgrade, 2015.

Presečnik, M., de Boor, J., Bernik, S., "Challenges in the synthesis and processing of p-type $Ca_3Co_4O_9$ ceramics for enhanced thermoelectric characteristics," in *the Programme and abstracts of the Ninth International Conference on High-Performance Ceramics*, Guilin, China: Chinese Ceramic Society, 2015.

Presečnik, M., Bernik, S., "Microstructural development and thermoelectric properties of $Ca_3Co_4O_9$ ceramics prepared by various processing methods," in the *Detailed programme & abstracts book of the 12th European Conference on Thermoelectrics, ECT 2014*, Madrid, Spain: The European Thermoelectric Society, 2014.

Presečnik, M., Bernik, S., "Microstroctural characteristics of thermoelectric $Ca_3Co_4O_9$ compound prepared by conventional sintering, hot-pressing and spark plasma sintering," in *the Program and abstract book of the 7th Young Researchers' Day*, Ljubljana, Slovenia: Institut Jožef Stefan, 2013.

Presečnik, M., Bernik, S., "Syntesis and microstructural analysis of calcium cobaltites as promising p-type thermoelectric materials," in *the 12th Conference of the European Ceramic Society, ECerS XII*, Stockholm, Sweden: ECERS, 2011.

Presečnik, M., Bernik, S. Synthesis and microstructural characterisation of Ca-cobaltites thermoelectric compound," in the *Program and the book of abstracts, 1CSCS-2011, 1st Conference of the Serbian Ceramic Society*, Belgrade, Serbia: The Serbian Ceramic Society, 2011.

Presečnik, M., Bernik, S., "Synthesis of the $Ca_3Co_4O_9$ thermoelectric compounds by mechano-chemical activation," v *Programu in knjigi povzetkov na 18. konferenci o materialih in tehnologijah*, Portorož, Slovenija: Inštitut za kovinske materiale in tehnologije, 2010.

Presečnik, M., Bernik, S., "Oxide thermoelectrics," in *Proceedings, of 2nd Jožef Stefan International Postgraduate School Students Conference*, Ljubljana, Slovenija: Mednarodna podiplomska šola Jožefa Stefana, 2010.

Presečnik, M., Bernik, S., "Mechano-chemical synthesis of Ca-cobaltates as promising oxide thermoelectrics ," *presented at ASON-1, 1st Adriatic School on Nanoscience*, Dubrovnik, Croatia, 2010.

Biography

The author of this thesis Mojca Presečnik was born on January 6th, 1981 in Slovenj Gradec, Slovenia. After finishing the Gymnasium in 2000, she enrolled in the Faculty of Natural and Technical Sciences at the Department for Geology at the University of Ljubljana. In between she organised or helped organise many educational excursions, such as, for example, the visit of the one of the largest mineral trade fairs in Europe, taking its place in Munich, the visit of the Velenje and Mežica mine, or even 10-day geological camps. Such events enabled students to practically experience the geology on the field, with the help of professional competence of many professors. During the study she organised and participated in setting up a few geological pillars with distinctive geologic rock formations of the selected area in three different parts of Slovenia, which now serve as an excellent tool for education about the history of Earth. Toward the end of her bachelor study she was the president of the voting committee in the Student Organisation of the University of Ljubljana and a member of the committee of the Student Board of the Faculty of Natural and Technical Sciences. She defended her bachelor thesis in 2008 entitled: »Geological storage of CO_2 in aquifers and assessment of its potential in Mura depression« under the supervision of Prof. Andrej Gosar. After college she employed herself in the CGP Group d.d., the group with services in the fields of civil engineering and construction, maintenance of roads and watercourses, and production of building materials and products. Towards the end of 2009 the possibility to enrol in the Jožef Stefan Postgraduate School appeared. Within the Young Researcher programme of the Slovenian Research Agency (ARRS), she started the programme of Nanosciences and Nanotechnologies, and began with the research. She studied the synthesis, microstructural and thermoelectric characteristics of the p-type ceramics in the Ca-Co-O system all under the supervision of Prof. Dr. Slavko Bernik. During her stay at the Institute she started a family with her partner and two kids. She presented her work on $Ca_3Co_4O_9$ ceramics at several international and Slovene conferences, and published five articles (four with first authorship) in recognized international journals.